SJSU SAN JOSÉ STATE UNIVERSITY

MTI MINETA TRANSPORTATION INSTITUTE

Exploring the Stress-Strain Relationship of Lightweight Concrete to Enhance the Lifecycle Performance of Transportation Highways and Bridges

Fariborz M. Tehrani, PhD, PE, ENV SP, PMP, SAP, F. ASCE

CSUTC California State University Transportation Consortium

FRESNO STATE Discovery. Diversity. Distinction.

CSU TRANSPORTATION CONSORTIUM

transweb.sjsu.edu/csutc

MINETA TRANSPORTATION INSTITUTE

Founded in 1991, the Mineta Transportation Institute (MTI), an organized research and training unit in partnership with the Lucas College and Graduate School of Business at San José State University (SJSU), increases mobility for all by improving the safety, efficiency, accessibility, and convenience of our nation's transportation system. Through research, education, workforce development, and technology transfer, we help create a connected world. MTI leads the California State University Transportation Consortium (CSUTC) funded by the State of California through Senate Bill 1 and the Climate Change and Extreme Events Training and Research (CCEETR) Program funded by the Federal Railroad Administration. MTI focuses on three primary responsibilities:

Research

MTI conducts multi-disciplinary research focused on surface transportation that contributes to effective decision making. Research areas include: active transportation; planning and policy; security and counterterrorism; sustainable transportation and land use; transit and passenger rail; transportation engineering; transportation finance; transportation technology; and workforce and labor. MTI research publications undergo expert peer review to ensure the quality of the research.

Education and Workforce Development

To ensure the efficient movement of people and goods, we must prepare the next generation of skilled transportation professionals who can lead a thriving, forward-thinking transportation industry for a more connected world. To help achieve this, MTI sponsors a suite of workforce development and education opportunities. The Institute supports educational programs offered by the Lucas Graduate School of Business: a Master of Science in Transportation Management, plus graduate certificates that include High-Speed and Intercity Rail Management and Transportation Security Management. These flexible programs offer live online classes so that working transportation professionals can pursue an advanced degree regardless of their location.

Information and Technology Transfer

MTI utilizes a diverse array of dissemination methods and media to ensure research results reach those responsible for managing change. These methods include publication, seminars, workshops, websites, social media, webinars, and other technology transfer mechanisms. Additionally, MTI promotes the availability of completed research to professional organizations and works to integrate the research findings into the graduate education program. MTI's extensive collection of transportation-related publications is integrated into San José State University's world-class Martin Luther King, Jr. Library.

Report 26-06

Exploring the Stress-Strain Relationship of Lightweight Concrete to Enhance the Lifecycle Performance of Transportation Highways and Bridges

Fariborz M. Tehrani, PhD, PE, ENV SP, PMP, SAP, F. ASCE

March 2026

A publication of the
Mineta Transportation Institute
Created by Congress in 1991

College of Business
San José State University
San José, CA 95192-0219

TECHNICAL REPORT DOCUMENTATION PAGE

1. Report No. 26-06	**2. Government Accession No.**	**3. Recipient's Catalog No.**	
4. Title and Subtitle Exploring the Stress-Strain Relationship of Lightweight Concrete to Enhance the Lifecycle Performance of Transportation Highways and Bridges		**5. Report Date** March 2026 **6. Performing Organization Code**	
7. Authors Fariborz M. Tehrani, https://orcid.org/0000–0002–7618–8009		**8. Performing Organization Report** CA-MTI-2531	
9. Performing Organization Name and Address Mineta Transportation Institute College of Business San José State University San José, CA 95192-0219		**10. Work Unit No.** **11. Contract or Grant No.** SB1-SJAUX_2023-26	
12. Sponsoring Agency Name and Address State of California SB1 2017/2018 Trustees of the California State University Sponsored Programs Administration 401 Golden Shore, 5th Floor Long Beach, CA 90802		**13. Type of Report and Period Covered** **14. Sponsoring Agency Code**	
15. Supplemental Notes 10.31979/mti.2026.2531			
16. Abstract Concrete is the primary construction material of bridges, roads, and other transportation infrastructure across the United States, but conventional normal-weight concrete (NWC) is heavy, prone to cracking, and expensive to maintain over time. This study examines the mechanical properties, durability, and lifecycle performance of lightweight aggregate concrete (LWC) and internally cured concrete (ICC) as alternatives in transportation infrastructure applications. Through laboratory testing, computer modeling, and lifecycle analysis, the research evaluates how these materials perform in terms of strength, flexibility, durability, cost, and environmental impact. The results show that LWC and ICC can meet required strength levels while being lighter and more flexible, which helps reduce cracking and long-term damage. These materials also improve internal moisture conditions, slowing deterioration caused by shrinkage and exposure to harsh environments such as deicing salts. The study finds that lightweight concrete can last nearly five times longer than conventional concrete in some applications, while significantly lowering maintenance needs. Over a structure's full lifespan, this can mean up to 85% lower lifecycle costs and up to 76% fewer greenhouse gas emissions. Current design codes often underestimate LWC performance, however, and therefore, revised empirical models are recommended. Overall, results confirm that LWC and ICC provide a structurally efficient, economically viable, and environmentally responsible solution for modern transportation infrastructure..			
17. Key Words Concrete, properties, elasticity, strength, durability, sustainability, emissions, cost	**18. Distribution Statement** No restrictions. This document is available to the public through The National Technical Information Service, Springfield, VA 22161.		
19. Security Classif. (of this report) Unclassified	**20. Security Classif. (of this page)** Unclassified	**21. No. of Pages115** 113	**22. Price**

Form DOT F 1700.7 (8-72)

DOI: 10.31979/mti.2026.2531

Mineta Transportation Institute
College of Business
San José State University
San José, CA 95192-0219

Tel: (408) 924-7560
Fax: (408) 924-7565
Email: mineta-institute@sjsu.edu

transweb.sjsu.edu/research/2531

ACKNOWLEDGMENTS

The California State University Transportation Council and the Fresno State Transportation Institute funded this project. The author would like to thank Dr. Reid Castrodale for sharing his expertise and key resources and Mr. Jody Wall for providing valuable data. Additionally, the author acknowledges the generous donations of materials from Amrize Utelite, Arcosa Lightweight, Buildex, and Stalite. The author is also grateful for the editorial services provided by the staff at the Mineta Transportation Institute (MTI). Any opinions, findings, conclusions, or recommendations expressed in this material are those of the author and do not necessarily reflect the views of these institutions.

Contents

LIST OF FIGURES

LIST OF TABLES

Executive Summary

Background

This report investigates the performance of lightweight aggregate concrete (LWC) and internally cured concrete (ICC) for transportation infrastructure applications. Traditional normal-weight concrete (NWC) imposes significant dead loads on structures, increasing material and construction costs, limiting design flexibility, and potentially negatively affecting seismic performance. LWC, particularly when combined with internal curing techniques, offers a promising alternative by reducing density, enhancing hydration, and improving long-term durability.

Objectives

The study aims to establish accurate stress–strain relationships for LWC and ICC, evaluate their mechanical properties in interaction with transport properties, and quantify their impact on service life, lifecycle cost, and environmental performance. It also seeks to provide design recommendations for updating ACI and AASHTO specifications to reflect the actual performance of modern lightweight concretes.

Methodology

The research employed a literature review, laboratory testing, analytical modeling, and life-cycle assessment. The literature review involved data mining and case studies on physical, mechanical, and durability characteristics of concrete containing lightweight aggregates. Laboratory tests measured compressive strength, modulus of elasticity, Poisson's ratio, and splitting tensile strength for multiple concrete mixes, including all-lightweight (ALW), sand-lightweight (SLW), internally cured concrete (ICC), and high-strength variants. Analytical models predicted service life based on chloride diffusion and evaluated structural performance under realistic loading conditions. Lifecycle assessments quantified environmental impacts, while lifecycle cost analysis assessed economic feasibility.

Key Findings

The results confirm that LWC and ICC achieve target compressive strengths while exhibiting lower moduli of elasticity than NWC, thereby reducing cracking under restraint and dynamic loads. Internally cured and lightweight mixes demonstrated improved durability due to enhanced hydration and reduced shrinkage. Analytical investigations of durability characteristics revealed that LWC produced with expanded shale, clay, and slate aggregates offers superior resistance to chloride ingress, extending service life by up to 4.8 times compared to NWC. Sustainability analysis showed reductions of up to 76% in greenhouse gas emissions over the structure's lifecycle. Lifecycle cost analysis also indicates savings of up to 85% due to reduced maintenance and

extended service life. Current design provisions underestimate LWC performance, and revised empirical models based on equilibrium density and compressive strength are recommended.

Overall Conclusion

Lightweight aggregate concrete and internally cured concrete represent a transformative solution for transportation infrastructure. They improve structural efficiency, durability, and sustainability while delivering substantial economic benefits over the lifecycle of bridges and pavements. Adoption of these materials supports federal initiatives and sustainability goals, making them essential for future infrastructure development.

1. Introduction

1.1 Background

Research on the modulus of elasticity of lightweight concrete has examined various factors that affect its mechanical properties. Studies cited in the Literature Review indicate that the modulus of elasticity is influenced by the type and proportion of lightweight aggregates used, the cementitious matrix, and the presence of fibers or other additives. For example, studies have reported that aggregate stiffness and porosity play a dominant role in controlling elastic modulus, while variations in binder composition and supplementary cementitious materials can significantly modify elastic behavior. Additionally, the incorporation of fibers has been shown to affect stiffness and deformation characteristics of lightweight concrete.

In practice, the modulus of elasticity plays a crucial role in structural design and analysis. Engineers rely on empirical formulas and guidelines—such as those provided by the American Concrete Institute (ACI) and the Expanded Shale, Clay & Slate Institute (ESCSI)—to estimate the modulus of elasticity based on the concrete's compressive strength and density. These guidelines help ensure that lightweight concrete structures meet the necessary performance standards and safety criteria.

1.2 Objective

Structural lightweight aggregate concrete materials are widely used in transportation infrastructure, including bridge decks and high-performance pavements. Recent advancements in the design and construction of these components have shifted the focus to understanding the stress-strain relationship and the elasticity modulus of concrete. This project aims to establish a comprehensive stress-strain relationship for lightweight concrete, specifically for high-performance pavements and bridge decks. Additionally, it examines the lifecycle impacts of this relationship on the service life of critical infrastructure, such as bridges.

Furthermore, the lifecycle analysis adheres to standard practices for communicating the environmental footprint of lightweight concrete bridge decks. This project aligns with the Federal Highway Administration (FHWA) Every Day Counts (EDC-7) Innovations, including the initiative "Enhancing Performance with Internally Cured Concrete" (EPIC2), as presented by FHWA in 2023 and 2024.

1.3 Scope

Experimental Investigations

The material properties of concrete specimens containing lightweight aggregates and control specimens will be investigated to develop the mix design. Concrete materials are readily available

in the local construction market. Lightweight aggregates can be donated and shipped from producers nationwide. Concrete samples will be prepared and tested in accordance with the proposed mix design. Additionally, specimens for measuring the modulus of elasticity and compressive strength will be created and evaluated.

Analytical Investigations

The analysis of material properties will be used to compare how lightweight aggregates affect concrete performance. Simulations will be carried out to assess the impact of these aggregates on the design and construction of road pavements and bridge decks. Additionally, the lifecycle impacts of lightweight concrete will be examined, focusing on the relationship between compressive strength and the modulus of elasticity. This analysis aims to determine how these factors affect the system's environmental footprint.

2. Literature Review

2.1 Lightweight Aggregate and Concrete in Transportation Infrastructure

Lightweight aggregate (LWA) and lightweight concrete (LWC) containing LWA have gained prominence in transportation infrastructure due to their reduced density, enhanced durability, and favorable mechanical properties (Gerami, Tehrani, and Esfahani 2007; Tehrani 2025). Lightweight materials also contribute to the economy of infrastructure development through lifecycle savings (Forouhi, Terhani, and Zand 1996). Chapman and Castrodale (2016); Cousins, Roberts-Wollmann, and Brown (2013); and Brown et al. (1995) demonstrated LWC's effectiveness in bridge girders and decks. Murillo, Thiman, and Smith (1994); Roberts (1997); Wolfe (2017); and Nunley (2018) presented case studies highlighting reduced weight, improved durability, and seismic resilience. Kalantari and Tehrani (2021), Kim and Chun (2015), and Tehrani (2021b) explored LWC in pavement applications, emphasizing internal curing and lifecycle benefits. Bonyadian et al. (2019, 2024) and Bonyadi et al. (2022) confirmed performance improvements in bridge deck pavements.

Durability and Transport Properties

The durability and lifecycle performance of transportation infrastructure are increasingly influenced by concrete material choices, particularly in the context of climate change and sustainability (Kalantari, Ehsani, and Tehrani 2023). Lightweight concrete, especially when enhanced with rotary-kiln-produced lightweight aggregates such as expanded shale, clay, or slate (ESCS), has emerged as a promising solution for improving the resilience and longevity of highway and bridge structures (Tehrani 1994, 1996, 1998, 2021a, 2025; Holm and Ries 2007; Tehrani and Ziarani 2010).

The cement paste, governed by the water-cementitious materials (w-cm) ratio, plays a pivotal role in determining the mechanical properties of concrete. A lower w-cm ratio improves hydration and reduces permeability, both of which are critical for durability. However, early deficiencies in cement paste can lead to shrinkage and cracking, compromising long-term performance. The interfacial transition zone (ITZ) between aggregates and paste is particularly sensitive to curing practices and pozzolanic activity, which influence shrinkage and cracking behavior (Kosmatka, Kerkhoff, and Panarese 2021; ACI 231; ACI 308; ACI 308-213; Schindler and McCullough 2002; Shakeri, Dardaei Joghan, and Tehrani 2024).

Durability under chloride exposure and freeze-thaw cycles is a critical concern for LWC in transportation. Pouramini et al. (2021) demonstrated degradation in saline environments. ESCSI (2024b) and Davodijam et al. (2022) confirmed LWC's superior resistance in marine and cold climates. Holm (1980), Holm and Bremner (2000), Helland (2005), and Hassanain (2010) provided field data from bridges in Norway, Bahrain, and the Persian Gulf.

Electrical resistivity and permeability are key indicators of concrete durability. Tanesi and Ardani (2012), Andrade et al. (2009), and Hooton and Charmchi (2015) supported resistivity testing as a reliable method. Tehrani (2020) linked transport properties to service-life predictions, reinforcing the value of resistivity and chloride-diffusion metrics.

Service Life Analyses

Life-365™ (2020); Ehlen, Thomas, and Bentz (2009); and Ehlen and Kojundic (2014) developed chloride-based models for service life estimation. Kalantari and Tehrani (2021, 2022, 2024) applied these models to various climate zones, demonstrating LWC's extended service life. Tehrani (2021b, 2022) emphasized the role of transport properties in lifecycle modeling.

Service life prediction models, such as Life-365™, utilize chloride diffusion equations based on Fick's second law to estimate the time to corrosion. Simulations have demonstrated that lightweight concrete mixtures can delay corrosion onset by up to 22%, with internal curing mixtures showing even greater improvements (Tehrani 2020). These findings are supported by field studies on bridges in marine and cold environments, where chloride penetration is a significant concern (Fluge and Blankvoll 1995; Henriksen and Stoltzner 1993).

Internal Curing

Internal curing using prewetted fine lightweight aggregates has been shown to reduce early-age shrinkage and thermal cracking, thereby enhancing durability and extending service life (Byard and Schindler 2010; ACI 213; ESCSI 2006; Tehrani 2019b). The use of ESCS aggregates enhances internal curing, leading to improved hydration and reduced autogenous shrinkage, thereby mitigating early-age cracking and contributing to long-term structural integrity (Bentz et al. 2005; Henkensiefken 2008). The existing literature indicates that internal curing not only reduces cracking and permeability but also improves compressive and flexural strength. For instance, compressive strength can increase by up to 20% and flexural strength by 15% (Kalantari et al. 2021; Mark 2006; Roberts 2004). These improvements contribute to reduced lifecycle costs and enhanced sustainability, as internally cured concrete requires less maintenance and offers longer service life, particularly in harsh environments such as marine or cold climates (Davodijam et al. 2022; Tehrani 2020).

Mechanical Properties

Mechanically, lightweight concrete exhibits lower thermal expansion and a lower modulus of elasticity, which helps mitigate thermal cracking. These properties are particularly beneficial for bridge infrastructure, improving seismic performance and fire resilience while facilitating accelerated construction. The porosity and mechanical properties of the aggregates influence the stress-strain behavior of lightweight concrete. While porosity reduces self-weight and modulus of elasticity, it can also affect tensile strength. However, studies have shown that ESCS aggregates

exhibit higher splitting tensile strength, shear strength, and modulus of elasticity than other lightweight aggregates (Kadkhodaie et al. 2024; Ghavami et al. 2024).

High-performance concrete (HPC) is used in bridge decks to improve durability, characterized by lower water-cement ratios and higher strength. While higher-strength concretes offer greater tensile capacity and reduced permeability to deicing salts, they can also lead to cracking due to volume changes. Hadidi and Saadeghvaziri (2005) noted a direct link between increased compressive strength and cracking, while Schmitt and Darwin (1995) found that higher strength correlates with higher cracking occurrences due to increased stiffness and reduced creep. Shah and Weiss (2000) also highlighted that a lower water-cement ratio raises the risk of early-age cracking. Hopper et al. (2015) recommended limiting the 28-day compressive strength of concrete to 5,000 psi (34.5 MPa) to minimize cracking. Hence, the application of lightweight aggregate to reduce modulus of elasticity while maintaining mechanical strength contributes to the structural performance of concrete (Khajehdehi and Darwin 2018).

Lowering concrete's elastic modulus can help reduce crack width in bridge decks and pavements subjected to dynamic loads from vehicular traffic. In addition, early-age concrete within the first 3 to 5 hours after placement experiences a higher rate of increase in modulus of elasticity than in strength. Hence, a higher modulus of elasticity can lead to stress levels exceeding the concrete's available strength (Mn/DOT 2011).

Concrete is typically restrained by surrounding structural elements such as girders in bridges, continuous slabs in pavements, and other concrete sections. When volume changes due to drying shrinkage or temperature fluctuations, a rigid concrete with a higher elastic modulus develops greater internal stresses under the same level of restraint than a less stiff concrete. An expected lower modulus of elasticity in lightweight concrete results in reduced rigidity, providing less internal restraint against volume changes such as shrinkage and thermal contraction, thereby reducing tensile stresses that cause cracking (Deng et al. 2016; Frosch, Blackman, and Radabaugh 2003; Ozyildirim and Nair 2023).

Further, a lower elasticity modulus allows the concrete to tolerate higher strains for a given stress level, meaning it can accommodate some of the deformations caused by traffic loads, temperature changes, and drying shrinkage without the stresses exceeding its tensile strength and leading to wide cracks. While traffic loads alone may not cause cracking in a properly designed deck, they contribute to the overall stress state. A 10% increase in elastic modulus can increase the cracking point stress by as much as 30–40% under load, due to the material's reduced plastic deformation capabilities (Figure 1). Therefore, a lower elasticity modulus helps mitigate the combined stresses from volume changes and external loads (Korolev et al. 2021).

Figure 1. Stress-Deflection Curves for Heavyweight Concrete, Reinforced by (a) Steel and (b) Composite, Adapted from Korolev et al. (2021)

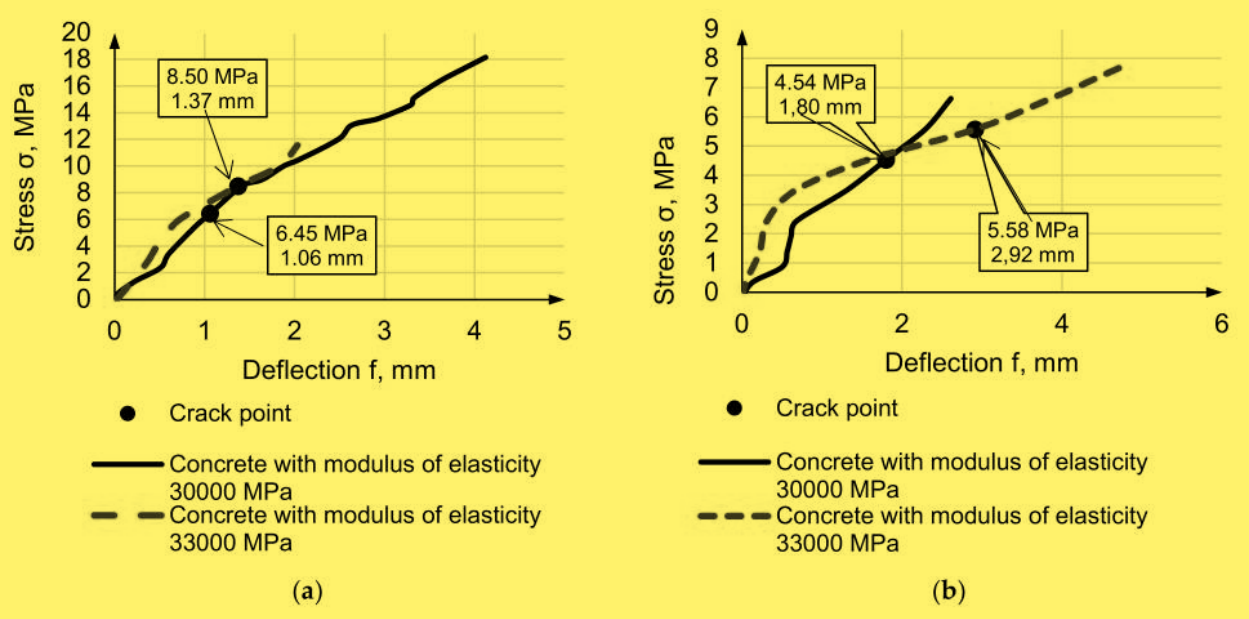

In practice, this is often achieved by using specific aggregate types, such as lightweight aggregates, which inherently have a lower modulus of elasticity but still provide adequate compressive strength. The use of concrete with strengths exceeding the specified design values should be avoided, as this often results in an undesirably high elastic modulus, which exacerbates cracking (Castrodale 2021; Ozyildirim and Nair 2023).

The effect of a lower elastic modulus on bridge deck crack width under dynamic vehicular loading is primarily quantified through numerical modeling, experimental testing with sensors, and design formulas specified in engineering codes. Vehicle-bridge interaction models can simulate the dynamic amplification factor (DAF) as a function of vehicle speed and road surface roughness (Han, Dan, and Wang 2018). A lower modulus changes the bridge's stiffness and natural frequency, affecting its dynamic response to traffic. Experimental testing, including field and laboratory dynamic load tests, is also conducted on actual bridge decks, pavements, or large-scale specimens. Test vehicles are driven across the deck at various speeds while sensors such as strain gauges and displacement transducers measure the structural response. The resulting crack widths can be directly measured using a crack comparator or digital imaging. Comparing results from decks with different E-moduli allows for a quantitative assessment of the effect (Dhungel et al. 2024).

Design codes provide formulas for estimating crack widths in reinforced concrete based on material properties, such as the elastic modulus and the stress in the steel reinforcement, as in the equations by Gergely and Lutz (1968), Kaar and Mattock (1963), and Frosch (1999). The general principle is that crack width is related to strain and crack spacing (Frosch, Blackman, and Radabaugh 2003).

A lower elastic modulus results in greater strain for a given stress, thereby influencing the calculated crack width. Research studies also collect data from in-service bridges and pavements with various concrete mix designs. By analyzing large datasets and using statistical methods, researchers establish correlations between mix parameters, including modulus of elasticity, and observed crack densities and widths (Mn/DOT 2011).

Sustainability

Lightweight aggregates contribute to sustainability by reducing the energy and emissions associated with transportation and construction. Their high absorption capacity and low thermal conductivity enhance fire safety, thermal comfort, and noise reduction, while also supporting environmental applications such as water preservation and waste cleanup (Tehrani et al. 2018; Pouramini, Torabian, and Tehrani 2021; Tehrani et al. 2025).

Lifecycle assessments (LCA) further validate the environmental and economic benefits of lightweight concrete. The use of Environmental Product Declarations (EPDs) enables quantification of carbon footprints and supports sustainable project delivery (Nelson and Tehrani 2018; Tehrani and Nelson 2022). For example, the global warming potential (GWP) of lightweight aggregates is significantly lower than that of traditional materials, thereby reducing emissions and energy consumption (ESCSI 2023; NRMCA 2020; PCA 2016; Tehrani et al. 2024, 2025).

Vosoughi et al. (2017) conducted a lifecycle cost analysis (LCCA) comparing internally cured and conventional pavements. Caltrans (2007), Kneifel and Lavappa (2024), and PBO (2018) provided cost data for construction and maintenance. ACCO (2004) offered regional economic insights.

Tehrani (2019a, 2023a, 2023b, 2024a, 2024b, 2024c) led efforts in environmental product declarations (EPDs) and lifecycle assessments (LCAs) for LWC. Ghavami et al. (2024) and ESCSI (2024a) quantified embodied energy and emissions. UL (2022), EPD (2021), NRMCA (2020), PCA (2016, 2019), CRSI (2017), and Vulcan (2016) provided standardized environmental data.

Experimental investigations have shown that LWC can achieve compressive strengths comparable to or exceeding those of NWC, particularly when high-strength lightweight aggregates are used. For instance, high-strength sand-lightweight concrete (HSSLW) demonstrated a predicted service life 4.76 times that of NWC in bridge decks in San Francisco, CA. HSSLW concrete exhibits the lowest lifecycle cost (0.14 relative to NWC), despite slightly higher initial costs. This cost efficiency is attributed to reduced maintenance needs and extended service life. Additionally, Figure 2 shows the annualized lifecycle greenhouse gas emissions, where HSSLW and ALW concrete types show reductions of up to 76% in global warming potential compared to NWC, underscoring the environmental benefits of LWC (Tehrani 2024b; Tehrani 2025).

Figure 2. Contributions of Lightweight Aggregates to Lifecycle Measures of Concrete, Adapted from Tehrani (2025)

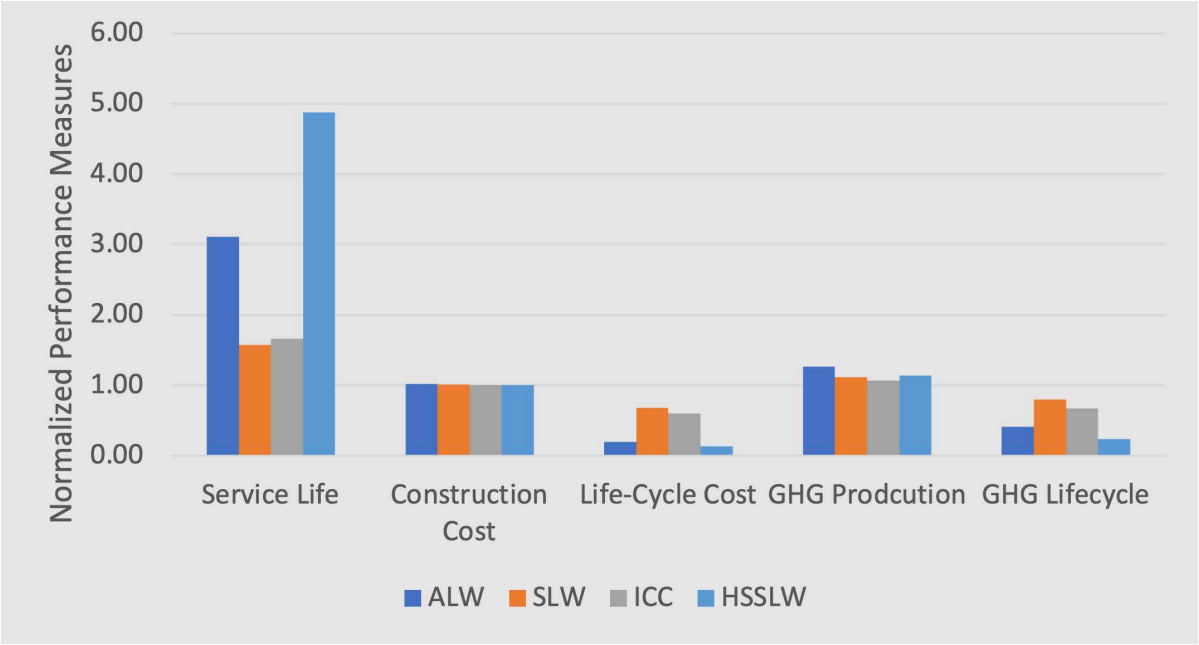

2.2 Early Investigations on Concrete Characteristics

Early research laid the groundwork for understanding concrete stress-strain behavior. Hognestad, Hanson, and McHenry (1955); Whitney (1937); Jensen (1943); Rosenblueth (1956); Cowan (1956); and Hruban (1956) contributed to the theory of ultimate strength design. Kaar, Hanson, and Capell (1977) and Ritchie and Graf (1951) focused on high-strength and lightweight concrete.

Stress-Strain Relations of Concrete

The seminal work by Hognestad, Hanson, and McHenry (1955) is a foundational contribution to understanding concrete stress distribution in ultimate strength design. Their study aimed to validate plasticity-based design theories by directly measuring the flexural stress distribution in concrete under high loads. The authors developed an innovative test method using eccentrically loaded, unreinforced concrete specimens to isolate and quantify the stress block properties, free from the confounding effects of reinforcement and tensile stresses. Five concrete mixes with water-cement (w/c) ratios ranging from 1.0 to 0.33 were tested at the ages of 7, 14, 28, and 90 days. The stress-strain curves obtained from these tests exhibited a descending branch beyond the peak stress, confirming the non-linear behavior of concrete in flexure and supporting the validity of ultimate strength design theories proposed by Whitney (1937), Jensen (1943), and others, as shown in Figure 3 (Hognestad, Hanson, and McHenry 1955).

Figure 3. Modulus of Elasticity Comparisons, Adapted from Hognestad, Hanson, and McHenry (1955)

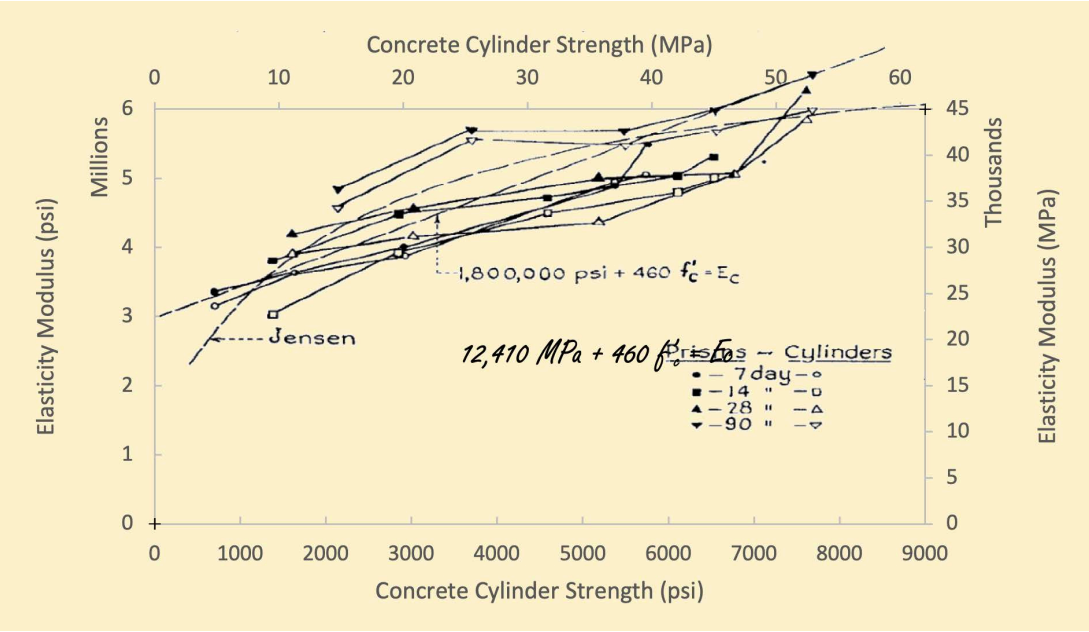

The study also addressed the phenomenon of "critical stress," defined as the point at which volume strain transitions from contraction to expansion, signaling the onset of internal cracking. This critical stress ranged from 71% to 96% of the maximum stress, depending on concrete strength. The authors emphasized that while concrete exhibits a descending stress-strain curve, the extent of plasticity is limited, and sudden failure can occur beyond certain strain thresholds (Hognestad, Hanson, and McHenry 1955).

The study conducted by Ritchie and Graf (1951) represents one of the earliest systematic investigations into the structural viability of lightweight concrete made with expanded shale aggregate. The research was motivated by the increasing use of lightweight concrete in large-scale infrastructure projects, such as the San Francisco–Oakland Bay Bridge and high-rise buildings, where reduced dead load could lead to significant cost savings and design flexibility. The primary objective of the study was to evaluate the mechanical and physical properties of structural concrete made with Lite-Rock, a proprietary expanded shale aggregate produced in Oregon. The authors compared the performance of Lite-Rock concrete with that of conventional gravel concrete and another expanded shale aggregate from California (Expanded Shale No. 2), focusing on parameters critical to structural applications such as compressive strength, modulus of elasticity, flexural strength, bond strength, shrinkage, and absorption (Ritchie and Graf 1951).

The experimental program involved nine different concrete mixes with varying cement contents (ranging from 3.7 to 9.2 sacks per cubic yard) and aggregate gradations. The mixes were tested using standard specimens, including 4"×8" and 6"×12" cylinders for compressive strength and

modulus of elasticity, and 6"×6"×36" beams for flexural and sonic modulus tests. The authors also conducted bond pull-out tests using 8"×8" cylinders with embedded deformed bars, as well as Dorry abrasion, absorption, and shrinkage tests (Ritchie and Graf, 1951).

The results demonstrated that Lite-Rock concrete could achieve compressive strengths up to 4,220 psi (Mix Dr) at 28 days, with a dry unit weight below 80 lb/ft^3. This performance exceeded the strength-to-weight benchmarks previously established by the Bureau of Reclamation and the National Bureau of Standards. The modulus of elasticity for Lite Rock concrete was approximately half that of gravel concrete and two thirds that of heavier shale (Figure 4). The authors derived a predictive equation that accurately estimated the elastic modulus based on compressive strength:

$$E = 750{,}000 + 250f_c' \qquad (1)$$

In this equation, E is the modulus of elasticity in psi and f_c' is the compressive strength in psi (Ritchie and Graf 1951).

Figure 4. Static and Sonic Moduli of Elasticity Versus Strength for Three Types of Concrete, Adapted from Ritchie and Graf (1951)

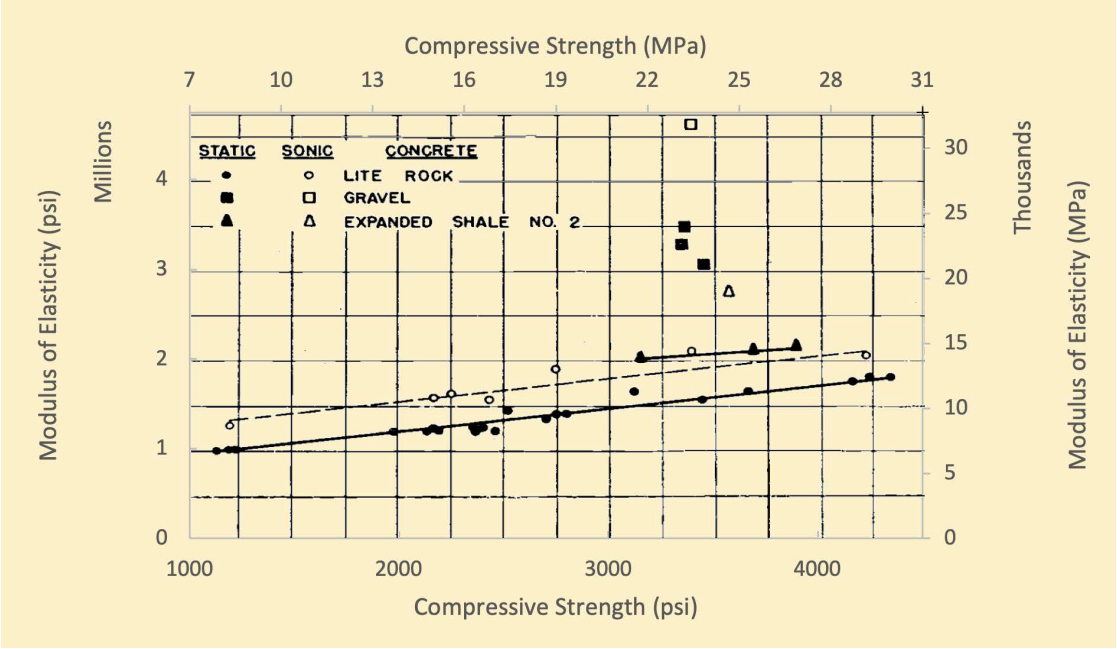

Flexural strength values ranged from 200 to 515 psi, with Lite-Rock mixes performing comparably to gravel and Expanded Shale No. 2 mixes. Bond strength was also satisfactory, with ultimate bond stresses reaching 1,178 psi (Mix H), and, in some cases, failure occurred in the steel rather than the concrete, indicating strong adhesion between the aggregate and reinforcement (Ritchie and Graf 1951).

From a structural design perspective, Lite-Rock concrete's low modulus of elasticity was found to be advantageous in reinforced concrete applications. The increased depth of the neutral axis and higher moment of inertia contributed to reduced deflections, despite the lower stiffness (Ritchie and Graf 1951).

Wang, Shah, and Naaman (1978) conducted a foundational investigation of the stress–strain behavior of both normal-weight and lightweight concrete under compression. The research is particularly significant for transportation infrastructure applications, where understanding the whole stress–strain profile—including the descending branch—is essential for predicting structural performance and durability. The authors developed a relatively simple experimental technique to obtain stress–strain curves up to a strain of 0.006. This method involved loading concrete cylinders in parallel with a case-hardened steel tube, which remained linearly elastic throughout the test. The steel tube allowed for controlled deformation and prevented sudden failure post-peak, enabling accurate measurement of the descending portion of the curve—a critical advancement over traditional load-controlled methods that often fail to capture post-peak behavior (Wang, Shah, and Naaman 1978).

The study included normal-weight concrete specimens with compressive strengths ranging from 3,000 to 11,000 psi and lightweight concrete specimens with compressive strengths ranging from 3,000 to 8,000 psi. The mix proportions and curing conditions were carefully controlled, and the results showed that both types of concrete exhibited gradual failure and reproducible descending curves. Notably, lightweight concrete demonstrated a steeper drop in the descending branch compared to normal-weight concrete of similar strength, indicating a more brittle post-peak behavior, as shown in Figure 5 (Wang, Shah, and Naaman 1978).

To analytically represent the stress–strain relationship, the authors proposed a rational expression:

$$f = \frac{A(\varepsilon/\varepsilon_0)+B(\varepsilon/\varepsilon_0)^2}{1+C(\varepsilon/\varepsilon_0)+D(\varepsilon/\varepsilon_0)^2} f_0 \qquad (2)$$

In this equation, f and ε are stress and strain, f_0 and ε_0 are peak stress and corresponding strain, and A, B, C, and D are constants determined separately for the ascending and descending portions of the curve using four key points: origin, 45% of peak stress, peak point, and a point symmetric to the peak with respect to the inflection point. Hence, the secant modulus of elasticity, E_0, follows:

$$E_0 = f_0/\varepsilon_0 \qquad (3)$$

The authors demonstrated that the coordinates of these key points could be statistically related to compressive strength, allowing the entire stress–strain curve to be predicted from strength alone. Regression equations were developed for both normal and lightweight concrete, with high correlation coefficients (up to 0.98), validating the robustness of the model:

$$E_0 = \begin{cases} 271{,}000\, {f_0}/{1000} + 978{,}000 \; for \; normalweight \; concrete \\ 180{,}900\, {f_0}/{1000} + 1{,}127{,}000 \; for \; lightweight \; concrete \end{cases} \quad (4)$$

Figure 5. Comparison of Experimental Data with the Generalized Analytic Curve for Normal Weight (Left) and Lightweight (Right) Concrete, Adapted from Wang, Shah, and Naaman (1978)

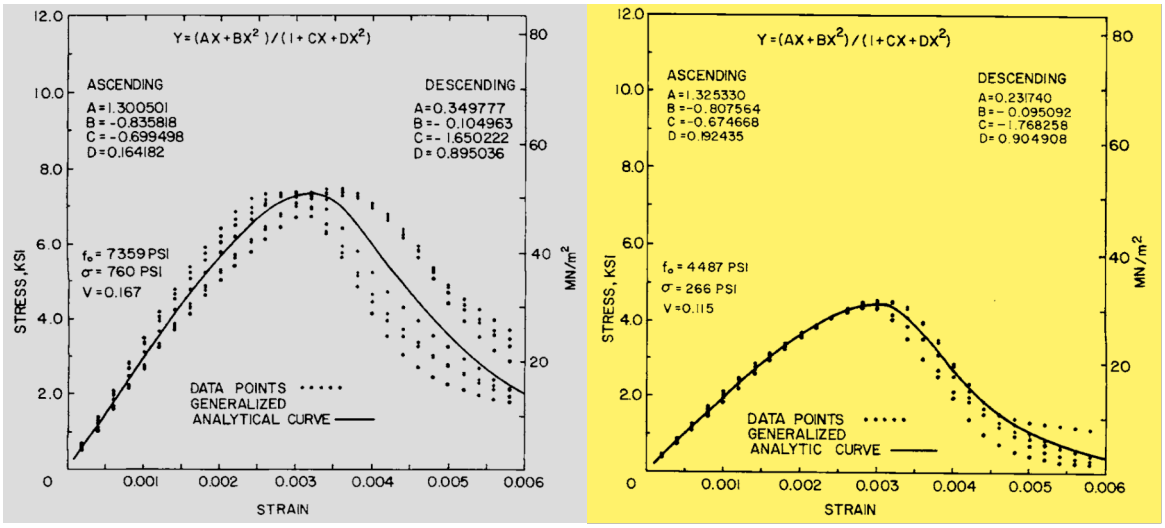

Notably, the study confirmed that the strain at the peak and inflection points of lightweight concrete increases almost linearly with compressive strength, unlike normal weight concrete, where these values remain relatively constant. This distinction underscores the need for separate analytical expressions for different concrete types when modeling structural behavior. The proposed model was validated against external data, including high-strength concrete specimens and extended strain ranges up to 0.020. The comparisons showed good agreement, confirming the model's applicability beyond the initial experimental limits (Wang, Shah, and Naaman 1978).

Hoyt (1961) presented an in-depth investigation into the load-deflection relationships of reinforced lightweight aggregate concrete beams, with a particular focus on the applicability of limit design theory. This research is highly relevant to the lifecycle performance of transportation infrastructure, especially bridges and highway components, where material efficiency, ductility, and long-term durability are critical. Hoyt begins by framing the concept of limit design, which emphasizes the ultimate strength and deformation capacity of structural materials rather than their elastic behavior. This approach is particularly suited to reinforced concrete structures, where plastic behavior and moment redistribution can significantly influence performance under service and ultimate loads. The thesis argues that limit design offers consistent safety factors and eliminates overdesign, making it a practical tool for reinforced concrete applications (Hoyt 1961).

The experimental program involved testing three simply-supported LWAC beams with central column stubs under pure flexure. The beams varied in depth—12", 16", and 20"—to assess the influence of section depth on rotation capacity. All beams were reinforced with tension and shear steel but lacked compression reinforcement, allowing the study to isolate flexural behavior. The concrete used was made with Idealite expanded shale aggregate, chosen for its local availability and relevance to lightweight construction practices (Hoyt 1961).

Stress-strain relationships for both steel and concrete were established through laboratory testing. The steel exhibited typical elastic-plastic behavior, with a well-defined yield point and strain hardening, in close agreement with theoretical expectations. The average yield stress was 45,900 psi, and the ultimate stress reached 75,800 psi, with strains up to 0.148 in./in. Concrete stress-strain curves showed that LWAC had a flatter curve than stone aggregate concrete, with ultimate strains ranging from 0.0029 to 0.00342 in./in., across the three beam depths. These values exceeded the theoretical strain limit of 0.0023 in./in., suggesting that LWAC can sustain higher deformations before failure (Hoyt 1961).

The moment-curvature relationship was analyzed using assumptions about strain distribution and stress blocks. The study found that the neutral axis shifted significantly during plastic deformation, affecting the internal lever arm and resisting moment. This behavior was confirmed through strain measurements and visual observations of crack progression. Further, load-deflection curves demonstrated clear yield points and substantial plastic ranges, validating the use of limit design for LWAC. The measured deflections at ultimate load were two to four times higher than theoretical predictions, indicating that LWAC beams possess considerable ductility (Table 1). This is a critical finding for transportation infrastructure, where structures must accommodate dynamic loads, thermal expansion, and long-term creep without catastrophic failure (Hoyt 1961).

Table 1. Load-Deflection Comparison, Adapted from Hoyt (1961)

Item	Beam Depth (in.)	Theoretical Value	Actual Value
Neutral Axis, from Compression-Edge (in.)	20	7.63	6.5
	16	6.45	6.1
	12	5.31	6.4
Yield Load (lbf)	20	33,400	38,000
	16	25,400	28,200
	12	17,700	16,300
Ultimate Load (lbf)	20	36,400	43.600
	16	27,800	32,200
	12	19,100	18,700
Yield Deflection (in.)	20	0.210	0.357
	16	0.295	0.433
	12	0.466	0.559
Ultimate Deflection (in.)	20	0.946	3.930
	16	0.938	2.844
	12	0.892	1.983

1 lbf = 4.44822 N and 1 in. = 0.0254 m

The study also explored the concept of the plastic hinge and its length, which influences rotation capacity and moment redistribution. While initial assumptions tied hinge length to beam depth, empirical data suggested that hinge length may be more closely related to loading conditions than geometry. This insight has implications for the design of bridge girders and highway slabs, where localized plasticity can enhance structural resilience (Hoyt 1961).

A comparison with a stone aggregate concrete beam tested at the University of Illinois revealed that while LWAC beams had higher initial deflections due to lower modulus of elasticity, stone concrete beams exhibited greater ultimate deflections (Figure 6). This difference was attributed to the abrupt failure of LWAC and the more gradual post-peak behavior of stone concrete, emphasizing the need for complete stress-strain curves that include descending branches (Hoyt 1961).

Figure 6. Load-Deflection Comparison – Stone and Lightweight Concrete, Adapted from Hoyt (1961)

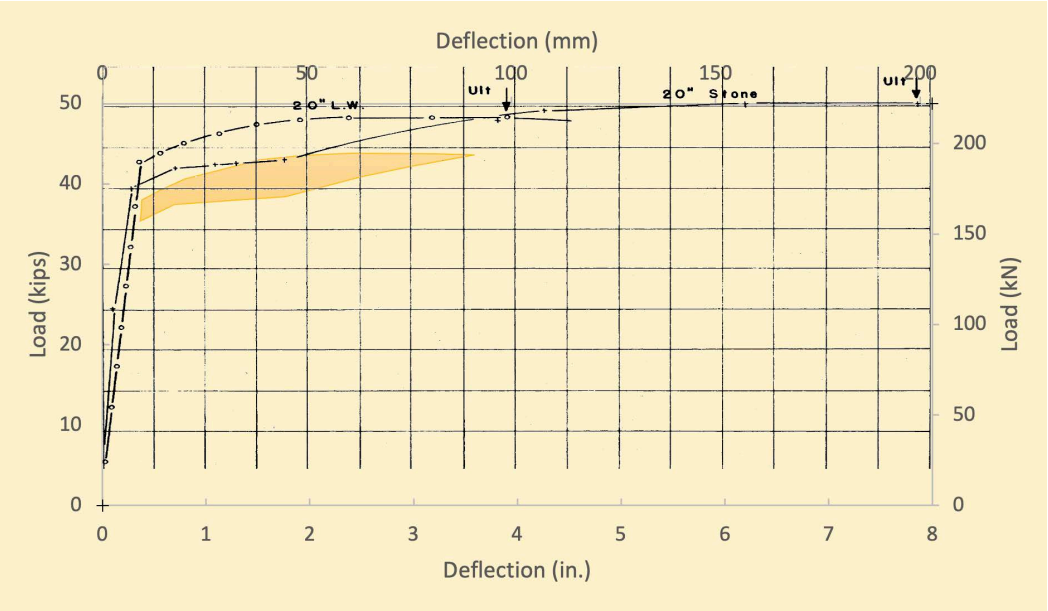

Kaar, Hanson, and Capell (1977) provided a foundational understanding of the stress-strain characteristics of high-strength concrete, including both normal-weight and lightweight aggregate concretes. The research was motivated by the increasing use of high-strength concrete in tall buildings and infrastructure, necessitating accurate flexural design constants for materials with compressive strengths exceeding 7,500 psi (51.7 MPa). The experimental program involved testing C-shaped specimens fabricated with concrete strengths ranging from 6,500 to 14,850 psi (44.8 to 102.4 MPa) for normal-weight concrete and from 3,560 to 12,490 psi (24.5 to 86.1 MPa) for lightweight concrete. The specimens incorporated three types of normal-weight aggregates and two types of lightweight aggregates, with Elgin sand used as the fine aggregate in all mixes. The water-cement ratios varied from 0.40 to 0.97 to achieve the desired strength levels (Kaar, Hanson, and Capell 1977).

Stress-strain curves were developed for each specimen, indicating that the commonly accepted ultimate strain of 0.003 remains suitable for design purposes despite observed data scatter. This is particularly relevant for confined concrete, where even minimal transverse reinforcement can extend the ultimate strain beyond 0.003 (Kaar, Hanson, and Capell 1977).

Moduli of elasticity were determined using both compressive cylinder tests and flexural stress-strain curves. The results indicated that values obtained from compression tests were approximately 10% higher than those from flexural tests, a trend consistent with earlier findings by Hognestad, Hanson, and McHenry (1955), as shown in Figure 7 (Kaar, Hanson, and Capell 1977).

Figure 7. Flexural Versus Compressive Moduli of Elasticity, Adapted from Kaar, Hanson, and Capell (1977)

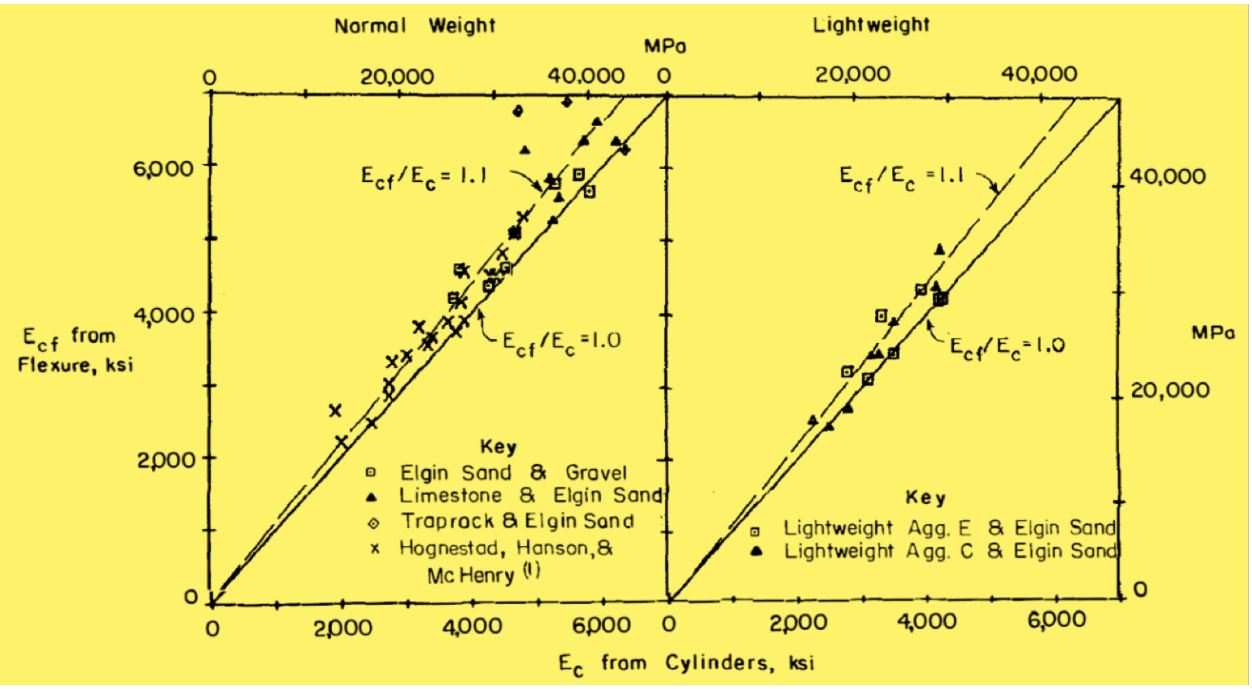

Ductility of Concrete

Early foundational work by Richart, Brandtzaeg, and Brown (1928) established that the compressive strength of concrete increases linearly with lateral confining pressure. Subsequent studies by Sheikh and Toklucu (1993) and Sheikh and Uzumeri (1980) expanded on this by examining the effects of spiral and hoop confinement, tie spacing, and reinforcement distribution. These studies consistently demonstrated that increased confinement enhances both strength and ductility, with circular hoops proving as effective as spirals in many cases (El-Dash, 1995).

Further investigations into high-strength concrete (HSC) and lightweight aggregate concrete (LWAC) revealed nuanced behaviors. For instance, Martinez, Nilson, and Slate (1984) found that LWAC could exhibit higher ductility than normal-weight concrete (NWC), while Bjerkeli, Tomaszewicz, and Jensen (1990) observed that LWAC had a steeper post-peak stress-strain curve, indicating more brittle failure. Ahmad and Shah (1982) and Wang, Shah, and Naaman (1978) also noted that confinement is generally less effective in LWAC and HSC due to their higher stiffness and lower tensile capacity (El-Dash, 1995).

El-Dash (1995) presented a detailed experimental and analytical investigation into the behavior of high-strength lightweight aggregate concrete (HS-LWAC) columns subjected to uniaxial compression. The study addressed a significant gap in the literature regarding the performance of lightweight concrete with compressive strengths exceeding 12,000 psi (83 MPa), particularly in structural applications such as transportation infrastructure (El-Dash, 1995).

The experimental program involved sixteen HS-LWAC columns with compressive strengths up to 14,640 psi (101 MPa) and unit weights below 120 pcf (1920 kg/m^3). The columns, with elliptical cross-sections, were confined using either single welded hoops or interlocking double spirals. The results demonstrated that interlocking spirals significantly improved both strength and ductility compared to single hoops. For example, columns with interlocking spirals and 1.5-inch pitch exhibited a 55% strength enhancement, while those with single hoops showed only 30% under similar conditions, as shown in Figure 8 (El-Dash, 1995).

Figure 8. Comparison Between the Observed and Predicted Modulus of Elasticity of High-Strength Lightweight Concrete, Adapted from El-Dash (1995)

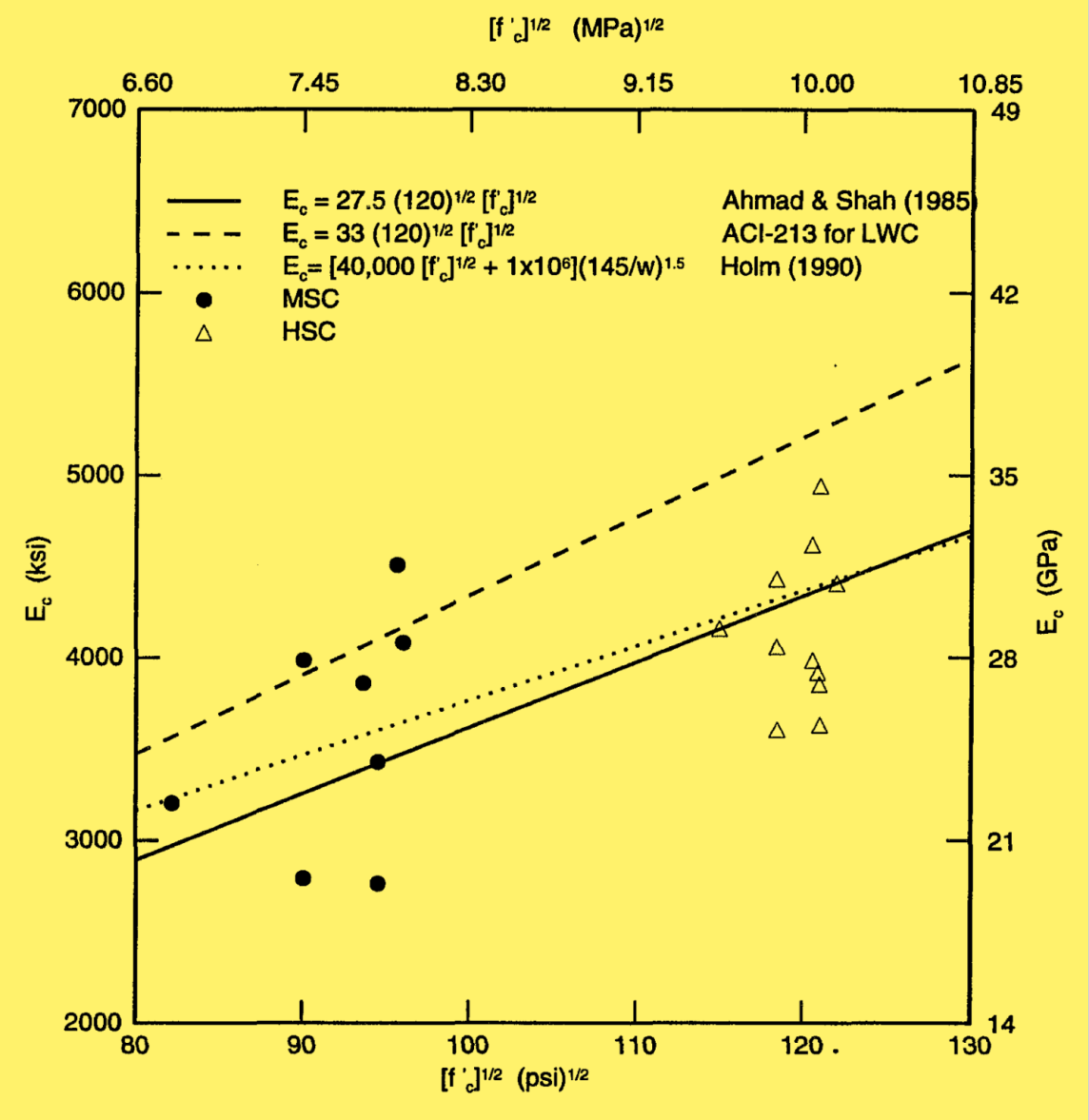

Results demonstrated that while LWAC exhibits lower strength and strain enhancements than NWC under similar confinement, effective confinement—particularly using interlocking spirals—can significantly improve performance. The findings have direct implications for the design of lightweight concrete elements in transportation infrastructure, where reduced self-weight and enhanced ductility are critical for seismic resilience and long-term durability (El-Dash 1995).

2.3 Mechanical Properties of Lightweight Concrete

The stress-strain relationship of LWC has been extensively studied to understand its deformation characteristics under axial and triaxial compression. Lim and Ozbakkaloglu (2014) developed a unified model for normal and lightweight concretes that incorporates confinement effects and specimen geometry. Cui et al. (2012b, 2012c) proposed analytical models for pre-peak stress-strain curves, emphasizing the influence of lightweight aggregate properties. Wang, Shah, and Naaman (1978) provided foundational experimental data on stress-strain curves for both normal and lightweight concretes, highlighting the importance of capturing the descending branch for lifecycle predictions. Further studies by Wei et al. (2020), Han and Xiang (2017), and Ashrafi and Farzam (2021) explored confined and unconfined LWC behavior, confirming its ductility and strain capacity. Wu et al. (2018) and El-Dash (1995) investigated the role of transverse reinforcement in enhancing compressive behavior, while Hoyt (1961) and Du et al. (2022) examined load-deflection and dynamic strain responses.

The elastic modulus of LWC is influenced by aggregate type, density, and curing conditions. Diogenes et al. (2011) and Popovics, Zemajtis, and Shkolnik (2008) compared static and dynamic modulus values, revealing discrepancies due to testing methods. Wall et al. (2002) and Wall and Maloof (2003) documented early strength development in LWC, while Myers and Morales (2000) provided kiln production data correlating with modulus trends. Mesbah, Lachemi, and Aïtcin (2002) and ASTM C469 offered standardized approaches for modulus determination, supported by Brazilian standards (ABNT NBR 8522).

LWC's tensile and shear capacities are essential for structural design. Ghavami (2022) assessed design strength modification factors for rotary-kiln aggregates. Historical studies by Ivey and Buth (1967) and Klein and Kluge (1961) evaluated shear and tensile behavior in beams. Li and Song (2019) analyzed prestressed hollow slabs, while Bogas, Gomes, and Real (2014) and Costa, Carmo, and Júlio (2018) focused on bond strength in LWC interfaces. Graybeal and Greene (2015) examined shear performance in prestressed girders.

Du et al. (2022) investigated LWC under high strain rates, revealing its resilience in dynamic applications. Shkolnik (1996, 2005) explored nonlinear responses affecting modulus and strength, and Subramaniam et al. (2000) used vibrational resonance to determine elastic properties.

Chord Modulus of Elasticity

Wall, Freeman, and Robinson (2002) presented a detailed experimental investigation of the modulus of elasticity (MOE) and compressive strength of LWC made with Stalite rotary kiln-expanded lightweight aggregate. The study evaluates nine concrete mixes with varying aggregate sizes (¾ inch, ½ inch, and ⅜ inch) and water-cementitious materials (w/cm) ratios ranging from 0.25 to 0.45, aiming to understand how these parameters influence the chord modulus of elasticity and overall structural performance (Wall, Freeman, and Robinson 2002).

The experimental program involved casting 15 4x8-inch cylinders per mix, curing them according to ASTM standards and testing for compressive strength at 7, 28, and 90 days. The results showed that compressive strength increased with lower w/c ratios and higher cement content. For example, Mix 7 (¾ inch aggregate, w/c = 0.25) achieved a 28-day strength of 14,469 psi, while Mix 9 (⅜ inch aggregate, w/c = 0.45) reached only 9,050 psi (Wall, Freeman, and Robinson 2002).

The modulus of elasticity was determined in accordance with ASTM C469, with samples tested to 40% of their ultimate compressive strength. The chord modulus values ranged from 3.40 x 10^6 psi to 4.72 x 10^6 psi, with higher values generally associated with mixes containing ¾ inch aggregate. Interestingly, despite lower compressive strengths, these mixes exhibited higher modulus values, suggesting that aggregate size and mortar content significantly influence stiffness. Predicted modulus values using ACI 318 (Eq. 5) and Morales (Eq. 6) equations showed varying degrees of accuracy:

$$E = W_c^{1.5}\sqrt{f_c'} \qquad (5)$$

$$E = \left(\frac{W_c}{145}\right)^{1.5}\left(40{,}000\sqrt{f_c'} + 1{,}000{,}000\right) \qquad (6)$$

In these equations, W_c is the density of concrete (pcf). ACI 318 tended to overestimate the modulus, especially for mixes with higher mortar content, with variances up to 29.6% (Mix 7 at 90 days). In contrast, the Morales equation provided closer estimates, particularly for mixes with mortar content around 17 ft^3/yd^3 (Figure 9) (Wall, Freeman, and Robinson 2002).

Figure 9. Chord Modulus, Adapted from Wall, Freeman, and Robinson (2002)

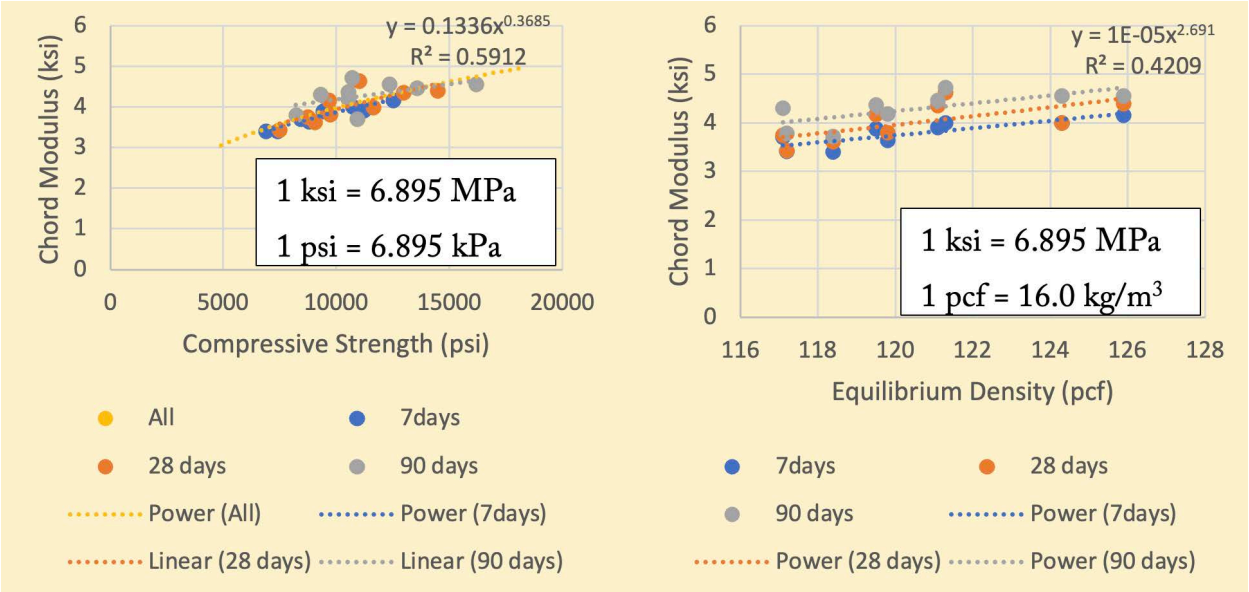

Long-term testing revealed continued gains in strength and modulus. For instance, LW3 achieved a compressive strength of 10,160 psi and a modulus of 3.98 x 10^6 psi at one year. Predictive models were evaluated, with the ACI 363 modified model and the Georgia Institute of Technology (GA Tech) model providing more accurate estimates than ACI 318. The GA Tech model was exact for strengths above 8,000 psi, with average variance around 6%. The stress-strain curves derived from axial load tests confirmed that LWC exhibits a nonlinear response at early ages, transitioning to a more linear elastic behavior as curing progresses. For example, LW2 at 365 days reached a stress level of 95,350 psi with a corresponding strain of 7.50E-03, indicating ductile behavior and energy absorption capacity (Wall, Freeman, and Robinson 2002).

Density measurements showed that LWC maintains a relatively stable unit weight of 121.10–124.00 PCF, which is significantly lower than NWC's unit weight. This reduction in density contributes to decreased dead load in bridge and highway structures, enhancing lifecycle performance through reduced structural demands and improved seismic resilience (Wall, Freeman, and Robinson 2002).

Stress-Strain Relations

Cui et al. (2012a) conducted a detailed experimental and analytical investigation of the pre-peak stress–strain behavior of structural lightweight aggregate concrete (LWAC), focusing on the influence of lightweight aggregate (LWA) properties. This research is particularly pertinent to the design and lifecycle performance of transportation infrastructure such as highways and bridges, where material efficiency and durability are critical. The authors emphasize that, unlike normal-weight concrete (NWC), the mechanical performance of LWAC is significantly influenced by the

properties of the LWA, which is often the composite system's weakest component. Specifically, the volume content, particle density, crushing strength, and shape index of the LWA are identified as key parameters affecting the compressive strength, modulus of elasticity, and strain characteristics of LWAC (Cui et al. 2012a).

Five types of LWA—expanded shale (LT, LS, YC), expanded clay (DG), and a mixture of shale and sintered pulverized fuel ash (SH)—were used in varying volume fractions (30%, 40%, and 50%) to produce LWAC specimens. The experimental results revealed that increasing the LWA volume content generally decreased both the peak compressive stress and the elastic modulus, confirming LWA's lower mechanical performance compared to the cement matrix (Cui et al. 2012a).

Interestingly, the study found that higher LWA particle density typically resulted in improved compressive strength and modulus of elasticity in LWAC. However, exceptions were noted, such as the YC aggregate, which, despite having lower crushing strength than LS and SH, produced LWAC with superior mechanical properties. This anomaly was attributed to the angular shape of the YC aggregate, highlighting the importance of the shape index as a determinant of concrete behavior. The shape index, defined as the ratio of sphericity to shape factor, was introduced as a novel parameter to quantify the influence of aggregate geometry. The study demonstrated that higher shape index values correlated with increased brittleness in LWAC, as evidenced by sharper post-peak strength declines and reduced ductility (Cui et al. 2012a; see Figure 10).

Figure 10. Effect of LWA Particle Density on Elastic Modulus of IAVAC, Adapted from Cui et al. (2012a)

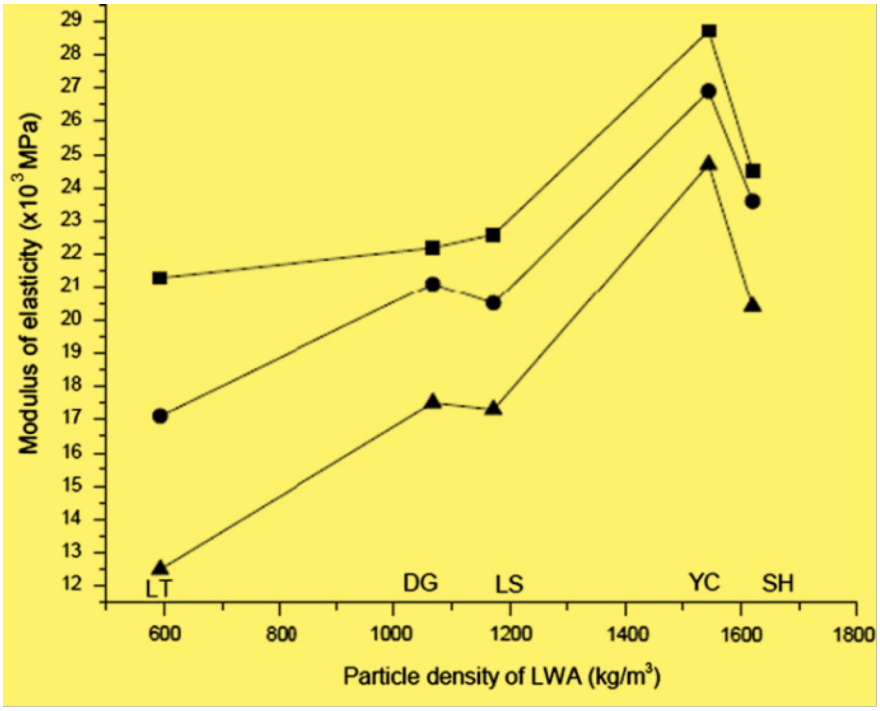

To model the pre-peak stress–strain behavior, the authors proposed a generalized quadratic equation of the form:

$$\sigma = \sigma_c[a(\varepsilon/\varepsilon_c)^2 + b(\varepsilon/\varepsilon_c)] \qquad (7)$$

In this equation, σ and ε represent stress and strain, σ_c and ε_c are their respective peak values, and the coefficients a and b were derived using curve-fitting techniques and regression analysis. The model was further refined to incorporate modification factors accounting for LWA volume content, crushing strength, and shape index. This formulation allows for the prediction of LWAC behavior across a range of aggregate types and mix designs. The model was validated using a new LWA (MOD) with distinct physical properties, and the predicted stress–strain curves closely matched experimental results, with a maximum error of less than 1.5% (Cui et al. 2012a).

Han and Xiang (2017) explored the mechanical behavior of LWAC produced using expanded shale as lightweight aggregate (LWA), focusing on its axial compressive stress-strain relationship and lateral expansion characteristics. Recognizing that replacing natural aggregates entirely with LWA significantly reduces concrete strength, the authors adopt a hybrid aggregate system that partially substitutes natural crushed stone with LWA. This approach aims to balance mechanical performance with sustainability goals in transportation infrastructure. Four concrete mixes were prepared with LWA volume fractions of 0%, 20%, 40%, and 60%. Compressive tests were conducted on cube and prism specimens at 28 days, with axial and lateral strains measured using strain gauges (Han and Xiang 2017).

Results showed that increasing the LWA volume fraction decreased the modulus of elasticity and increased the axial and lateral peak strains. The compressive strength of prism specimens varied more significantly than that of cube specimens, indicating that lateral expansion plays a critical role in LWAC failure. Notably, the compressive strength initially decreased at 20% LWA but increased at higher LWA fractions, suggesting an optimal LWA content range that enhances deformation compatibility between aggregates and the matrix (Han and Xiang 2017).

The Poisson effect was analyzed by computing the ratio of lateral to axial strain. LWAC exhibited a more pronounced lateral expansion than standard concrete, especially at higher stress levels. For example, at 60% LWA content, lateral peak strain increased by approximately 75%, while axial peak strain increased by only 8% (Figure 11). This enhanced lateral ductility is attributed to the deformability of LWA and to improved interfacial transition zones resulting from internal curing (Han and Xiang 2017).

Figure 11. Poisson Ratio, Adapted from Han and Xiang (2017)

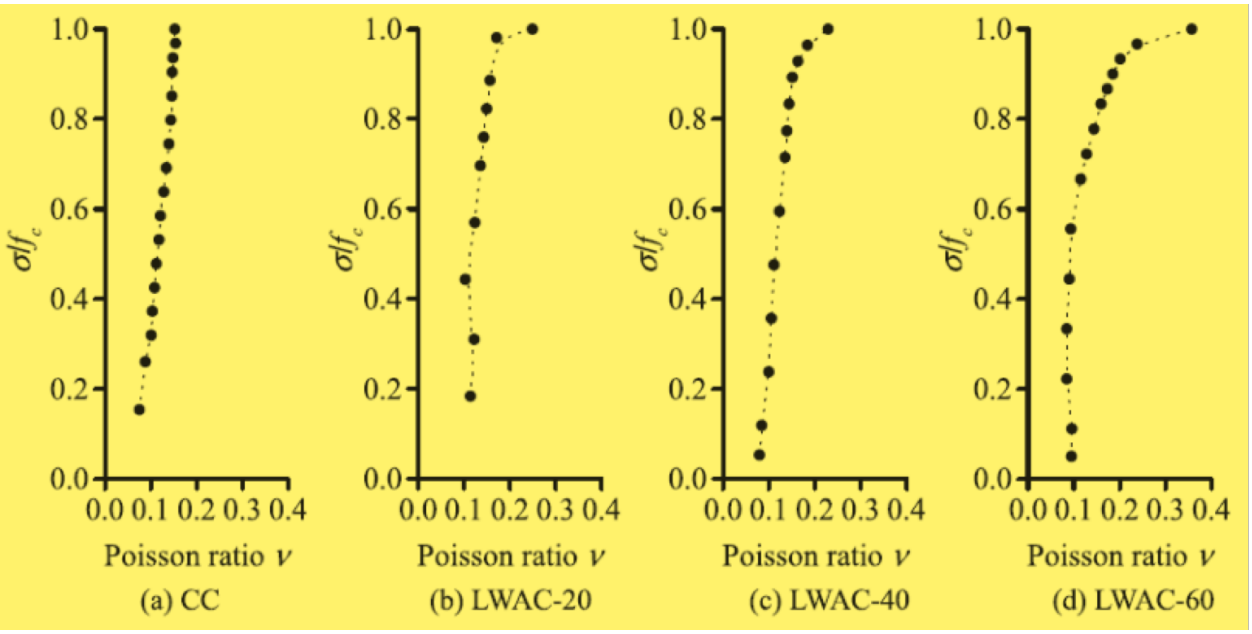

To model the stress-strain behavior, the authors adopted the Sazen model, which incorporates initial modulus of elasticity (E_0), peak secant modulus (E_s), and peak strain (ε_0):

$$\sigma = \frac{E_0 \varepsilon}{1+\left(\frac{E_0}{E_s}-2\right)\frac{\varepsilon}{\varepsilon_0}+\left(\frac{\varepsilon}{\varepsilon_0}\right)^2} \qquad (8)$$

These parameters were fitted as functions of LWA volume fraction. The model accurately simulated experimental stress-strain curves, making it suitable for nonlinear structural analysis and design of LWAC components (Han and Xiang 2017).

Dynamic Modulus of Elasticity and Poisson's Ratio

Popovics, Zemajtis, and Shkolnik (2008) conducted a detailed investigation of the relationship between concrete's static and dynamic moduli of elasticity. The research addresses two primary objectives: improving the accuracy of dynamic test methods for estimating the dynamic modulus and clarifying the relationship between dynamic and static moduli of elasticity. Dynamic testing methods, including vibrational resonance and ultrasonic pulse velocity (UPV), offer non-destructive alternatives for estimating dynamic modulus. However, discrepancies exist among methods and specimen geometries. For instance, dynamic modulus values from UPV are generally higher than those from resonance methods, and beam specimens yield higher dynamic modulus than cylinders of the same mix (Popovics, Zemajtis, and Shkolnik 2008).

Researchers used standard methods, including ASTM C469 for static modulus, ASTM C215 for vibrational resonance, and ASTM C597 for UPV. Modified methods such as Love's correction and the two-frequency method were also employed. The two-frequency method allows

simultaneous estimation of the dynamic Poisson's ratio and dynamic modulus from longitudinal resonance frequencies. Findings revealed that ASTM C215 longitudinal resonance underestimated the dynamic modulus, while transverse resonance overestimated it. Love's correction and the two-frequency method provided more accurate estimates, especially when Poisson's ratio was correctly assumed. The influence of Poisson's ratio was significant, particularly in UPV-based estimates, where incorrect assumptions led to substantial errors. Interestingly, assuming a higher Poisson's ratio (e.g., 0.28) improved agreement between UPV and resonance-based dynamic modulus values, though this contradicts the conventional theory (Popovics, Zemajtis, and Shkolnik 2008).

The composite nature of concrete was identified as a key factor in the discrepancy between static and dynamic moduli. Tests on two-phase specimens (cement paste and aggregate) showed that the dynamic modulus followed the Voigt upper-bound mixture rule, while the static modulus lay between the Voigt and Reuss bounds. This suggests that the dynamic modulus's elevation over the static one may stem from composite behavior rather than strain-level nonlinearity. Several empirical relationships were evaluated, including those by Lydon and Balendran (1986), BS8110 in Swamy and Bandyopadhyay (1982), Shkolnik's (1996, 2005) thermofluctuation theory, and Popovics's (1982) density-based model. Statistical analysis showed that the best-fit linear models provided the most accurate predictions, with mean absolute errors below 1.3 GPa. The BS8110 equation performed best for longitudinal resonance, while Popovics' model excelled for transverse resonance and Love's (1944) correction, as shown in Figure 12 (Popovics, Zemajtis, and Shkolnik 2008).

Figure 12. Comparison of Static (ASTM C469) Versus Dynamic Elasticity Moduli (ASTM C215) Data (Points) Using Longitudinal Resonance for Concrete Cylinders, Adapted from Popovics, Zemajtis, and Shkolnik (2008)

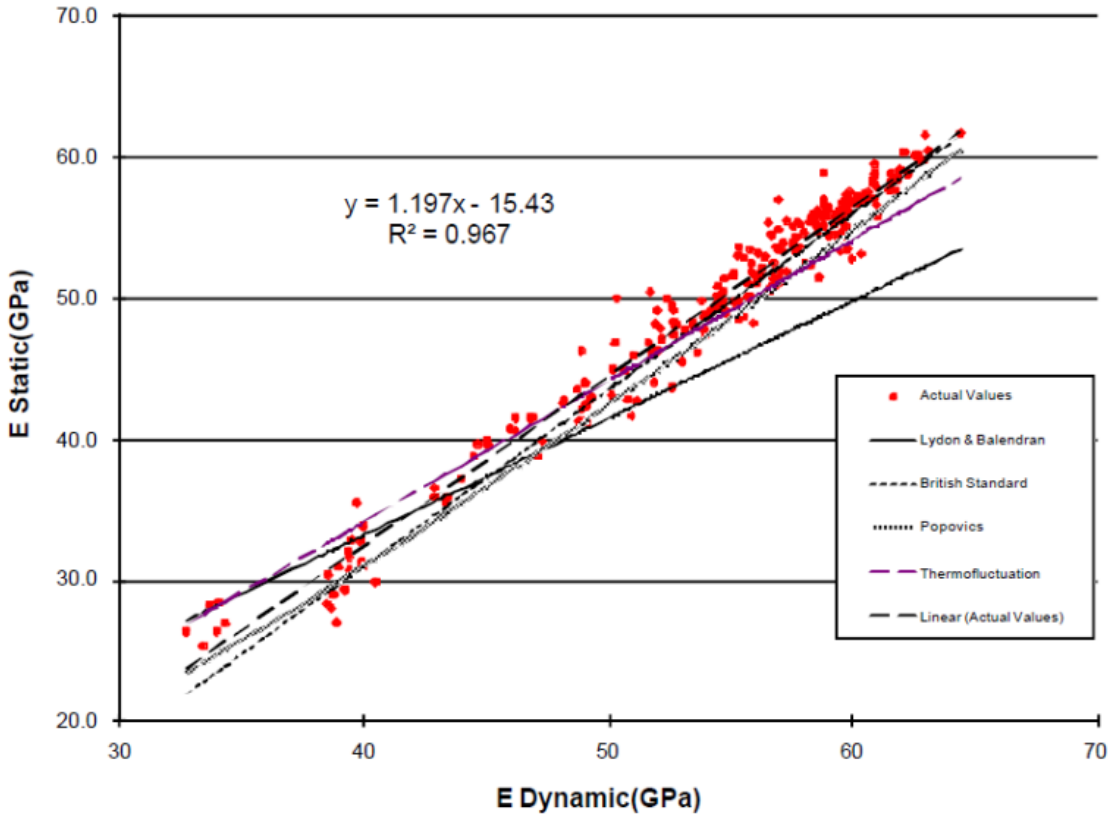

In this context, Diogenes et al. (2011) present an innovative methodology for determining the dynamic modulus of elasticity of concrete using acoustic response techniques. This approach provides integrated, repeatable insights into material stiffness and damping, with potential applications in structural health monitoring and design optimization. The study compares traditional static testing methods with dynamic techniques, including impulse excitation, sonic velocity, and resonance frequency. Among these, the resonance frequency method—based on longitudinal, transverse, and torsional vibrations—is highlighted for its reliability and widespread use in engineering applications. The impulse excitation technique, implemented using the Sonelastic® system, involves striking the specimen and analyzing the resulting acoustic response to determine its natural frequencies and associated elastic properties (Diogenes et al. 2011).

Static modulus determination, typically derived from stress-strain curves under compression, is complicated by concrete's nonlinear behavior. Dynamic testing, by contrast, applies low-level vibrations that avoid creep effects and yield values closer to the initial tangent modulus. The dynamic modulus is generally 20–40% higher than the static modulus, depending on concrete strength (Diogenes et al., 2011). Empirical relationships between static and dynamic moduli are

also provided by BS 8110-2 (BSI, 1985), Lyndon and Baladran (1986), and Popovics (1982), though these vary based on concrete type and testing conditions.

The experimental program involved testing cylindrical and prismatic specimens using both Sonelastic® and ACE® Data Physics systems. Static tests included axial compression and four-point flexural loading, while dynamic tests followed ASTM C215 protocols. Results showed that dynamic modulus values from prismatic specimens were approximately 26% higher than static values, while cylindrical specimens showed a 20% increase in dynamic modulus of elasticity. Flexural modulus values were significantly lower than those from compression tests, which can be attributed to concrete's cracking behavior and the limitations of linear elastic assumptions in flexural analysis. The modulus of rupture, expressed as the ratio of flexural tensile strength to compressive strength, averaged 9.52%, aligning with literature values of 10–12% (Diogenes et al. 2011).

The study also explored dynamic Poisson's ratio and torsional modulus, finding values consistent with theoretical expectations. The dynamic Poisson's ratio averaged 0.206, slightly above the standard design value of 0.2 but below the 0.24 suggested by Neville (1997). The torsional modulus was approximately 40% of the dynamic modulus, supporting the assumptions in Brazilian design standards (Diogenes et al. 2011).

The dynamic behavior of lightweight concrete (LWC), particularly under high strain rates, is a critical factor in assessing its suitability for transportation infrastructure subjected to impact loads, such as bridges and highway structures. In this context, Du et al. (2022) conducted a detailed experimental investigation of the dynamic response of expanded shale lightweight concrete (ESLWC) using a large-diameter Split Hopkinson Pressure Bar (SHPB) apparatus. The research focused on ESLWC specimens with static compressive strengths of 50 MPa and 60 MPa, designated as LWC50 and LWC60, respectively. These specimens were subjected to strain rates ranging from 30 to 100 s^{-1} to simulate high-impact conditions. The SHPB tests revealed that ESLWC exhibits a characteristic failure mode of fragmentation into small particles, with fragment size decreasing as strain rate increases. This behavior is attributed to the progressive development and coalescence of microcracks under increasing impact energy (Du et al. 2022).

A key finding of the study is the dynamic increase factor (DIF), defined as the ratio of dynamic to static compressive strength. While the dynamic compressive strength of ESLWC increased with strain rate, the DIF decreased with increasing static compressive strength. For instance, LWC50 showed a higher DIF than LWC60 at strain rates above 60 s^{-1}, indicating that lower-strength ESLWC may exhibit more pronounced dynamic enhancement. This trend is illustrated in Figure 7, which compares measured DIFs with predictions from existing models, including the CEB-FIP code and Hao and Hao's aggregate-based model. The study found that these models overestimated the DIF for ESLWC, prompting the authors to propose a new empirical formula tailored to ESLWC, which demonstrated a mean relative error of only 3.1% compared to test results (Du et al. 2022).

The stress–strain behavior of ESLWC under dynamic loading was also characterized. At lower strain rates (e.g., 40 s^{-1}), the stress–strain curve exhibited three distinct stages: linear elastic, yield platform, and brittle failure. However, at higher strain rates (≥ 60 s^{-1}), the yield platform disappeared, and the material transitioned directly from elastic behavior to brittle failure. This shift is attributed to rapid deformation, which prevents the material from undergoing gradual yielding. Figure 9 presents these stress–strain curves for both LWC50 and LWC60 under varying impact pressures, clearly illustrating the evolution of mechanical response with increasing strain rate (Du et al. 2022).

Energy absorption capacity, a critical parameter for impact-resistant materials, was evaluated by calculating the area under the stress–strain curve. ESLWC demonstrated superior energy absorption compared to normal weight concrete (NWC), ceramics–cement porous materials (CCPM), rubberized concrete (RuC), and even fiber-reinforced concretes such as basalt fiber-reinforced geopolymeric concrete (BFRGC) and steel fiber-reinforced concrete (SFRC). Results showed that ESLWC achieved higher total energy absorption densities across the tested strain rate range, confirming its potential for high-impact applications (Du et al. 2022).

To understand the microstructural mechanisms underlying these behaviors, scanning electron microscopy (SEM) was used to examine the interfacial transition zone (ITZ) and crack development. The ITZ in ESLWC was found to be more porous and microcracked than the surrounding cement paste, with a thickness of approximately 40 μm—thinner than that typically observed in normal-weight concrete. At lower strain rates (e.g., 40 s^{-1}), cracks propagated along the ITZ, while at higher strain rates (e.g., 100 s^{-1}), cracks penetrated directly through the lightweight aggregates. This shift indicates that the ITZ governs dynamic behavior at moderate strain rates, whereas the aggregates dominate at higher strain rates (Du et al. 2022).

Triaxial State of Stress-Strain Relationships and Confinement

The study by Lim and Ozbakkaloglu (2014) presents a unified stress–strain model for both normal-weight concrete (NWC) and lightweight concrete (LWC) under uniaxial and triaxial compression, addressing a critical gap in modeling concrete behavior across a wide range of densities and strengths. The authors begin by assembling two extensive experimental databases: one for unconfined concrete and another for actively confined concrete. The unconfined database comprises 4,353 datasets from 209 studies, including both NWC and LWC specimens with varied geometries and material compositions. The confined concrete database includes 377 datasets, with specimens subjected to triaxial compression to simulate active confinement conditions (Lim and Ozbakkaloglu 2014).

A key contribution of the study is the development of predictive expressions for the elastic modulus, compressive strength, and axial strain at peak stress for both NWC and LWC. The compressive strength model incorporates water-to-cementitious binder ratio (w/c), silica fume

ratio (sf/c), and concrete density (ρc,f), demonstrating that strength increases with lower w/c ratios and higher densities and silica fume content (Figure 13):

$$f'_{c0} = \left(\frac{21}{w/c} + 32\sqrt{sf/c}\right)\left(\frac{\rho_{cf}}{2400}\right)^{1.6} \quad (9)$$

$$E_c = 4400\sqrt{f'_{c0}}\left(\frac{\rho_{cf}}{2400}\right)^{1.4} \quad (10)$$

In these equations, f'_{c0} is the compressive strength (MPa), w/c is the water-to-cement ratio, sf/c is the silica fume to cement ratio, ρ_{cf} is the concrete density (kg/m^3), and E_c is the modulus of elasticity (MPa). For elastic modulus prediction, the authors compare existing models and propose a new expression that accounts for both compressive strength and density. The proposed model shows improved accuracy over previous models, particularly for LWC, which is often underrepresented in traditional formulations (Lim and Ozbakkaloglu 2014).

Figure 13. Comparison of Concrete Elastic Moduli with Model Predictions, Adapted from Lim and Ozbakkaloglu (2014)

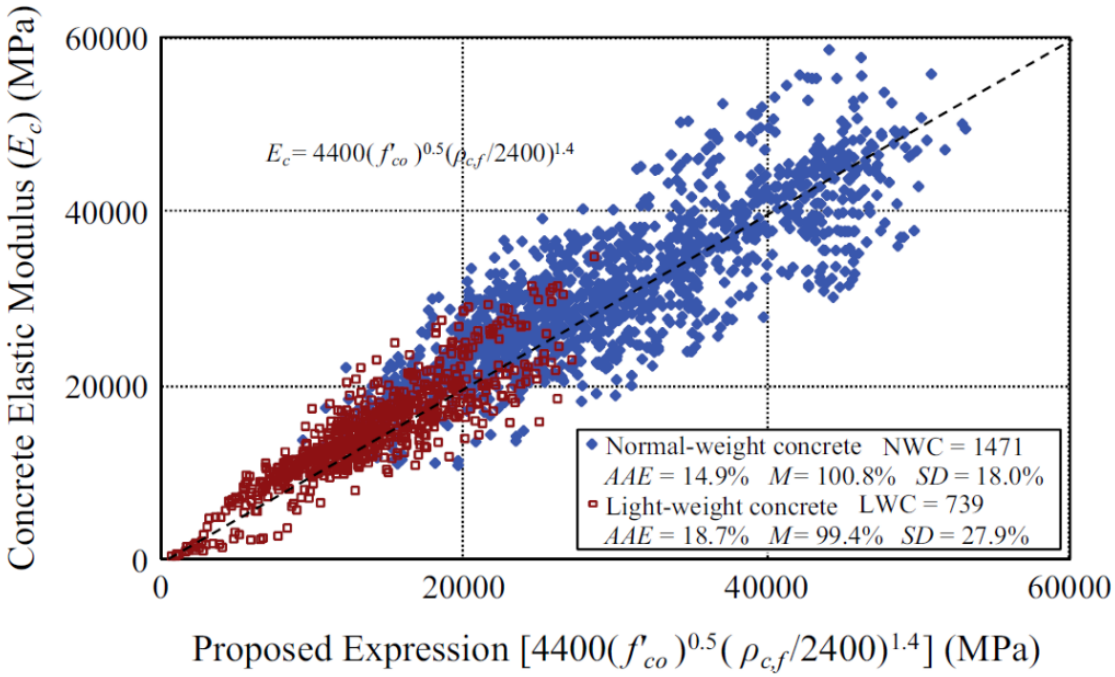

The axial strain at peak compressive stress is another critical parameter for lifecycle performance. Lim and Ozbakkaloglu (2014) identify that axial strain decreases with increasing concrete density and specimen size, and they incorporate these effects into a multivariable regression model.

Numerical Simulation of Elasticity Modulus Prediction

The study by Bonifácio et al. (2020) addresses a critical gap in the design and analysis of lightweight aggregate concrete (LWAC), particularly in the context of transportation infrastructure. Despite LWAC's increasing use in structural applications due to its reduced density and improved thermal and acoustic properties, its mechanical behavior is still largely predicted using empirical charts and formulae, which are often inadequate for capturing the complexity of its stress-strain response. To overcome these limitations, the authors propose a numerical simulation approach using the Finite Element Method (FEM), modeling LWAC as a biphasic material composed of lightweight aggregates (LWA) and surrounding mortar. Each phase is assigned distinct mechanical properties, including compressive strength, tensile strength, and Young's modulus. The simulation is validated against experimental data from 48 concrete formulations, incorporating combinations of three mortar types and four aggregate types at four volume fractions (Bonifácio et al. 2020).

The LWAs used include expanded clay and expanded shale, with physical characteristics including bulk density, shape index, and the proportion of broken grains. Expanded shale aggregates generally exhibited higher bulk densities and shape indices, which influenced the mechanical performance of the resulting LWAC. The mortar types ranged from normal (40 MPa) to very high performance (86 MPa). The FEM simulations were conducted using the CAST3M software, employing a 2D model of a cylindrical specimen cross-section. Aggregates were modeled as perfect spheres randomly distributed within the mortar matrix, and elastoplastic behavior was assumed using the Drucker-Prager yield criterion. The simulation parameters included experimentally derived values for compressive and tensile strengths and elastic moduli of both phases (Bonifácio et al. 2020).

Results demonstrated strong agreement between numerical predictions and experimental measurements. The Mean Absolute Percentage Error (MAPE) for Young's modulus and compressive strength was lowest for expanded shale aggregates (1.75% and 4.19%, respectively) and highest for expanded clay aggregates (4.21% and 9.89%). Pearson correlation coefficients exceeded 0.96 for all aggregate types and mechanical properties, indicating robust predictive accuracy. Further analysis revealed no clear trend in error relative to aggregate volume or mortar type, suggesting that the model's generalization capacity is strong. The use of a 2D model, despite its geometric simplifications, proved effective and computationally efficient, with negligible distortion in the central region of the specimen (Bonifácio et al. 2020).

2.4 Modulus of Elasticity of Internally Cured Concrete

The study by Kim and Chun (2015) investigates the potential of internally cured concrete (ICC) for use in rigid pavements under Florida conditions. ICC is designed to mitigate early-age cracking in high-strength-high-performance concrete (HSHPC), which is prone to shrinkage and thermal cracking due to its high early chemical shrinkage and heat generation. ICC incorporates internal

reservoirs of water through lightweight aggregates (LWA), which release water during hydration, improving cement paste hydration and reducing self-desiccation. The authors constructed three full-scale instrumented concrete slabs with different mix designs: a standard mix with a 0.40 water-cement ratio; ICC-1 with a 0.32 water-cement ratio and increased cement content; and ICC-2 with the same water-cement ratio as the standard mix but with fine aggregates replaced by LWA. ICC-1 showed the highest compressive and flexural strength, while ICC-2 had slightly lower strength than the standard mix due to the inclusion of LWA as listed in Table 2 (Kim and Chun 2015).

Table 2. Compressive Strength, Elastic Modulus, Flexural Strength, and Drying Shrinkage Data, Adapted from Kim and Chun (2015)

Test	Mix Type		
	Standard Mix	ICC-1	ICC-2
Compressive Strength (MPa)	47.1	54.1	45.6
Modulus of Elasticity (MPa)	30,682	26,890	26,200
Modulus of Rupture (kPa)	4999	5640	4861
Drying Shrinkage at 28 days	3.7×10^{-4}	3.1×10^{-4}	3.8×10^{-4}
Drying Shrinkage at 91 days	5.3×10^{-4}	3.8×10^{-4}	5.0×10^{-4}

Environmental responses were measured using strain gauges, thermocouples, and linear variable differential transformers (LVDTs) embedded in the slabs. Temperature gradients were monitored across the slab thickness, revealing that ICC slabs exhibited higher temperature differentials than the standard mix slab, likely due to their lower thermal conductivity resulting from the denser microstructure formed by improved hydration. Curling measurements using LVDTs showed that ICC slabs experienced less vertical movement than the standard mix slab, suggesting reduced curling stress. This is attributed to the higher and more uniform relative humidity maintained by the internal curing effect of LWA. Environmental strain measurements also indicated that ICC slabs had lower strain changes, which correlates with their lower elastic modulus and reduced cracking potential (Kim and Chun 2015).

To further evaluate performance, a three-dimensional finite element (FE) model was developed using ADINA software. The model incorporated hexahedral and spring elements to simulate slab joints and subgrade interactions. Material properties were calibrated using laboratory and back-calculated data from falling weight deflectometer (FWD) tests. The model was validated by comparing computed strains with measured strains from full-scale tests (Kim and Chun 2015).

2.5 Design Approach to Mechanical Properties of Lightweight Aggregate Concrete

The mechanical behavior of lightweight concrete (LWC) has long been a subject of interest in structural engineering, particularly for its potential to enhance the lifecycle performance of transportation infrastructure such as highways and bridges. The Federal Highway Administration (FHWA) addressed a critical gap in the design specifications by investigating high-strength LWC with unit weights between traditional LWC and normal weight concrete (NWC), a range not currently covered by the AASHTO LRFD (2015) Bridge Design Specifications (Greene and Graybeal 2013).

The FHWA's research program included extensive mechanical testing of 27 precast/prestressed girders and 40 reinforced concrete beams fabricated with LWC. The study focused on compressive strength, elastic modulus, and splitting tensile strength, using mix designs that incorporated Haydite, Stalite, and Utelite lightweight aggregates, combined with natural sand and Type III Portland cement. The target equilibrium densities ranged from 0.125 to 0.135 kcf (2,000–2,160 kg/m^3), representing a transitional zone between traditional LWC and NWC (Greene and Graybeal 2013).

The mechanical properties of the tested mixes revealed compressive strengths ranging from 4.0 to 10.0 ksi at 28 days. Notably, the elastic modulus values were found to be overestimated by the AASHTO LRFD (2015) expression and underestimated by both the NCHRP 12-64 and ACI 363R-10 expressions (Figure 14). The proposed expression for modulus of elasticity in ksi ($_c$), based on unit weight in kcf (w_c) and compressive strength in ksi (f_c'), is given as follows:

$$E_c = 120{,}000 K_1 {w_c}^{2.0} {f_c'}^{0.33} \quad (11)$$

The correction factor K_1 relates to the source of aggregate. This equation demonstrated the lowest coefficient of variation among the evaluated models (Greene and Graybeal 2013).

Figure 14. Test-to-Prediction Ratio Compared to Compressive Strength for AASHTO LRFD (2015) Equation, Adapted from Greene and Graybeal (2013)

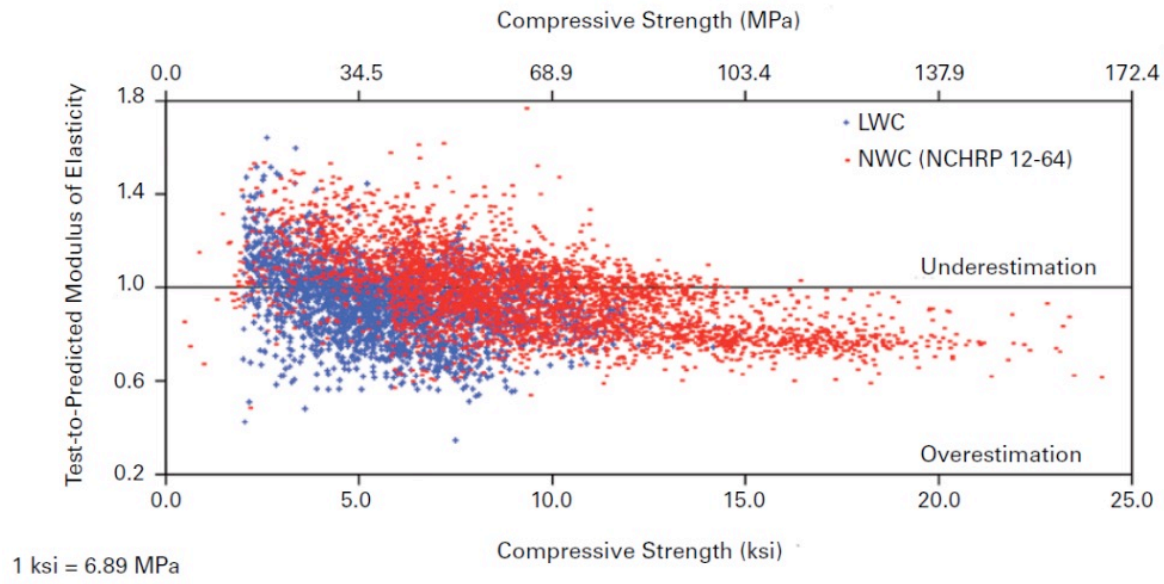

Splitting tensile strength tests showed that the splitting ratio often exceeded the threshold requiring modification factors in the AASHTO LRFD (2015) specifications. The study proposed a piecewise linear expression for splitting ratio based on unit weight, with a constant value of 0.159 for wc ≤ 0.100 kcf and a linear increase to 0.212 for wc ≥ 0.135 kcf (Figure 15).

To support these findings, the Turner-Fairbank Highway Research Center (TFHRC) compiled a comprehensive LWC database consisting of 3,835 data lines from 128 publications. This database included compressive strength, modulus of elasticity, splitting tensile strength, modulus of rupture, and Poisson's ratio, and was used to validate the proposed design expressions (Greene and Graybeal 2013).

Figure 15. Modulus of Elasticity for Proposed Expression, Adapted from Greene and Graybeal (2013)

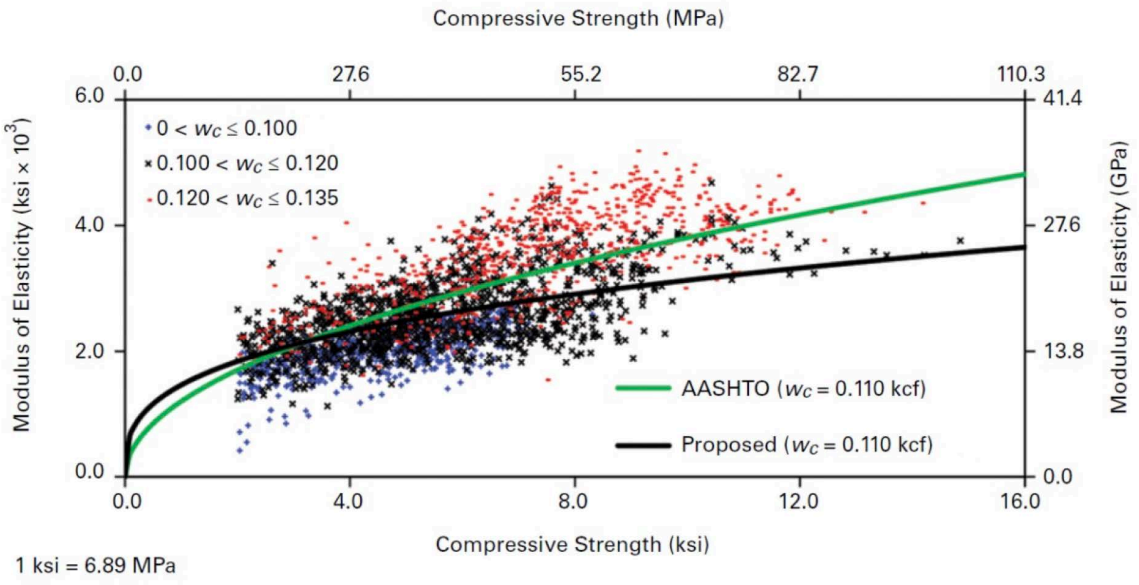

The study also introduced a unified LWC modification factor (λ-factor) to replace the current AASHTO LRFD (2015) factors based on constituent materials. Finally, the study recommends redefining LWC as concrete containing lightweight aggregate with an equilibrium density not exceeding 0.135 kcf, as determined by ASTM C567. This definition eliminates the need for terms such as "sand-lightweight" and "all-lightweight" concrete, aligning classification with measurable density rather than constituent ratios (Greene and Graybeal 2013).

Nava Ghavami (2022) investigates the design strength modification factors (λ) applied to SLWAC, particularly those produced using rotary-kiln expanded aggregates such as expanded shale, clay, and slate (ESCS). The study critically evaluates the current American Concrete Institute (ACI) code provisions, especially ACI 318, and proposes refinements based on statistical and experimental data, similar to those provided by Greene and Graybeal (2013). Despite recent findings by Greene and Graybeal (2013), the ACI 318 code applies a uniform modification factor (λ) to account for the reduced mechanical properties of SLWAC compared to NWC. However, this approach does not differentiate between aggregate types or design purposes. Ghavami (2022) argues that this generalization may lead to either conservative or non-conservative designs, depending on the specific aggregate used and the structural application (Ghavami 2022).

Ghavami (2022) also reviews the performance of different aggregate types, including rotary-kiln manufactured aggregates (e.g., expanded shale, clay, slate), industrial byproducts (e.g., blast furnace slag, fly ash), natural lightweight aggregates (e.g., pumice, expanded silicate), and recycled materials (e.g., oil palm shell, expanded polystyrene). These studies consistently show that aggregate source and composition significantly influence mechanical properties such as compressive strength, modulus of elasticity, and bond strength. To quantify these effects, Ghavami

(2022) conducted statistical analyses using data from over 200 peer-reviewed articles published between 2003 and 2020. One-way ANOVA tests revealed significant differences in λ values across aggregate types and design purposes. For instance, the λ value for blast furnace slag was significantly higher than that for pumice, while ESCS aggregates showed the highest λ values for flexural strength and modulus of rupture (Ghavami 2022).

Multiple regression analyses further identified key parameters influencing λ, including equilibrium density, volume fraction of fine lightweight aggregate, water-cementitious materials ratio, and compressive strength. For example, the regression model for ESCS aggregates showed a strong correlation (R^2 = 0.99998) between λ and these parameters, suggesting that a more nuanced approach to λ determination is warranted (Ghavami 2022).

Ghavami et al. (2024) attempt to revise the following design equations for the modulus of elasticity of lightweight concrete containing expanded shale, clay, and slate LWA:

$$E_c = \begin{cases} 0.043 {w_c}^{1.5} {f'_c}^{0.5}, ACI318 \\ 0.0017 {w_c}^{2} {f'_c}^{0.33}, AASHTO \end{cases} \quad (12)$$

In these equations, E_c is the modulus of elasticity (MPa) and f'_c and w_c are specified compressive strength (MPa) and equilibrium density (kg/m^3) of lightweight concrete, respectively. Revised equations reflect equivalent modification factors for modulus of elasticity using empirical results and the prescribed equation based on equilibrium density, indicating the scatterings of results concerning the solid unity line. The dependent two-tail t-test of difference between the equivalent modification factor based on the empirical modulus of elasticity (M = 0.740, SD = 0.136) and the prescribed equation using equilibrium density (M = 0.752, SD = 0.0849) is significantly different (t(832) = 3.09, p = 0.0020). Regression analyses of observed data result in alternative equations for the modulus of elasticity:

$$E_c = \begin{cases} 0.0418 {w_c}^{1.5} {f'_c}^{0.5}, ACI318 compatible fit (R^2 = 0.6016) \\ 0.00182 {w_c}^{2} {f'_c}^{0.33}, AASHTO compatible fit (R^2 = 0.5596) \\ 0.419 {w_c}^{1.23} {f'_c}^{0.43}, Best fit (R^2 = 0.6207) \end{cases} \quad (13)$$

Statistical ANOVA tests on the experimental to prescribed modification factor ratio reveal no significant difference (F(780) = 0.615, p = 0.433) between rotary-kiln manufactured expanded aggregates (M = 0.976, SD = 0.14) and industrial byproducts such as slag (M=0.957, SD = 0.084). But, there is a significant difference (F(2,785) = 5.267, p = 0.00534) between these aggregates and recycled natural aggregate sources (M=0.795, SD = 0.26) as illustrated in Figure 16.

Figure 16. Experimental Modulus of Elasticity Modification Factors for Various Aggregate Types, Adapted from Ghavami et al. (2024)

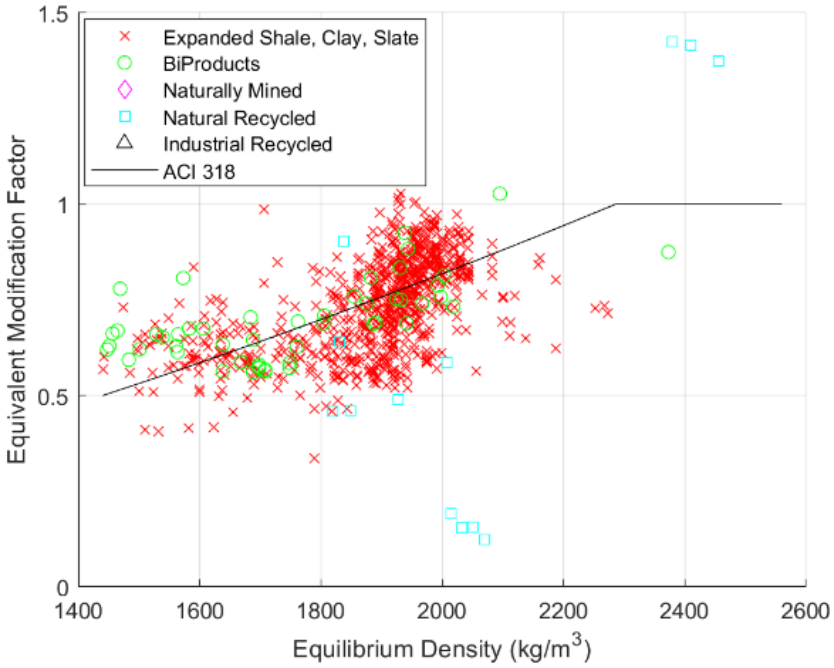

Kadkhodaie et al. (2024) presented the regression analysis of modulus of elasticity using 424 experimental data points. Results revealed 4% increase compared with the ACI 318 equations (Figure 17). Further, it was concluded that the ACI 318 equation underestimates the modulus of elasticity of lightweight concrete with an equilibrium density of less than 1700 kg/m^3. Regression analyses lead to the following equation:

$$E_c = 0.138 w_c^{1.37} {f'_c}^{0.438}, 1440\, kg/m^3 < w_c \leq 2160\, kg/m^3 \; (R^2{=}0.6209) \qquad (14)$$

Figure 17. Experimental and Prescribed Equivalent Modification Factors for the Modulus of Elasticity, Adapted from Kadkhodaie et al. (2024)

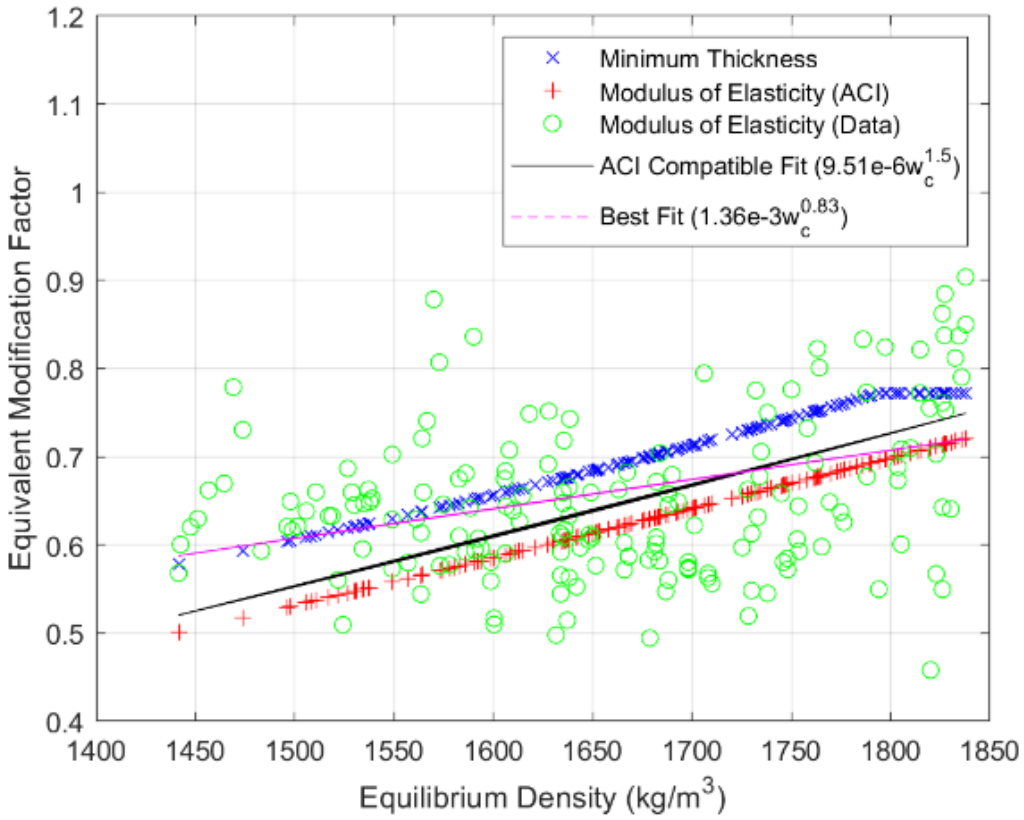

2.6 Selected Case Studies on Bridge Applications

The use of sand lightweight concrete (LWC) in prestressed bridge girders has gained traction in recent years due to its potential to reduce dead load and improve structural efficiency. Chapman and Castrodale (2016) document the successful implementation of high-strength sand LWC in three bridge projects in Washington State: the Airport Way South Viaduct Replacement, the Skagit River Bridge replacement on Interstate 5, and the SR162 Puyallup River Bridge. Each project utilized the same sand LWC mixture to achieve weight reduction without compromising structural performance (Chapman and Castrodale 2016).

The Airport Way South project was the first to specify sand LWC to match the dead load of the original 1928 structure and avoid retrofitting the substructure. The Skagit River Bridge replacement followed a similar strategy after a span collapse, using decked bulb tee girders to maintain dead load equivalence. The SR162 project served as a demonstration of sand LWC in WSDOT WF74G girders, with spans of 110 and 160 feet (Chapman and Castrodale 2016).

The sand LWC mixture was developed through lab trials and consultation with aggregate suppliers. It used lightweight coarse aggregate and natural sand, with Class F fly ash added to improve workability. The final mix achieved a 28-day compressive strength of 9,000 psi and a fresh unit weight below 128 pcf, as required by the Airport Way South project. Compared to a normal weight concrete (NWC) mix, the LWC had a lower water-cement ratio (0.283 vs. 0.300) and a calculated fresh density of 122.2 pcf versus 154.4 pcf for NWC (Chapman and Castrodale 2016).

Despite the higher cost of lightweight aggregate—five times more expensive than local coarse aggregate and with freight costs up to 25 times higher—the overall cost increase for LWC girders was modest. The cost of sand LWC was approximately double that of NWC per cubic yard, but the total girder cost increased by only 13–14% (Table 3). This cost premium does not account for potential savings in transportation, erection, and substructure design due to reduced weight (Chapman and Castrodale 2016).

Table 3. Relative Cost Comparison, Adapted from Chapman and Castrodale (2016)

Item	LWC to NWC Ratio
Aggregate	5
Aggregate Freight	25
Fresh Concrete	2.0
WF50G Girder Cost	1.14
WF83G Girder Cost	1.13

Performance data from all three projects confirmed the reliability of the sand LWC. Fresh unit weight measurements from over 500 batches at Airport Way South averaged 123.1 pcf, with a standard deviation of 1.5 pcf. Compressive strength data showed that LWC achieved similar strength and strength gain rates as NWC. The average 28-day compressive strengths for LWC ranged from 10,832 to 11,845 psi across the three projects (Chapman and Castrodale 2016).

Modulus of elasticity (MOE) measurements showed that LWC values were approximately 10% lower than predicted by ACI and AASHTO equations, while NWC values aligned closely with predictions. Using the AASHTO LRFD (2015) equation with a unit weight of 123 pcf and correction factor of one, the predicted MOE was 4,270 ksi, which matched measured values at later ages (Figures 18 and 19) (Chapman and Castrodale 2016).

Figure 18. Graphs of Compressive Strength, Modulus of Elasticity, Creep, Shrinkage, Splitting Tensile Strength, and Camber, Adapted from Chapman and Castrodale (2016)

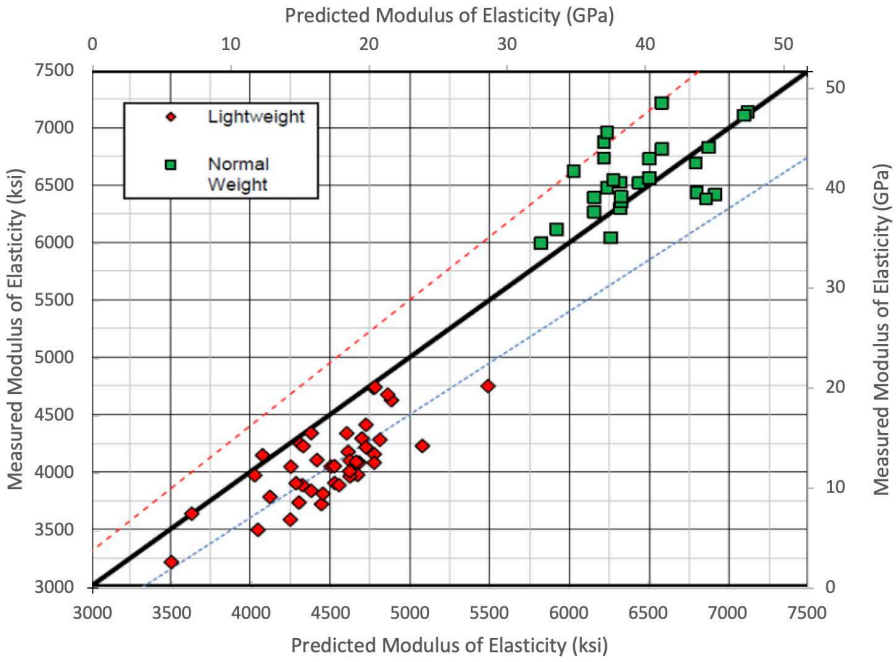

Figure 19. Measured Modulus of Elasticity for Sand Lightweight Concrete (All Three Projects), Adapted from Chapman and Castrodale (2016)

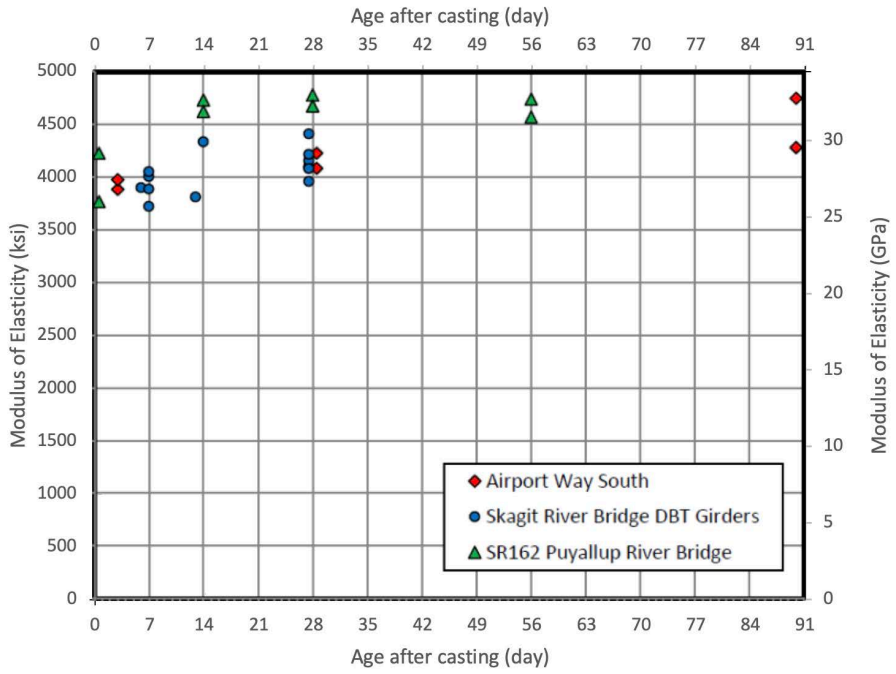

Creep and shrinkage behavior of LWC was also favorable. Measured creep coefficients and specific creep values were close to AASHTO predictions. Shrinkage data collected in 2012 and 2015 showed consistent performance, with the 2015 data being more uniform (Chapman and Castrodale 2016).

Splitting tensile strength tests revealed that LWC exceeded the expected values for NWC based on AASHTO LRFD (2015). Average 28-day splitting tensile strengths ranged from 663 to 700 psi, compared to a predicted value of 638 psi for NWC at 9,000 psi compressive strength. This suggests that LWC can be specified without applying the 0.85 shear reduction factor typically required when fct is not specified (Chapman and Castrodale 2016).

Camber behavior of LWC girders was also well-controlled. For the Airport Way South project, formwork was pre-deflected to counteract camber, resulting in acceptable field performance. For the Skagit River and SR162 projects, measured camber values generally fell within predicted bounds, with minor deviations attributed to temperature effects during measurement (Chapman and Castrodale 2016).

The authors recommend using 123 pcf for design calculations, 128 pcf for fresh concrete acceptance, and 138 pcf for reinforced concrete self-weight. They also suggest limiting release strength to 7,500 psi and 28-day strength to 10,000 psi. AASHTO LRFD (2015) equations for modulus of elasticity, creep, shrinkage, and splitting tensile strength can be used without modification, provided appropriate input values are used (Chapman and Castrodale 2016).

These case studies revealed that the use of sand LWC in these three Washington State bridge projects demonstrates that it can match or exceed the performance of NWC in terms of strength, durability, and predictability. While material costs are higher, the overall cost impact is modest, and potential savings in construction logistics and substructure design may offset the premium. These findings support broader adoption of sand LWC in bridge applications (Chapman and Castrodale 2016).

2.7 Significance of the Research

Lightweight concrete represents a strategic material choice for resilient, durable, and sustainable transportation systems. Its favorable stress-strain characteristics, combined with lifecycle and environmental advantages, position it as a key component in the future of infrastructure design and maintenance. Existing literature has examined the stress-strain relationship of lightweight concrete (LWC) and its implications for enhancing the lifecycle performance of transportation infrastructure, particularly highways and bridges. The mechanical properties of LWC—including its stress-strain behavior, modulus of elasticity, tensile and shear strength, and dynamic response—have been shown to meet or exceed those of normal-weight concrete (NWC) when properly designed and cured. These properties contribute to reduced dead loads, improved ductility, and enhanced seismic resilience, making LWC a suitable material for modern infrastructure systems.

Durability and transport properties such as chloride permeability (AASHTO T 277, ASTM C1202), electrical resistivity (AASHTO T 358, ASTM C1760, and C1876), and sorptivity are critical to the long-term performance of concrete structures. Internally cured LWC, using expanded shale, clay, and slate aggregates, has demonstrated superior resistance to environmental stressors, including freeze-thaw cycles and chloride ingress. These improvements translate into extended service life and reduced maintenance requirements, as confirmed by service life prediction models and field studies. Lifecycle cost analysis and environmental impact assessments further support the adoption of LWC. Despite slightly higher initial costs, LWC offers significant savings over time due to its durability and reduced repair frequency. Environmental Product Declarations (EPDs) and Lifecycle Assessments (LCAs) have quantified the sustainability benefits of LWC, including lower embodied energy and greenhouse gas emissions.

Applications in transportation infrastructure—from bridge decks and girders to pavements—have demonstrated the practical advantages of LWC. Case studies and experimental investigations confirm its effectiveness in improving constructability, reducing cracking, and enhancing long-term performance. Design specifications and building codes have evolved to accommodate the unique properties of LWC, with updates to AASHTO, ACI, ASTM, and international standards. These changes ensure that LWC can be safely and effectively integrated into structural designs, supporting performance-based approaches and resilience planning.

AASHTO (American Association of State Highway and Transportation Officials) has been actively working on updating and refining the modulus of elasticity for lightweight concrete in their bridge design specifications. AASHTO has updated the empirical expression for the modulus of elasticity of lightweight concrete in their LRFD Bridge Design Specifications. These updates aim to better reflect the properties of modern lightweight concrete materials. Although focused on high-strength concrete, recent studies by AASHTO have also provided insights into the modulus of elasticity, shrinkage, and creep of concrete. These studies help improve the accuracy of long-term material property predictions for both high-strength and lightweight concrete. These guidelines assist engineers and designers in accurately determining the elastic properties of lightweight concrete for various applications. This project contributes to better understanding of the stress-strain relationship of lightweight and internally-cured concrete containing lightweight aggregates, emphasizing expanded shale, clay, and slate as viable materials for transportation infrastructure. The current research offers practical solutions for designing concrete bridges and pavements using rotary-kiln expanded aggregates.

3. Methodology

3.1 Experimental Investigations

This study uses a quantitative, experimental approach to determine the static and dynamic modulus of elasticity of various lightweight aggregate concrete (LWAC) and internally cured concrete (ICC) mixes. The research aims to compare the elastic properties of LWAC with those of normal-weight concrete (NWC) and assess the trends for normal and high-strength concrete mixtures. All experimental procedures will follow relevant American Society for Testing and Materials (ASTM) standards to ensure reliability and repeatability.

Materials and Specimens

The constituent materials will include Portland cement Type 1L (Portland-Limestone Cement, PLC), cementitious materials as needed (e.g., fly ash Class F and ground granulated blast furnace slag, GGBFS, Grade 100), normal-weight fine and coarse aggregates (e.g., gravel and sand, specified by ASTM C33), potable water, chemical admixtures (e.g., air-entraining, water-reducing, and high-range water reducing or superplasticizers to achieve desired properties), and various types of LWA (e.g., expanded shale, clay, or slate, specified by ASTM C330 as demonstrated in Table 4 and Figure 20.

Table 4. Sources of Lightweight Aggregate and Concrete

Producers	Plants
Arcosa Lightweight	Brooks (KY), Livingston (AL)
Buildex	Dearborn (MO)
Carolina Stalite	Salisbury (NC)
Amrize Utelite	Coalville (UT)

Figure 20. Geographical Distribution of Lightweight Aggregate and Concrete Sources

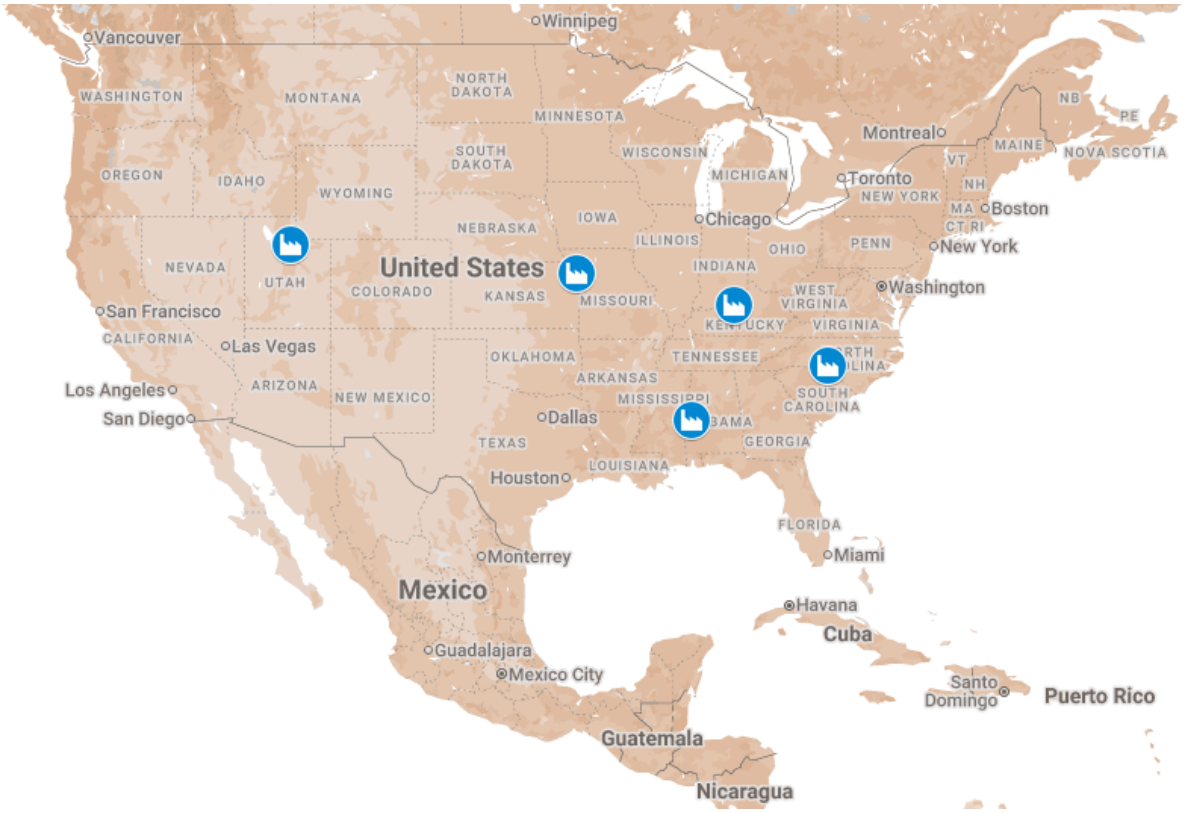

Multiple concrete mix designs will be prepared, including a control NWC mix and several LWAC and ICC mixes with a target air content of 5–8%. Lightweight concrete specimens include all lightweight (ALW) and sand lightweight (SLW) concrete with a target specified compressive strength of 28 MPa (4000 psi). The target equilibrium density of SLW was 1,760–1,920 kg/m^3 (110–120 pcf). Samples also included two high-strength mixtures (NWC and SLW) with a target compressive strength of 41 MPa (6,000 psi) and 48 MPa (7,000 psi). The water-cementitious materials (w/cm) ratio and total aggregate volume were optimized for each mix to achieve the target compressive strength while maintaining adequate workability and consistent density ranges. Internal curing followed ASTM C1761 (Table 5).

Table 5. Concrete Mix Design Specifications

Mix Design	ALW	SLW	ICC	NW	HSSLW1	HSNW1	HSSLW2	HSNW2
Compressive Strength, MPa (psi)		28 (4,000)			41 (6,000)		48 (7,000)	
Air Content (%)		5–8			5–8		5–8	
Equilibrium Density, kg/m^3 (pcf)	None	1,760–1,920 (110–120)	None	None	None	None	None	None
Normal Weight Coarse Aggregate			+	+		+		+
Normal Weight Fine Aggregate		+	+	+	+	+	+	+
Lightweight Coarse Aggregate	+	+			+		+	
Lightweight Fine Aggregate	+		+					

For each mix proportion, at least six cylindrical specimens were cast: three for determining compressive strength and three for modulus of elasticity testing. The standard specimen size was 4 x 8 inches (102 x 203 mm), with a length-to-diameter ratio of 2:1, as recommended by ASTM standards.

Specimens were molded in three layers, with each layer compacted using a steel rod to ensure consistency. After casting, all specimens were covered and left in their molds for 24 hours at room temperature. They were then demolded and transferred to a curing tank with clean water maintained at a constant temperature (e.g., 23 ± 2°C) for 7 days (ASTM C31 and C192). Specimens were kept in sealed conditions until the day of testing (typically 28 days) as shown in Figure 21.

Figure 21. Protecting (Top) and Sealing (Bottom) Samples

Testing and Data Collection

Fresh concrete tests included density, air content, and workability (ASTM C138, C143, C231, and C567). The ultimate compressive strength of companion cylinders was determined according to ASTM C39/C39M using a universal testing machine (Figure 22). This value is essential for establishing the target load for the modulus of elasticity test (40% of ultimate strength). The splitting tensile strength (ASTM C496) was also measured for determination of modification factors.

Figure 22. Compressive Strength Sample (Left) and Testing (Right)

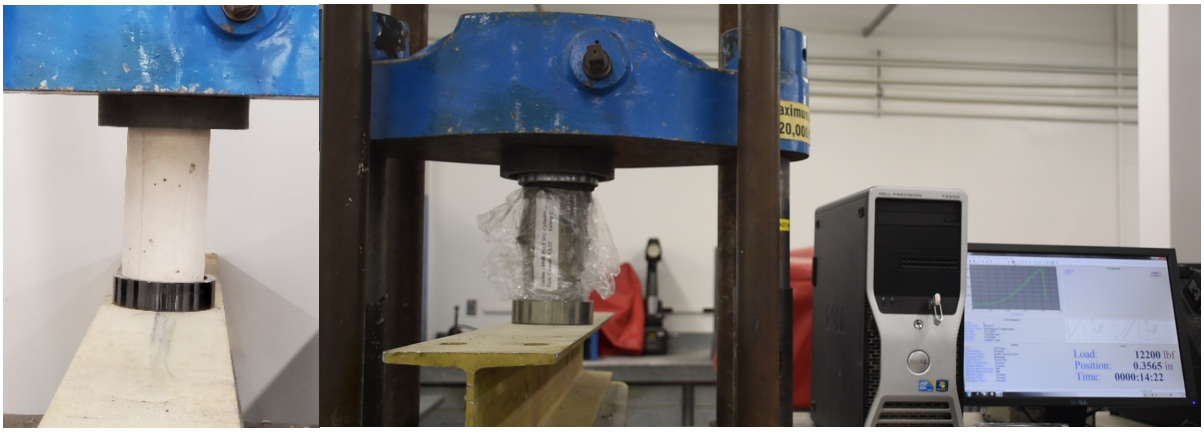

The static modulus of elasticity was determined using the ASTM C469/C469M standard test method. A compressometer was mounted at the mid-height of each test specimen to measure longitudinal deformation under axial load (Figure 23). The specimen was placed in a compression testing machine capable of maintaining a constant loading and unloading rate of approximately 35 psi/s (0.25 MPa/s). A preload was applied to seat the instrumentation, followed by at least two loading and unloading cycles up to 40% of the previously determined ultimate compressive strength. Applied load and longitudinal strain data were continuously recorded during the loading cycles using a data acquisition system.

Figure 23. Static Modulus of Elasticity Test Sample (Left) and Testing (Right)

The dynamic modulus of elasticity was measured using non-destructive methods, specifically the fundamental resonant frequency method as per the ASTM C215 standard. In the resonant frequency method, prismatic specimens were supported on soft supports at specific locations to facilitate free-end vibration in the fundamental flexural (transverse) or longitudinal modes. An impact was manually applied to the specimen's surface using a small hammer, and an acoustic sensor captured the resulting vibrations and sent the data to a signal analyzer. Fast Fourier Transform (FFT) analysis was used to identify the fundamental resonant frequency (Figure 24).

Figure 24. Dynamic Modulus of Elasticity Sample and Testing Apparatus

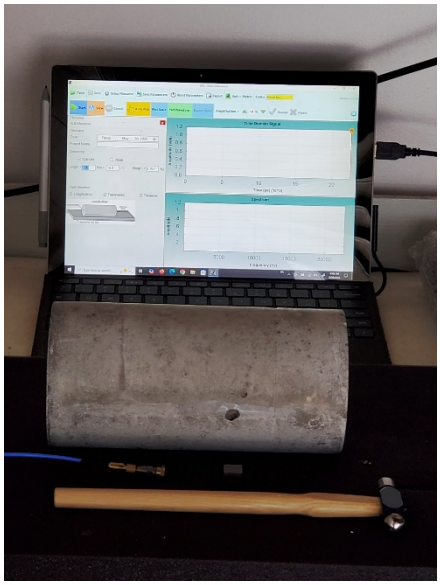

Data Analysis

The static modulus of elasticity (E_c) for each sample was calculated as the chord modulus, which is the slope of the stress-strain curve between a longitudinal strain of 50 microstrains (0.000050 in./in.), σ_1 and ε_1, and the stress corresponding to 40% of the ultimate compressive strength, σ_2, with corresponding strain, ε_2:

$$E_c = \frac{\sigma_2 - \sigma_1}{\varepsilon_2 - \varepsilon_1} \qquad (15)$$

The average E_c value from the repeatable cycles for each specimen is reported. Statistical analysis is performed to compare the modulus of elasticity across the different LWAC mixes and the NWC control, correlating the results with the compressive strength.

The dynamic modulus of elasticity (E_d) was calculated from the fundamental resonant frequency data using the equations provided in the ASTM C215 standard, which account for the specimen's mass, dimensions, and shape correction factors. A comparative analysis was conducted to evaluate the relationship between the static modulus and the dynamic modulus for the different LWAC and ICC mixes. Statistical methods were applied to correlate both moduli with compressive strength.

3.2 Analytical Investigations

These tasks assess the lifecycle impact of the lightweight concrete modulus of elasticity on design, construction, and environmental footprints of transportation components. This phase links the

modulus of elasticity to structural performance, service life, and durability characteristics using established engineering models.

Durability

Service life prediction utilizes durability models related to specific degradation mechanisms (e.g., chloride ingress-induced corrosion, freeze-thaw damage). The interaction between structural response and these mechanisms (e.g., a more flexible structure may require different protective measures) provides a better prediction of the service life.

Service life prediction based on durability factors relies on chloride diffusion in reinforced concrete and the total time for the chloride buildup and ingression plus corrosion of steel bars. The Fick's second law is a common approach to such a prediction (Ehlen, Thomas, and Bentz 2009; Ehlen and Kojundic 2014; Life-365™ 2020):

$$\frac{dC}{dt} = D\frac{d^2C}{dx^2} \qquad (16)$$

where C is the chloride content, D is the diffusion coefficient, x is the depth of the chloride intrusion with the maximum value equal to the depth of reinforcing steel or concrete cover, and t is time. The chloride content follows:

$$\mathrm{C}(x,t) = C_0\left(1 - erf\frac{x}{2\sqrt{Dt}}\right) \quad (17)$$

where C_0 is the chloride content at depth zero. Hence, the diffusion coefficient varies with time and temperature, benchmarked at the 28-day and 293K referenced time and temperature, respectively (Davodijam, Dastan Diznab, and Tehrani 2022):

$$D(T) = D_{ref}\left(\frac{t_{ref}}{t}\right)^m exp\left[\frac{U}{R}\left(\frac{1}{T_{ref}} - \frac{1}{T}\right)\right] \qquad (18)$$

where U is the activation energy of the diffusion process (35 *kJ/mol*), R is the gas constant (8.3145 *J/mol/K*), and T is the absolute temperature (K).

The Nernst-Einstein equation (Lu, 1997) follows:

$$D = \frac{RT\sigma}{Z^2F^2C} \qquad (19)$$

where D is the diffusion coefficient, R is the gas constant (8.3145 *J/mol/K*), T is the absolute temperature (K), σ is the partial conductivity (S/cm), Z is the charge (Coul), F is the Faraday's constant (96,500 Coul/mol), and C is the concentration (mol/cm^3).

Structural Response

The stress and strain distribution in bridge decks and pavement slabs under various loading conditions (traffic, thermal changes, seismic events) influences the predicted service life of concrete. This influence determines the need for maintenance, retrofit, and rehabilitation of transportation elements and hence interacts with lifecycle analyses, including cost and emissions.

Performance models predict the initiation and progression of damage (e.g., fatigue cracking, rutting, deflection) as a function of the modulus of elasticity and traffic loads. The analysis will specifically investigate how lower values might influence flexibility and potentially affect durability performance (e.g., by altering stress levels) and required maintenance frequency.

Tehrani (2025) has detailed the investigation approach to predict the service life of concrete as a homogenous material, i.e., uncracked, meaning that the analysis assumes no pre-existing or load-induced cracking and neglects crack-assisted transport mechanisms. The superposition of structural response and durability factors demand an extension of these methods to combine the chloride diffusion for cracked and uncracked concrete. The chloride diffusion of cracked concrete (D_{cr}) follows the estimated crack width (ΔL_x) in mm (Kwon et al., 2009):

$$\frac{D_{cr}}{D_{ref}} = 31.61\Delta {L_x}^2 + 4.73\Delta L_x + 1 \quad (20)$$

Hence, the equivalent diffusion for a section of concrete (D_{avg}) can follow a weighted average approach (Hassan and Amleh, 2025):

$$D_{avg} = \frac{[(A_g - A_{cr}) \times D_{ref}] + (A_{cr} \times D_{cr})}{A_g} \quad (21)$$

In this equation, A_g and A_{cr} are gross and cracked areas, respectively.

Climate Data

Table 6 presents the rates of chloride accumulation for urban bridges, following the guidelines from Life-365™ (2020). The primary factor influencing the severity of chloride accumulation in each area is the frequency of freeze-and-thaw cycles; hence, the lowest recommended rate applies to regions that are hot and dry. For urban bridges, the accumulation rate is established at 85% of the rates intended for parking structures because they are more exposed to de-icing agents. For marine structures located 1.5 km from the coastline, the advised chloride accumulation rate is 0.02% (Kalantari and Tehrani, 2021; Kalantari, Dastan Diznab, and Tehrani, 2021).

Table 6. Chloride Build-Up Rate for Urban Bridges, Adopted from Tehrani (2025)

Climate Zone	Chloride Build-Up Rate (% per Year)[a]
Very Cold	0.085
Cold	0.068
Moderate	0.0255
Semi-Moderate	0.0170
Semi-Arid to Very Hot	0.0085

The forecast for the service life of each concrete mixture was derived from an urban bridge situated at or near the manufacturing site, with the objective of evaluating the impact of lightweight aggregates, irrespective of the specific site. A comparable evaluation can also be employed to predict the service life for other intended locations, such as California. The temperature history for chosen plant sites is detailed in Life-365™ (2020), utilizing available data sources (Figure 25).

Figure 25. Temperature History of Selected Plant Locations (After Life-365™)

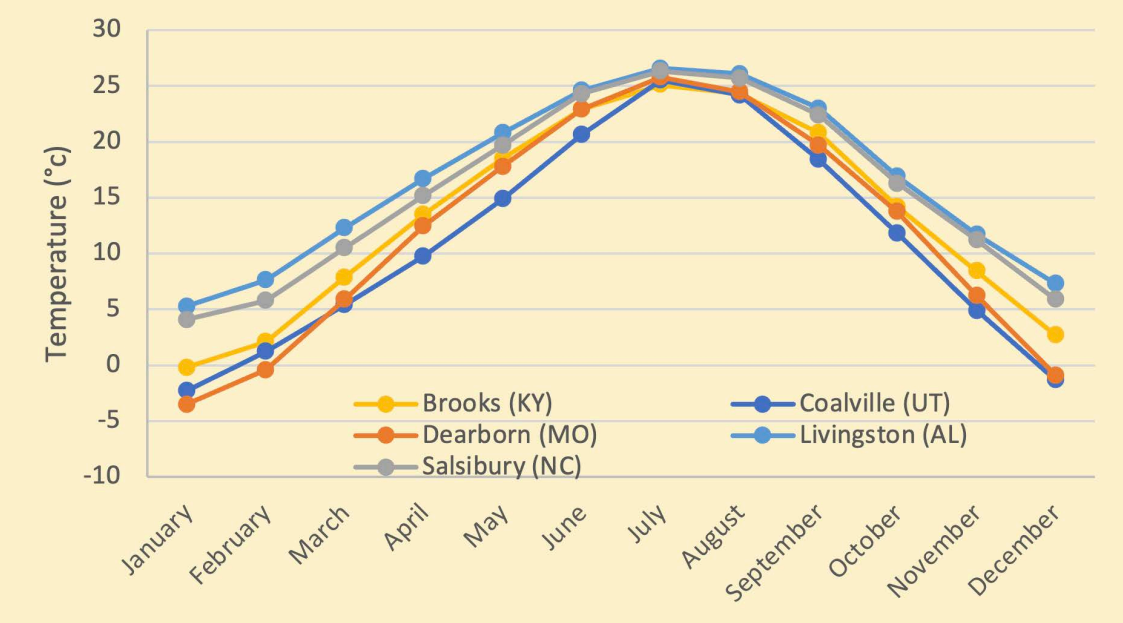

The construction of concrete decks or slabs follows established protocols as indicated in the appropriate guidelines (Table 7). In environments that are corrosive, concrete generally demands additional cover, increased thickness, and extra reinforcement to withstand the adverse effects of corrosive substances. In contrast, parking structures with shorter spans require less thickness and reinforcement. Urban bridges, which have longer spans and greater exposure to harmful agents, are designed with thicker slabs and enhanced concrete cover. Furthermore, in colder regions, the concrete cover for slabs and decks is somewhat thicker than normal due to the more frequent use

of de-icing agents. This principle also applies to cities located near water bodies with higher chloride levels (Davodijam, Dastan Diznab, and Tehrani 2022).

Table 7. Input Data for the Service Life Prediction

Exposure	Pavement	Urban Highway Bridges
Thickness (mm)	300	200
Concrete Cover (mm)	75	60
Reinforcing Ratio (%)	1.5	1.2
Water-to-Cementitious Materials Ratio (w-cm)	Varies [a]	Varies [a]
Maximum Chloride Concentration (%)	0.60 [b]	0.68 [b]

[a] Mix Design Specific; [b] 85% of the frigid climate

Lifecycle Assessment

The lifecycle assessment analyzes the expected lifespan of concrete applications in relation to their transport properties. It takes into account both financial and environmental impacts. The evaluation of costs includes expenses related to construction and repairs. Construction costs encompass the expenses for concrete and rebar, which maintain similar unit prices across different applications and locations, adjusted for thickness and reinforcement ratios. Repair expenses entail the replacement of damaged sections according to a planned schedule and the grinding of surfaces. To determine the total repair costs, adjustments need to be made based on the frequency and severity of damages (Vosoughi et al. 2017). Standard maintenance generally includes replacing 1% of the area, grinding the entire surface, and joint replacement every decade (SUDAS 2021). The cost data was generated based on existing research and updated bid data from transportation projects managed by CA DOT (Caltrans 2007) as of January 2025. The cost estimates were formulated for approximately 2,000 cubic meters of concrete covering an area of 10,000 square meters. Economic characteristics are provided by NIST (Table 8) (Kneifel and Lavappa 2024).

Utilizing Environmental Product Declarations (EPDs) enables precise assessment of the carbon footprints linked to different concrete designs. These evaluations emphasize the ecological advantages of the suggested solutions, including extended durability, enhanced use of natural resources, and reduced energy use and emissions (Tehrani 2021b).

Table 8. Cost Data

Item	Unit	Estimated Cost ($)
Ordinary Concrete Materials	m^3	1000
High Strength Concrete	m^3	1050
Reinforcing Steel Bars	tonne	4500
Grinding Existing Concrete	m^2	14
Grinding Existing Bridge Deck	m^2	30
Membrane Waterproof	m^2	140
Deck Seal	m^2	70
Removing Concrete Pavement	m^3	150
Removing Structural Concrete	m^3	380
Inflation Rate	%	1.8
Discount Rate	%	2.0

Lifecycle assessment evaluates economic and environmental impacts, specifically focusing on cost and greenhouse gas emissions. To compare different scenarios, we use equivalent annual cost (EAC) estimates, which account for construction, periodic operation (maintenance and repairs), and decommissioning costs (Tehrani 2025):

$$EAC(i,L) = \frac{[i(1+i)^L]}{[(1+i)^L-1]}\left\{C + \sum \frac{1}{(1+i)^t} O_t + D\frac{1}{(1+i)^L}\right\} \quad (22)$$

In this equation, C is the cost of construction, O_t is the cost of operation at time t, say maintenance, repair, or retrofit, L is the service life, i is the applicable interest rate, and D is the cost of decommissioning, including removal, discarding, and recycling. A zero-interest assumption simplifies this equation to the following (Tehrani 2025):

$$EAC = (C + \sum O_t + D)\frac{N}{L} \quad (23)$$

where N is the analysis period, say 500 years, or any number more significant than the maximum service life of concrete specimens to allow a meaningful comparison (Tehrani 2025).

The lifecycle assessment follows the system boundary described in Table 9. The chosen modules constitute a partial selection necessary for a cradle-to-gate Environmental Product Declaration (EPD) as discussed by Tehrani (2024b, 2024c), particularly for uses in transportation such as roads and bridges. The production phase is assessed independently for Expanded Shale Clay and Slate (ESCS) as well as concrete manufacturing processes, which include ready-mix concrete. Modules that pertain to refurbishment and the energy and water consumption during the usage phase are excluded from the focus of this analysis. Data for each module, as illustrated in Table 10, are

obtained from existing Product Category Rules (PCR), EPD, and Lifecycle Assessment (LCA) publications (EPD 2021; ISO 14025) related to diverse materials, including cement (PCA 2016), concrete (NRMCA 2020), steel (CRSI 2017), normal-weight aggregate (Vulcan 2016), and ESCS (ESCSI 2024a; UL 2022). Furthermore, cited engineering manuals and guides offer insights into productivity and anticipated performance indicators, such as service life (Peurifoy et al. 2018; ACCO 2004; PBO 2018; SUDAS 2021).

Table 9. System Boundary Modules

Phase	Module	Stage
ESCS Production	A1	Mining Shale, Clay, and Slate
	A2	Transport to Rotary Kiln
	A3	Manufacturing ESCS
Concrete Production	A2'	Transport to Concrete Plant
	A3'	Produce Ready Mix Concrete
Pavement Construction	A4	Transport Concrete to the Site
	A5	Concrete Placement
Pavement Service Life	B1	Pavement Use
	B2	Joint Maintenance
	B3	Grinding Repair
	B4	Slab Replacement
Pavement End of Life	C1	Deconstruction
	C2	Transport Waste
	C3	Waste Processing and Crushing
	C4	Disposal
Benefits & Loads Beyond System Boundary	D	Reuse, Recovery, Recycling Potential

Table 10. Global Warming Potential (GWP)

Item	Unit	Global Warming Potential (kg CO_2 eq)	Reference
Cement	Tonne	1040	PCA 2016
Concrete (28-34 MPa) 0-20% SCM	m^3	523.68	NRMCA 2020
Concrete (41-55 MPa) 0-20% SCM	m^3	642.02	NRMCA 2020
Fabricated Steel Reinforcement	Tonne	979	CRSI 2017
Lightweight Aggregates (ESCS)	m^3	111	ESCSI 2023
Gravel	Tonne	6.06	Vulcan 2016
Sand	Tonne	4.89	Vulcan 2016

This Life Cycle Assessment (LCA) evaluates the productivity rates of construction activities to assess resource usage. However, the energy consumption and emissions linked to construction teams remain beneath an assumed cut-off threshold of 1%. Furthermore, the system boundary excludes the energy contributions and emissions resulting from the production of construction machinery and equipment. The durability of this equipment minimizes its effect to below the cut-off limit (Tehrani 2023b).

4. Results

4.1 Physical and Mechanical Properties

Mix Design and Physical Properties

Table 11 contains the plastic density, slump, and air content of mixtures. Figure 26 details the mixture design of concrete specimens.

Table 11. Fresh Concrete Properties

Concrete Mix	Plastic Density (kg/m^3)	Slump (mm)	Air Content (%)
All Lightweight (ALW)	1,648	152	–
Sand Lightweight (SLW)	1,807–2,010	127–229	3.4–9.5
Internally Cured (ICC)	2,079–2,223	108–146	8.0
Normal Weight (NW)	2,113–2,289	25–152	2.0–9.5
High Strength Sand Lightweight 1 (HSSLW1)	1,852–1,853	114–159	8.0
High Strength Normal Weight 1 (HSNW1)	2,180–2,334	95–152	5.5
High Strength Sand Lightweight 2 (HSSLW2)	1,893	146	7.0
High Strength Normal Weight 2 (HSNW2)	2,196	165	3.7

Figure 26. Mixture Design of Concrete Specimens

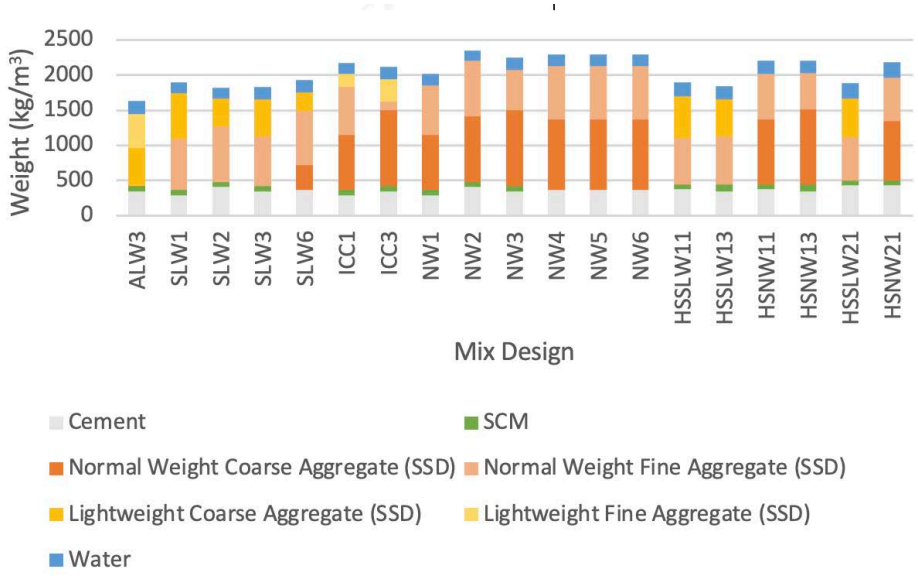

Figures 27 and 28 compare the specific gravity and water absorption of aggregates used in mix designs. The average specific gravity of coarse and fine lightweight aggregates is respectively 55% and 62% of normalweight aggregates. The average water absorption of lightweight aggregates was 19–20 times that of normalweight aggregates.

Figure 27. Specific Gravity of Aggregates

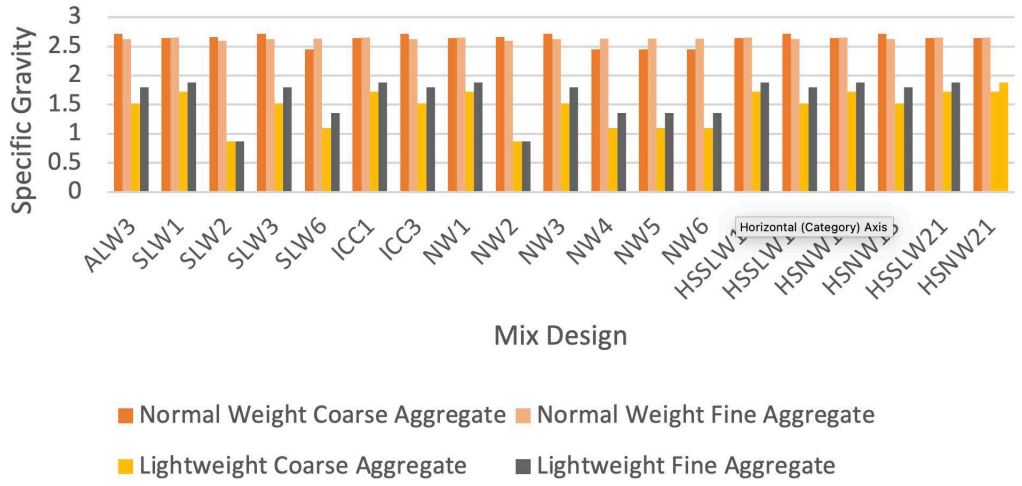

Figure 28. Water Absorption of Aggregates

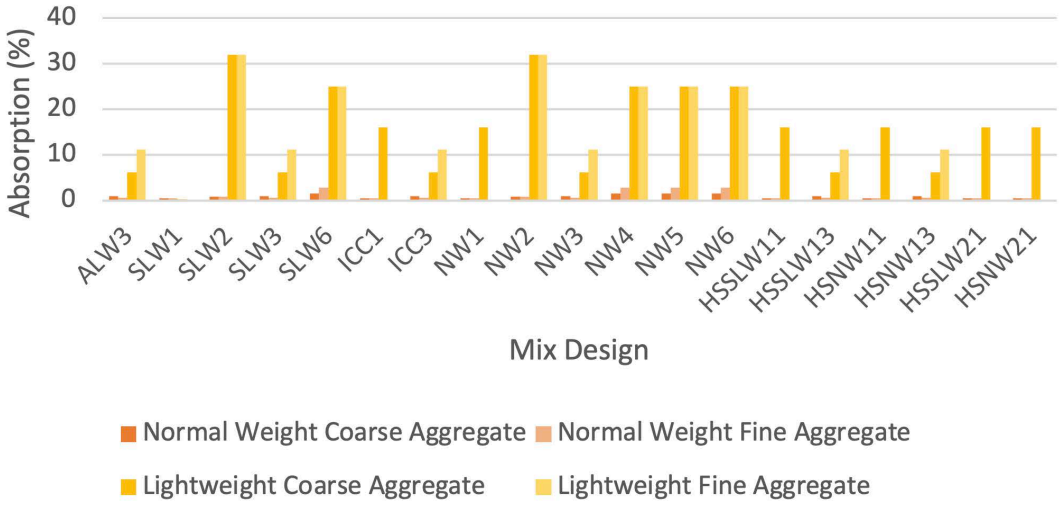

Mechanical Strengths

Figure 29 illustrates the compressive strength of concrete specimens. Logarithmic trendlines estimate the variation in compressive strength between 1 and 128 days, when available. The results show that all ALW, SLW, ICC, and NW samples exceeded the specified target compressive strength of 28 MPa for normal concrete. Also, HSSLW and HSNW exceeded their targets of 41 and 48 MPa for high-strength concrete. However, the samples from one source, including

lightweight and normalweight, achieved the value at 128 days, which indicates a potential problem with cementitious materials and admixtures proportioning. The ratio of the compressive strength of concrete containing lightweight aggregates to normal-weight concrete was 94% for ALW, 79–136% for SLW, 93–101% for ICC, 96–99% for HSSLW1, and 102% for HSSLW2.

Figure 29. Compressive Strengths of Concrete Specimens

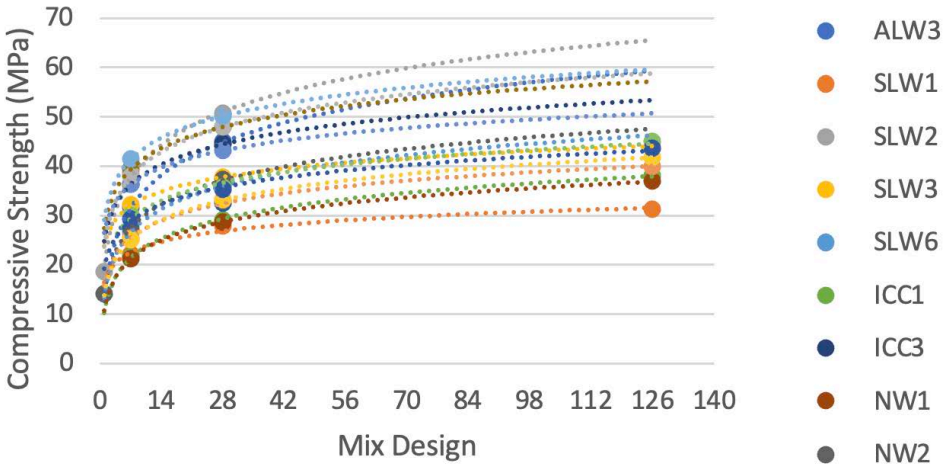

Figure 30 illustrates the splitting tensile strengths of concrete specimens. The ratio of the splitting tensile strength of concrete with lightweight aggregates to normalweight concrete was 83% for ALW, 95–96% for SLW, 118% for ICC, and 91% for HSSLW1.

Figure 30. Splitting Tensile Strengths of Concrete Specimens

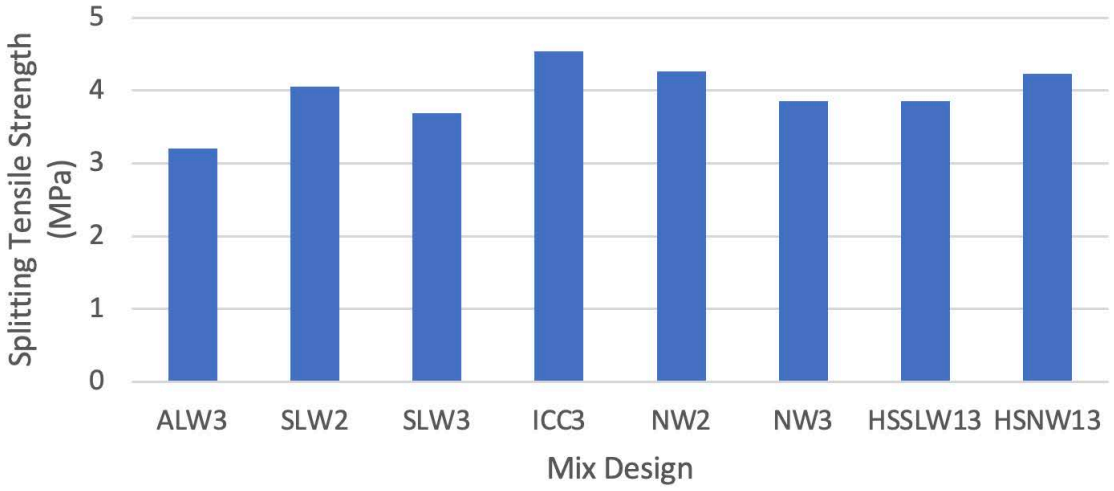

Figure 31 shows the trends of splitting tensile strength as a function of compressive strength. Data points show that all concrete samples containing lightweight aggregates, excluding ALW, have the same or higher splitting tensile strength than normalweight aggregate with the comparative compressive strengths. The ACI equation is also presented for comparison:

$$f_t = 0.53\sqrt{f_c'} \qquad (22)$$

Figure 31. Relationship Between Compressive and Splitting Tensile Strengths

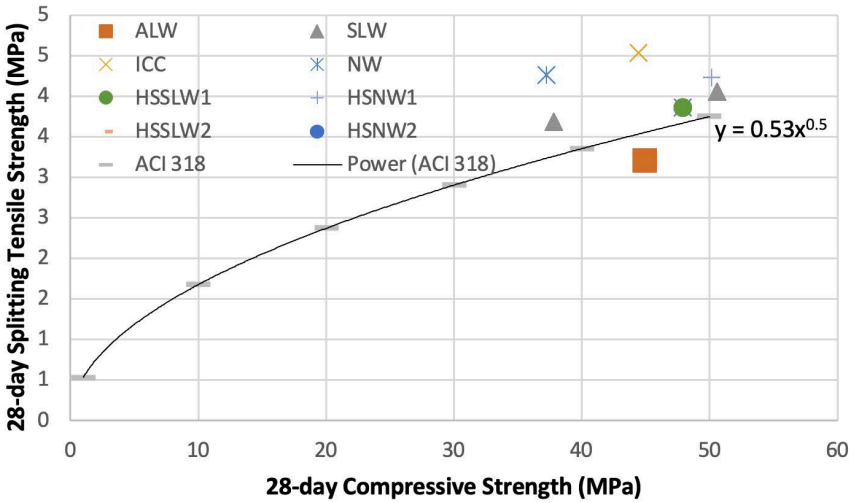

The ratio of splitting tensile strength to compressive strength leads to a modification factor (Figure 32) in design codes, such as ACI 318, for lightweight concrete. The prescriptive equation for the modification factor, λ, relies on equilibrium density, w_c, and disregards the source of aggregates:

$$\lambda = \begin{cases} 0.75, w_c \leq 1600\, kg/m^3 \\ 0.000463\sqrt{w_c}, 1600 < w_c \leq 2160\, kg/m^3 \\ 1.0, w_c > 2160\, kg/m^3 \end{cases} \qquad (23)$$

Hence, the modification factor does not apply to ICC samples. An experimental value of the modification factor may follow mechanical properites:

$$\lambda = 1.79\frac{f_{ct}}{\sqrt{f_c'}} \qquad (24)$$

where f_{ct} and f_c' are the splitting tensile and compressive strengths (MPa), respectively.

Figure 32. Experimental and Prescriptive Modification Factors

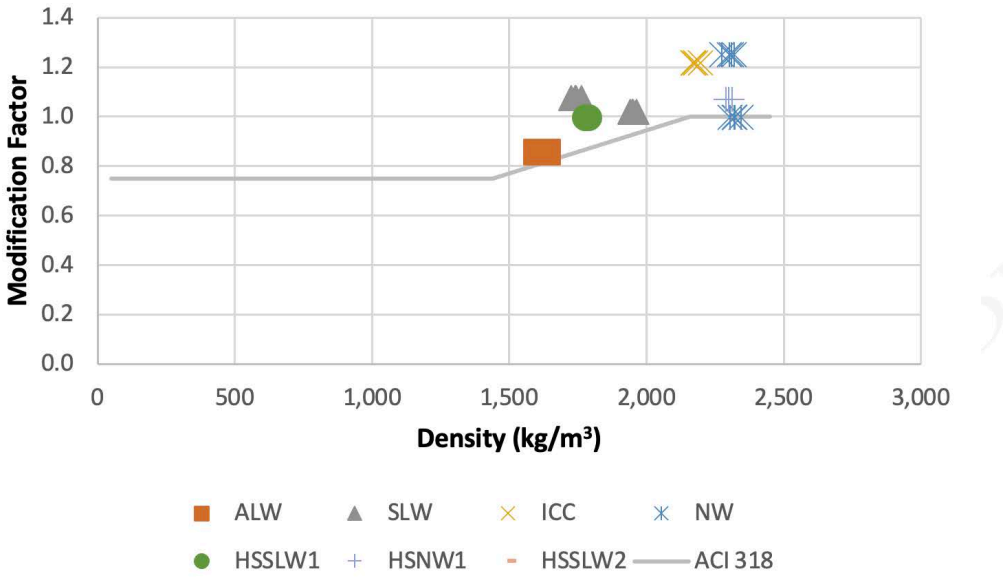

Figure 33 compares experimental modification factors with the results of the ACI prescriptive equation. This comparison reveals that experimental values obtained for specific ESCS aggregates outperformed ACI generic values. All SLW specimens had a modification factor of 1 or higher, which voids the concept of a modification factor for ESCS lightweight concrete. The modification factor of ALW was also 13% higher than the ACI value.

Figure 33. Modification Factors of Lightweight Concrete Specimens

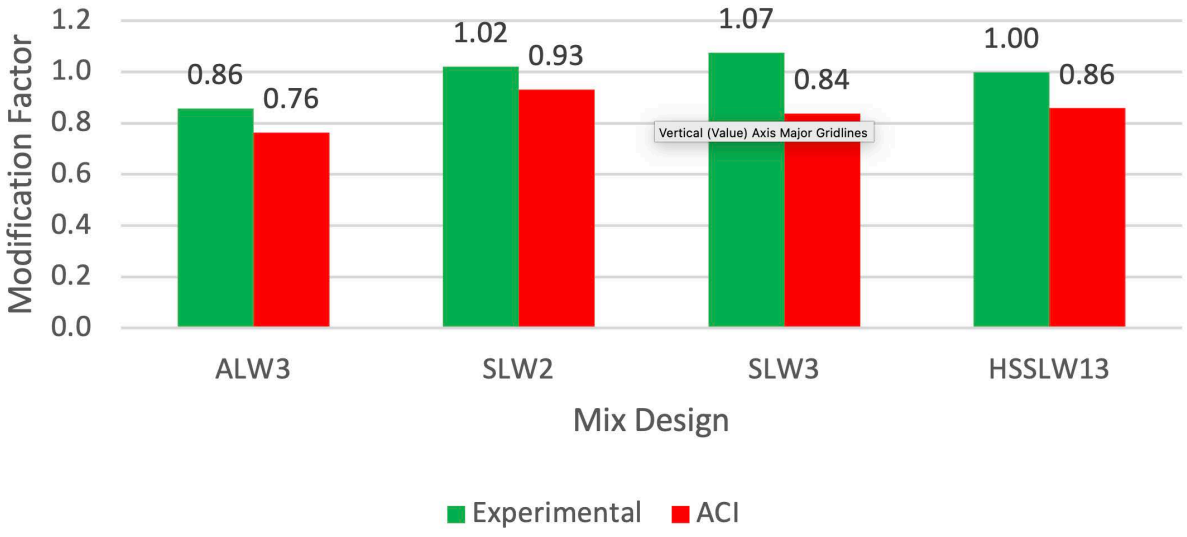

Modulus of Elasticity

Figure 34 shows the variation of static modulus of elasticity per compressive strength of concrete specimens. The trend line indicates the ACI 318 equation for normalweight concrete:

$$E = 4.7\sqrt{f_c'} \quad (25)$$

The ratio of measured static modulus of elasticity to the prescribed value in the ACI equation is 57% for ALW, 68–90% for SLW, 85–133% for ICC, 93–107% for NW, 44–75% for HSSLW, and 114–124% for HSNW samples.

Figure 34. Static Modulus of Elasticity and Compressive Strength of Concrete Specimens

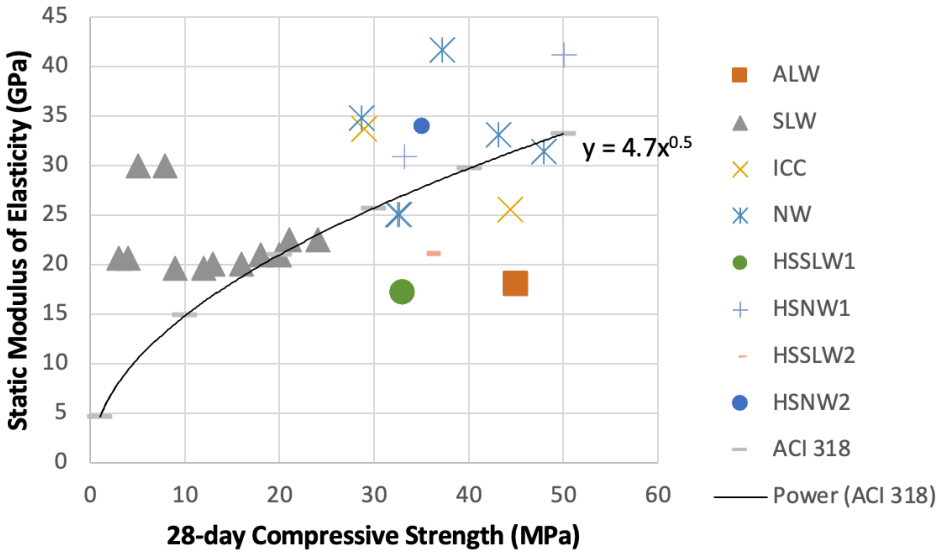

Figure 35 shows similar relationships between static modulus of elasticity and density of concrete specimens. Three trend lines indicate the ACI 318 equations for three target compressive strength values of 28, 41, and 50 MPa:

$$E = 0.043 w_c^{1.5} \sqrt{f_c'} \quad (26)$$

All samples, except HSSLW1, have outperformed the predicted modulus of elasticity based on their target compressive strength values.

Figure 35. Static Modulus of Elasticity and Density of Concrete Specimens

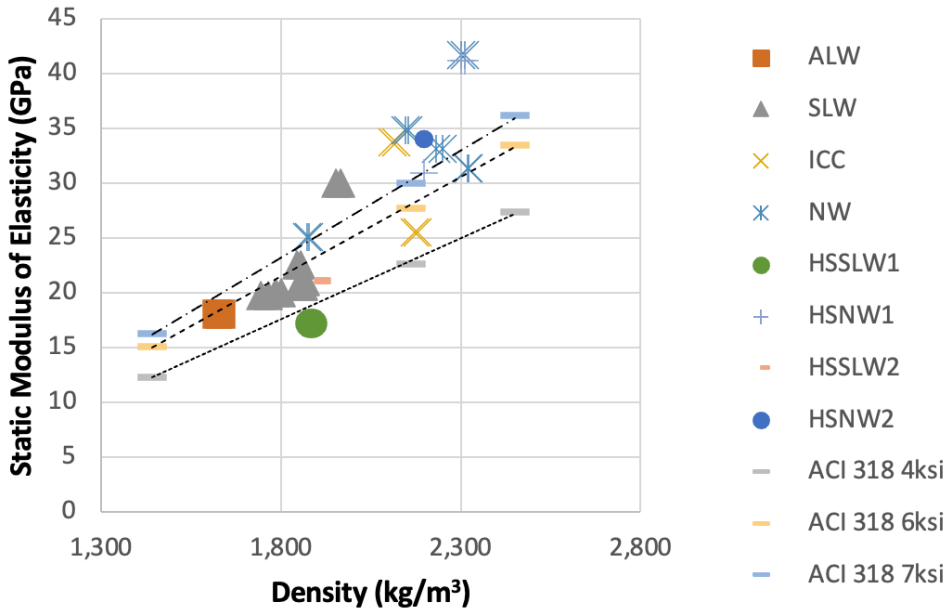

Figure 36 demonstrates the increase of modulus of elasticity through time between 28 days and one year of age. The average rate of increase is 8% for SLW and insignificant for others.

Figure 36. Static Modulus of Elasticity and Age of Concrete Specimens

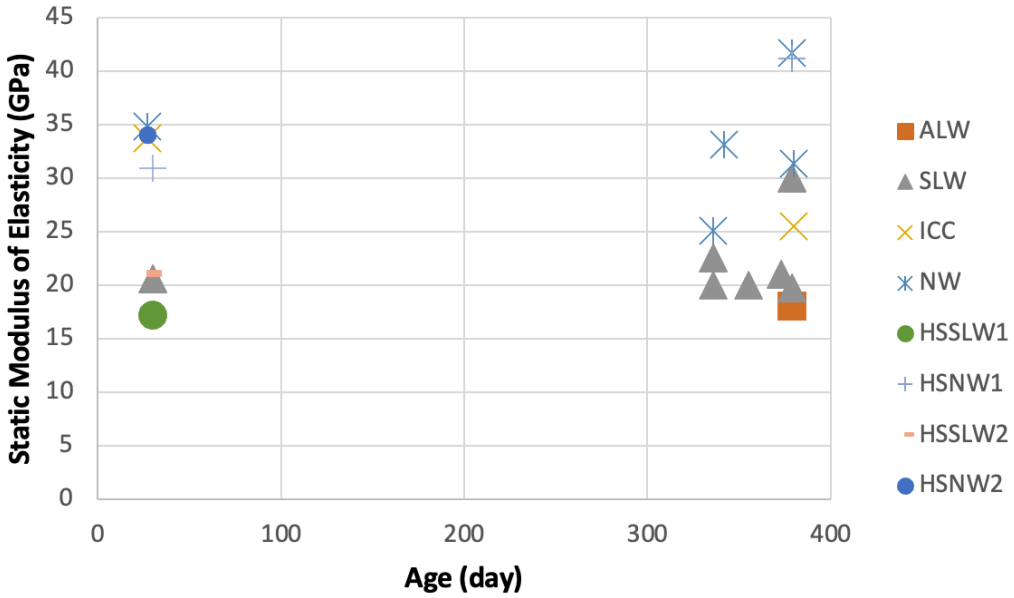

Figure 38 shows the measured Poisson's ratios for concrete specimens. These values vary from 0.11 to 0.47 with a tendency of increase for concrete specimens containing lightweight aggregates, except for ICC. This trend is more visible for high-strength concrete samples.

Figure 37. Static Poisson's Ratio of Concrete Specimens

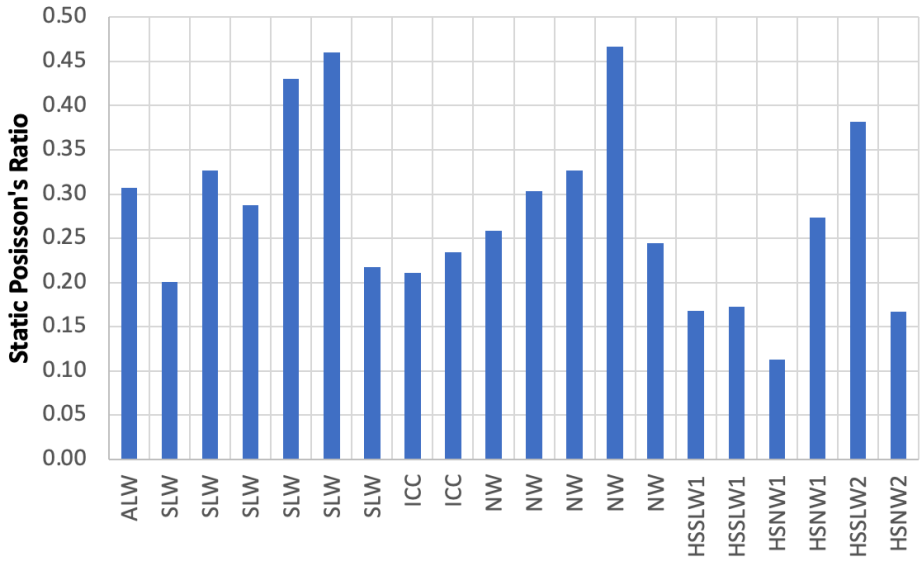

Figures 38, 39, and 40 represent the trends of static Poisson's ratio of concrete specimens with respect to compressive strength, density, and age. These trends do not indicate a significant correlation between concerning parameters.

Figure 38. Static Poisson's Ratio and Compressive Strength of Concrete Specimens

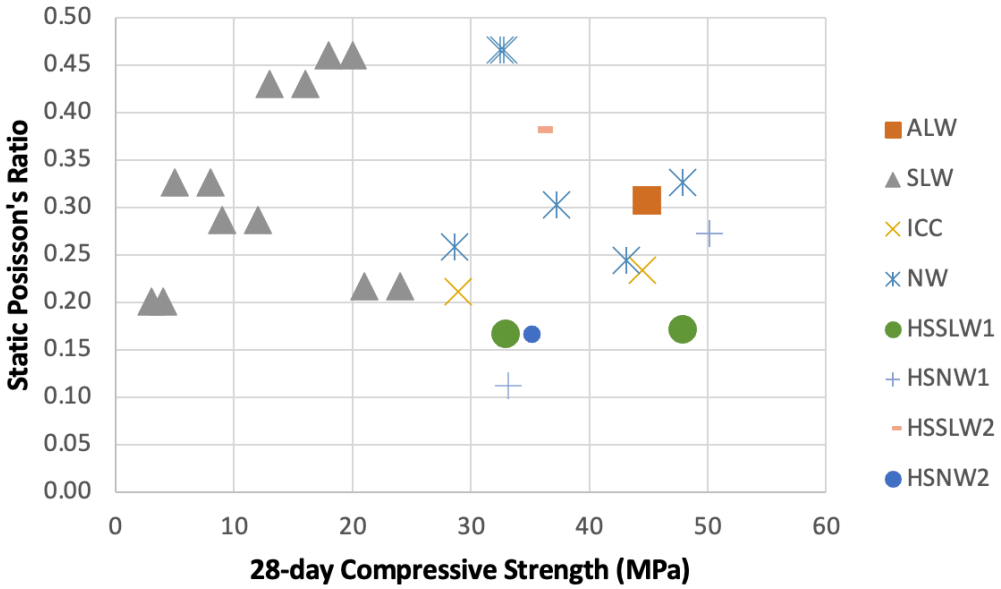

Figure 39. Static Poisson's Ratio and Density of Concrete Specimens

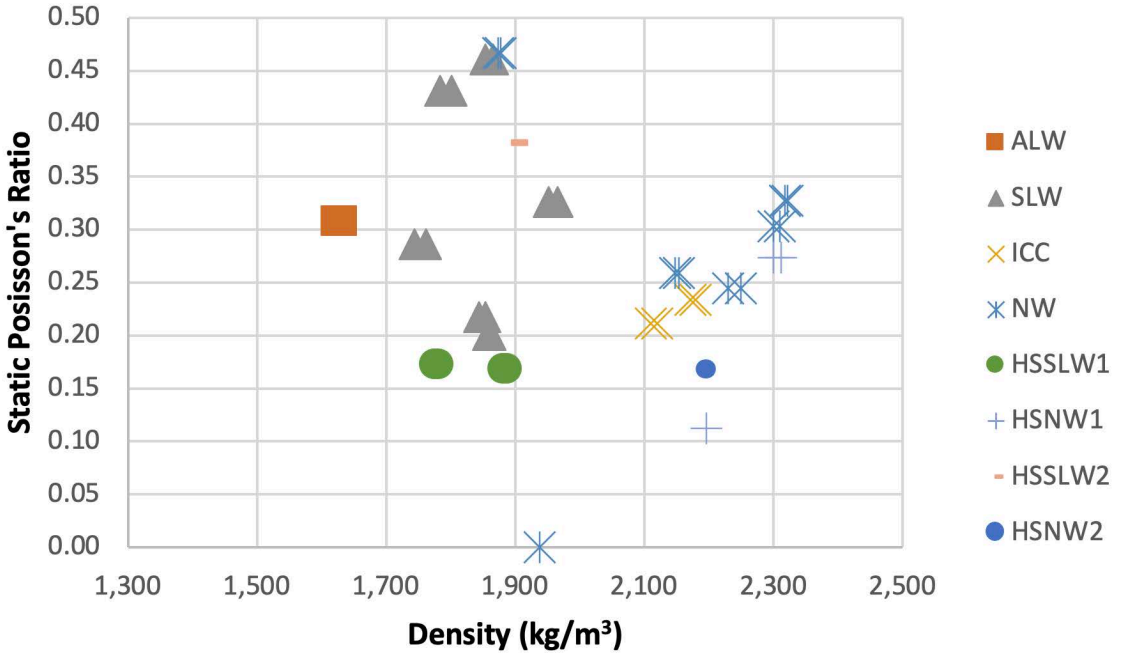

Figure 40. Static Poisson's Ratio and Age of Concrete Specimens

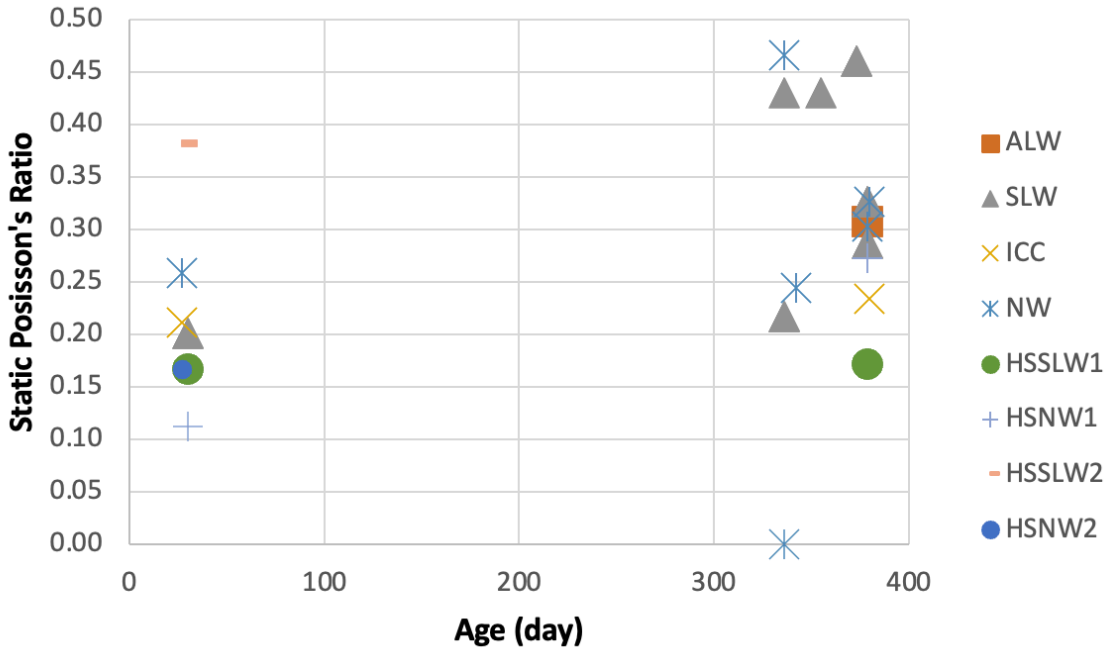

Figure 41 presents the relationship between static and dynamic moduli of elasticity in longitudinal direction. Three proposed models for this relationship include the following equations by Neville (1997), BS 8110, and Shkolnik (1996) as reported by Diógenes et al. (2011):

$$E = 0.83E_d \quad (27)$$

$$E = 1.25E_d - 19 \quad (28)$$

$$E = E_d - 5.864 \quad (29)$$

All lines underestimate the static modulus of elasticity calculated based on the dynamic longitudinal value, with the BS 8110 offering the most conservative value. Equations in this figure represent regression lines with the highest coefficient of determination for NW and SLW samples. These equations are very close to each other and confirm the Neville (1997) relations with zero intercept and with a higher slope.

Figure 41. Longitudinal Dynamic and Static Moduli of Elasticity of Concrete Specimens

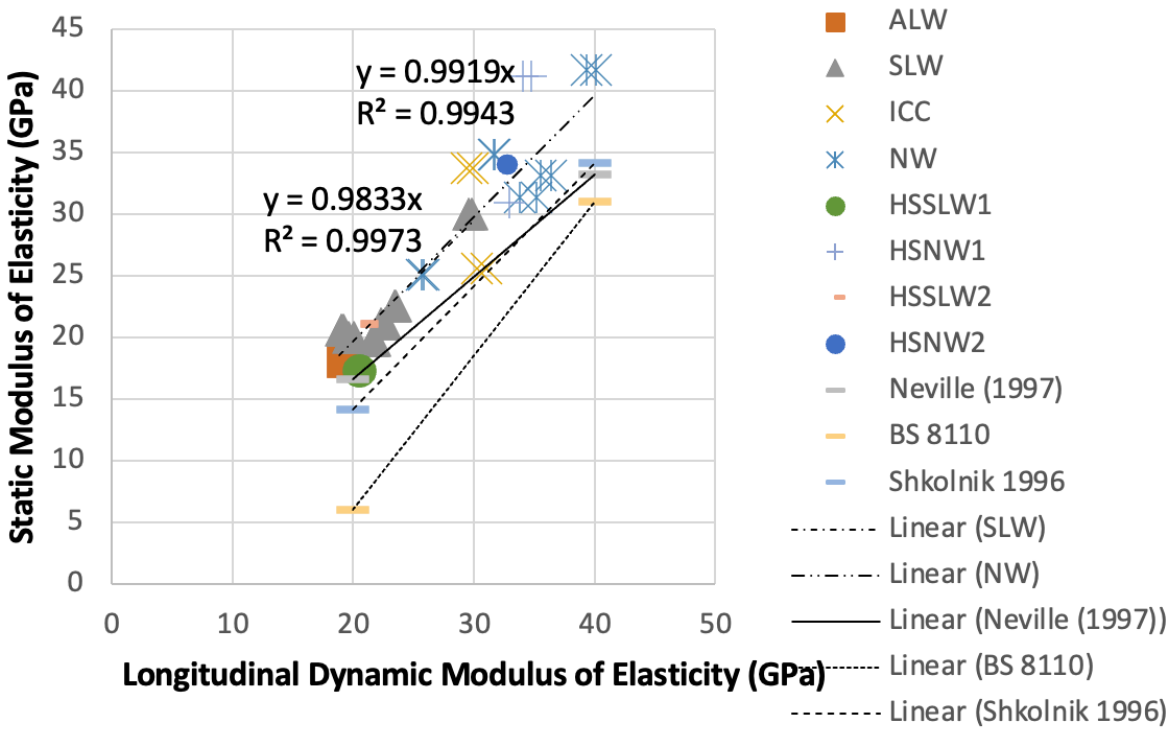

Figures 42, 43, and 44 show the trends of dynamic modulus of elasticity in the longitudinal direction with respect to compressive strength, density, and age of concrete specimens. These trends are comparable with those of static modulus of elasticity, as suggested by their linear relationship, with a scaled value due to the dynamic effect.

Figure 42. Longitudinal Dynamic Modulus of Elasticity and Compressive Strength of Concrete Specimens

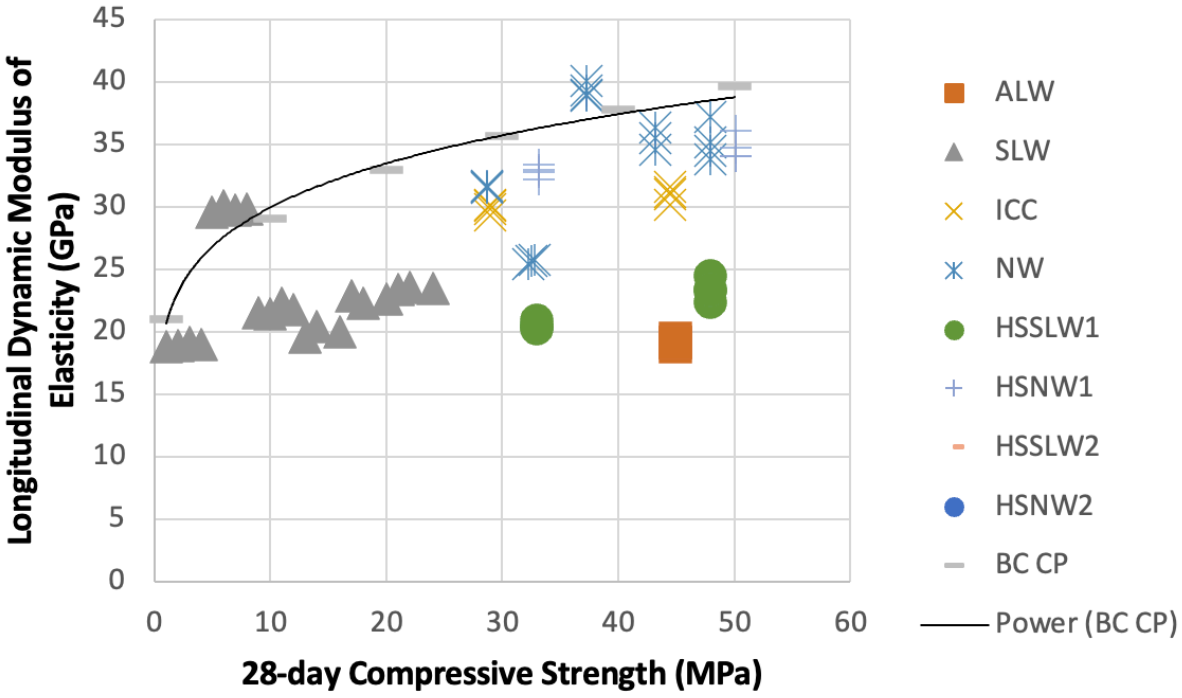

Figure 43. Longitudinal Dynamic Modulus of Elasticity and Density of Concrete Specimens

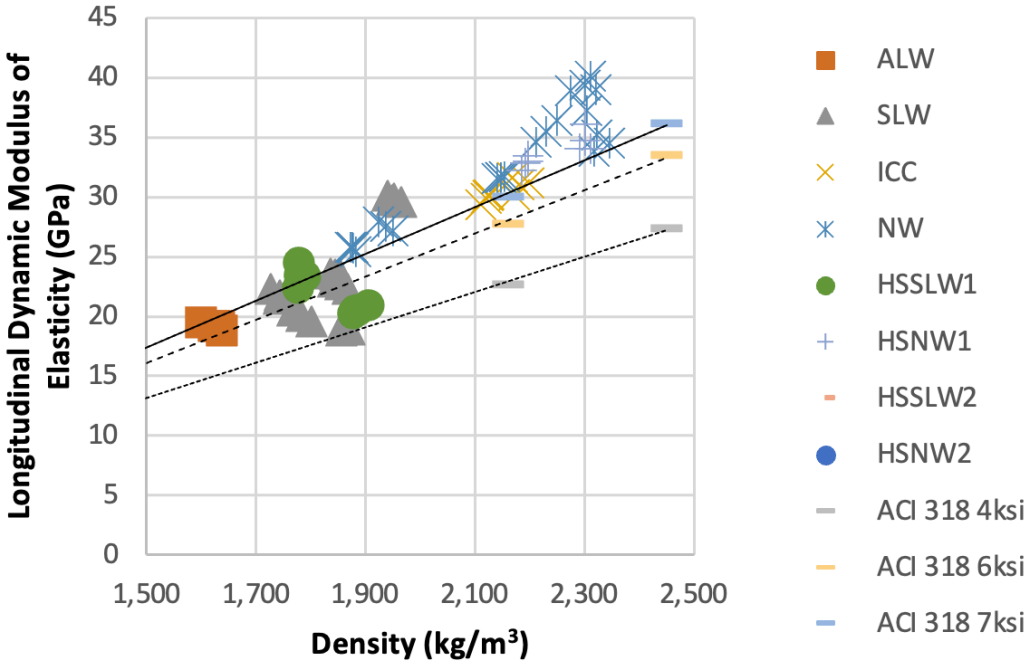

Figure 44. Longitudinal Dynamic Modulus of Elasticity and Age of Concrete Specimens

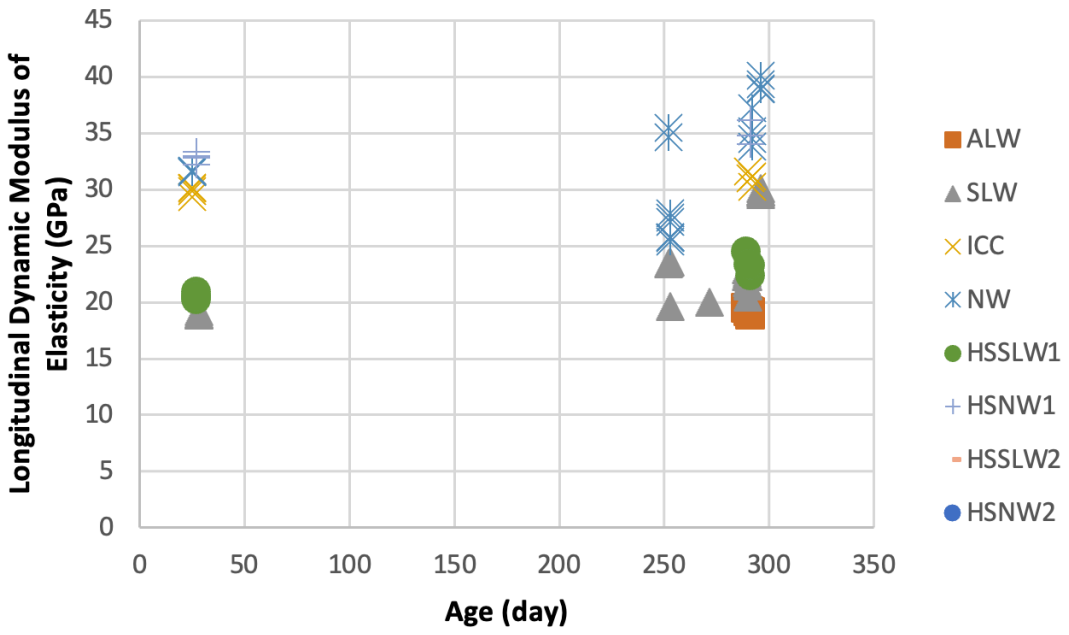

Figures 45 and 46 exhibit linear relationships between longitudinal, transverse, and torsional moduli of elasticity for concrete specimens. These trends are independent of concrete characteristics and the influence of aggregate types.

Figure 45. Longitudinal and Transverse Dynamic Elasticity Moduli of Concrete Specimens

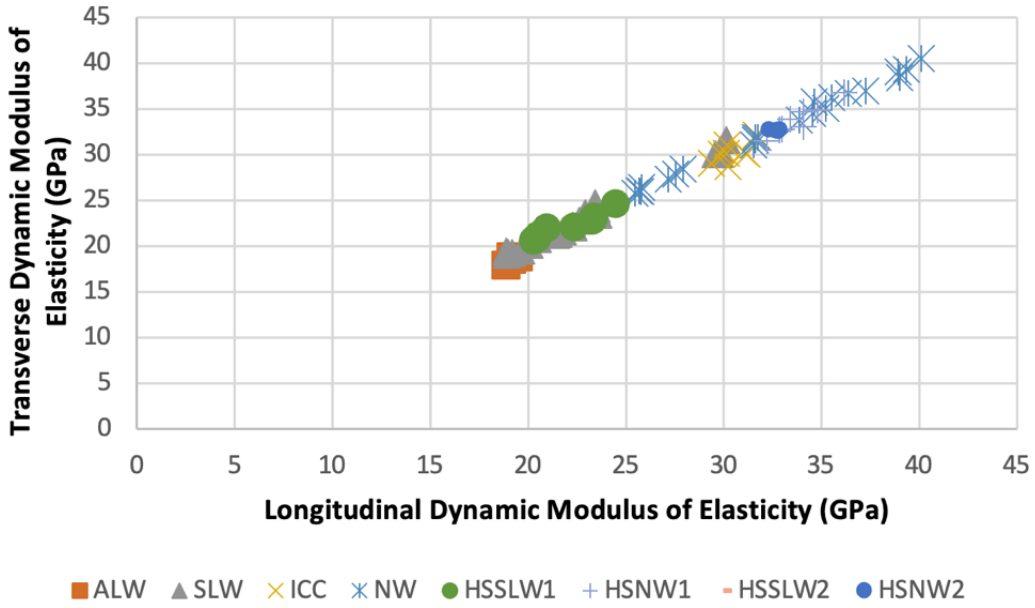

Figure 46. Transverse and Torsional Dynamic Elasticity Moduli of Concrete Specimens

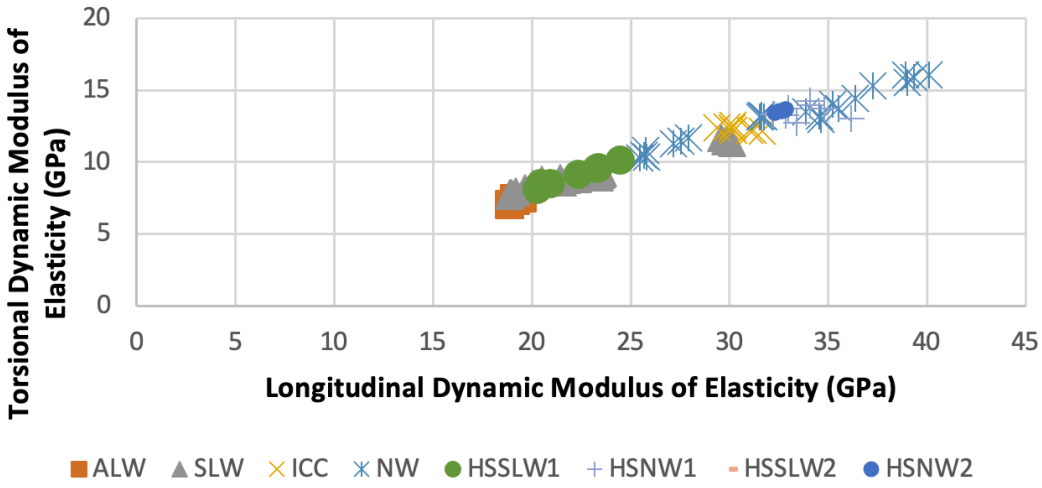

Figures 47 to 52 show the trends of transverse and torsional dynamic moduli of elasticity with respect to compressive strength, density, and age of concrete specimens. These trends follow the same trends for the longitudinal direction.

Figure 47. Transverse Dynamic Modulus of Elasticity and Compressive Strength of Concrete Specimens

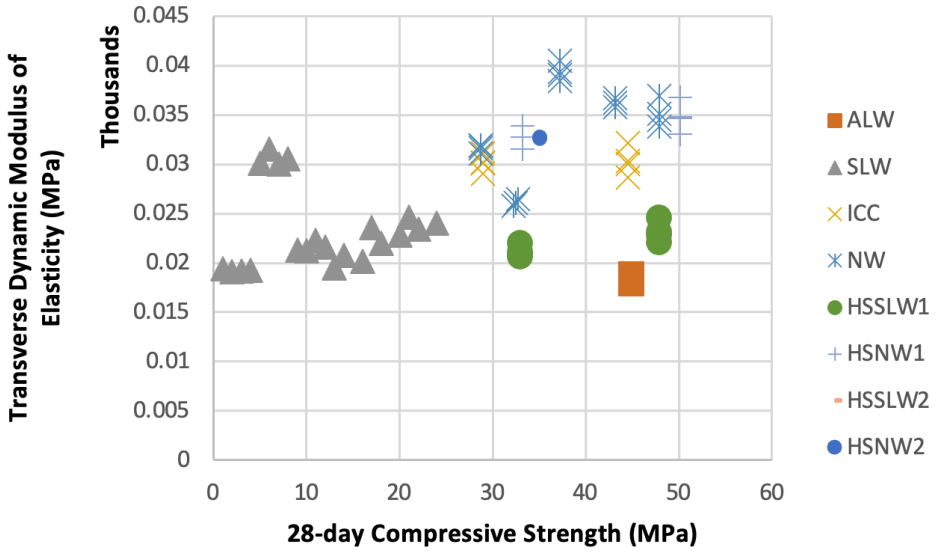

Figure 48. Transverse Dynamic Modulus of Elasticity and Density of Concrete Specimens

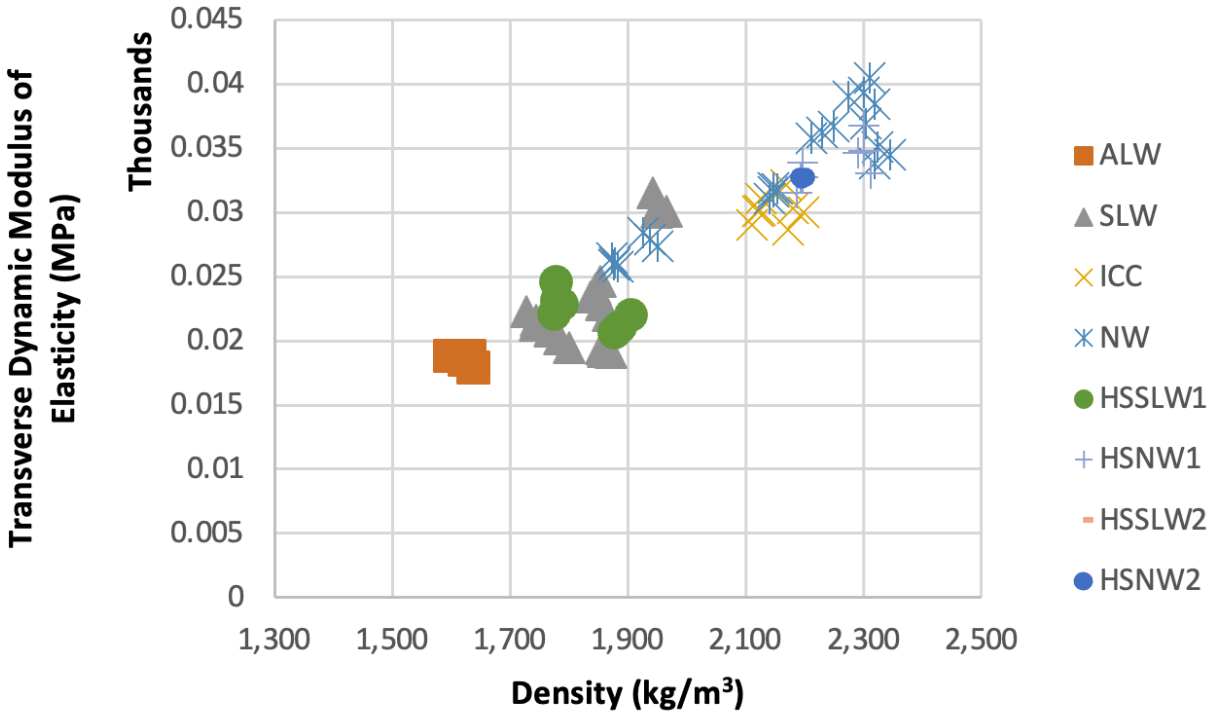

Figure 49. Transverse Dynamic Modulus of Elasticity and Age of Concrete Specimens

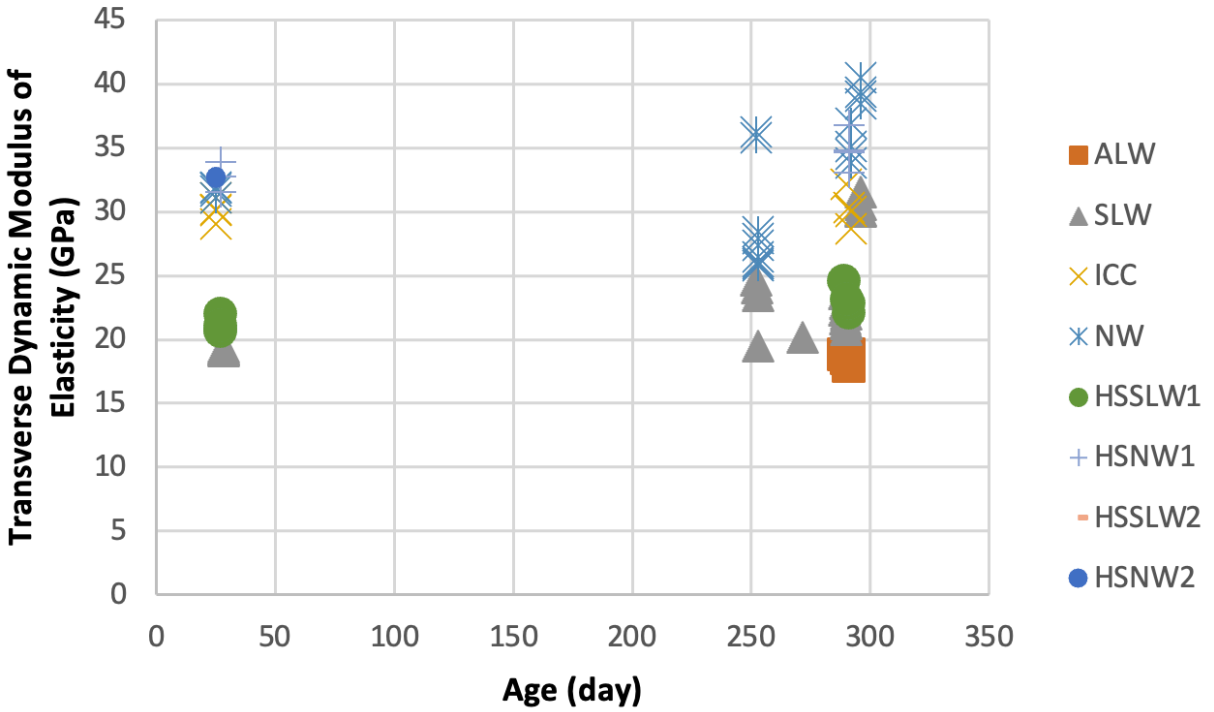

Figure 50. Torsional Dynamic Modulus of Elasticity and Compressive Strength of Concrete Specimens

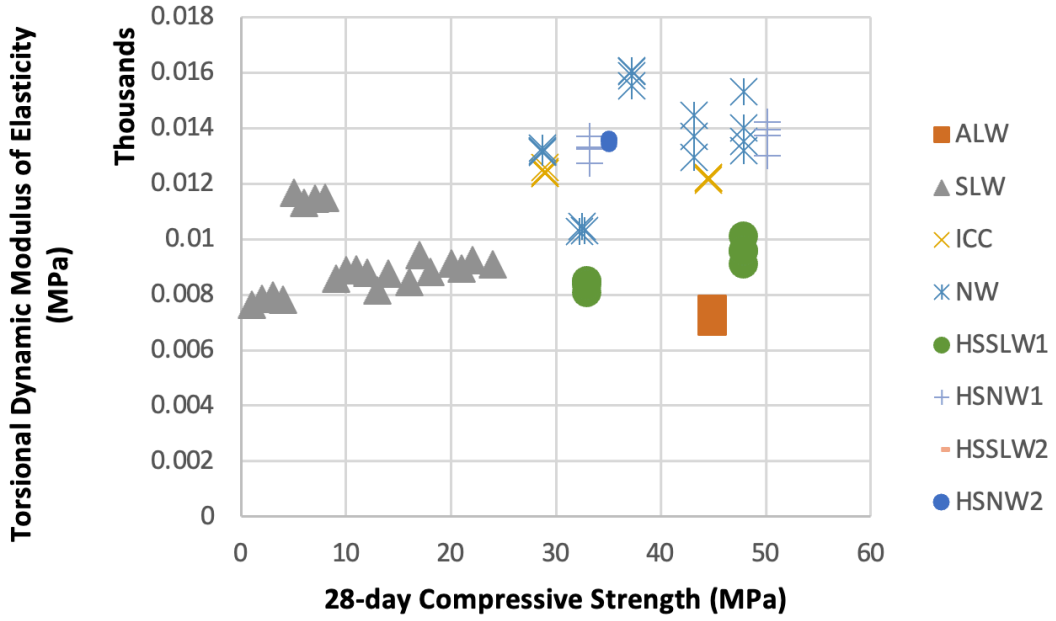

Figure 51. Torsional Dynamic Modulus of Elasticity and Density of Concrete Specimens

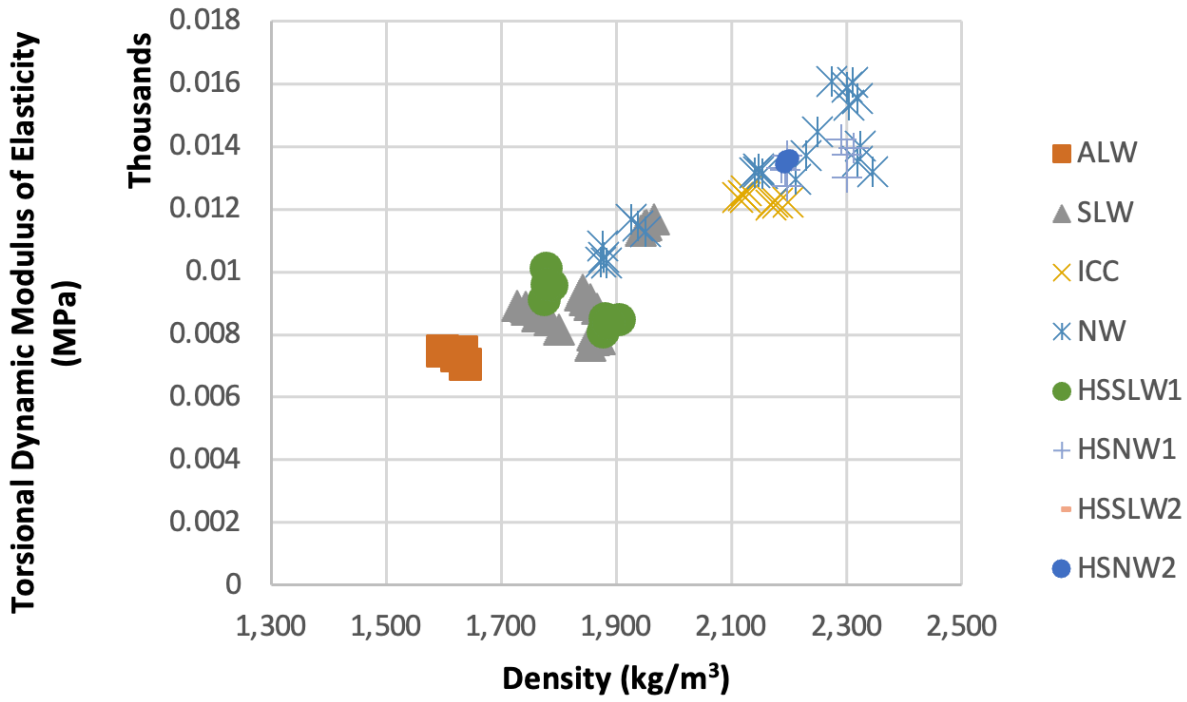

Figure 52. Torsional Dynamic Modulus of Elasticity and Age of Concrete Specimens

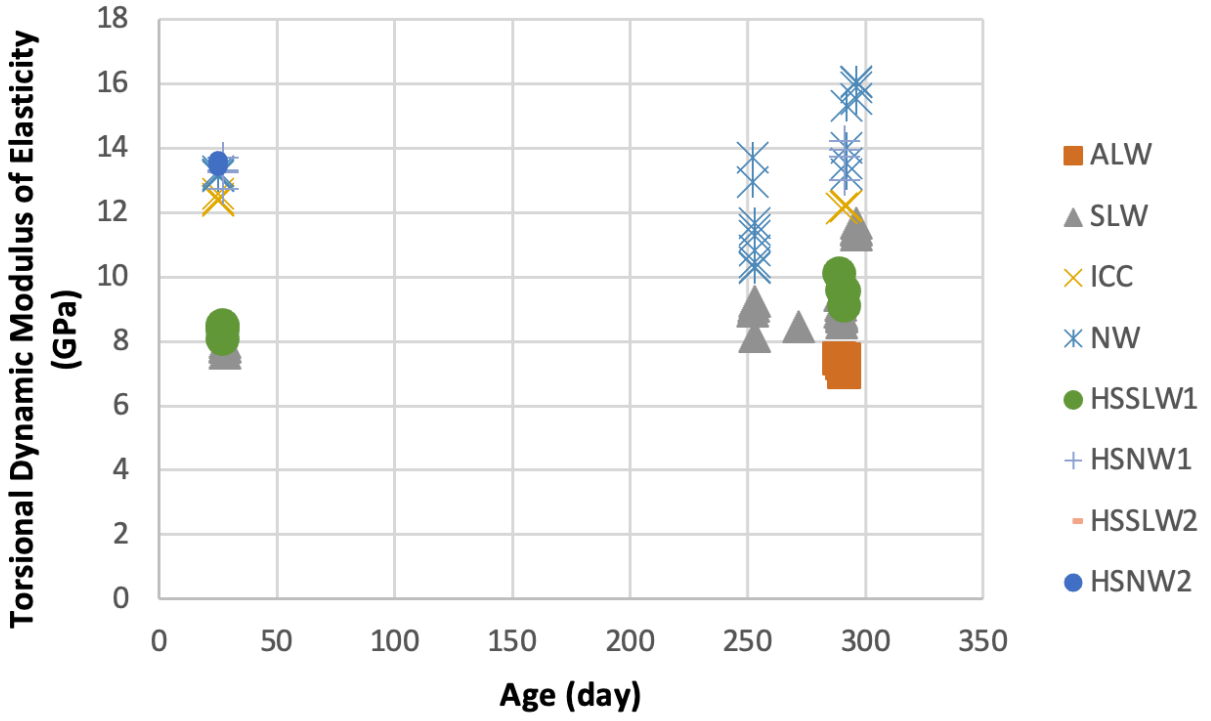

Figure 53 shows the dynamic Poisson's ratio of concrete specimens. Compared with static Poisson's ratios, these values also hint at a slight increase in Poisson's ratio for concrete containing lightweight aggregates, but less than those observed for the static ratios.

Figure 53. Dynamic Poisson's Ratios of Concrete Specimens

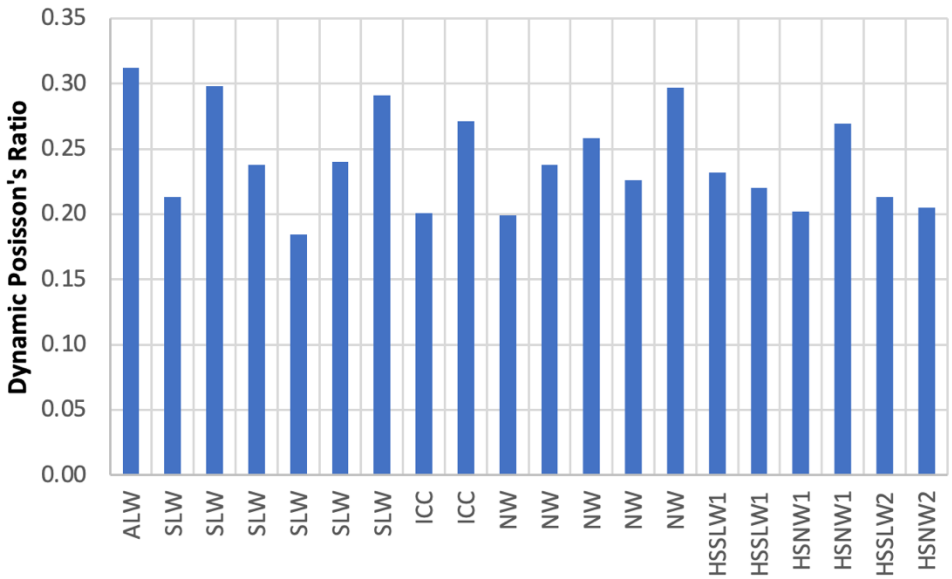

Figure 54 shows static and dynamic Poisson's ratios for concrete specimens. Observations indicate that the range of measured values from the dynamic method is between 0.18 and 0.31, which is considerably narrower than that from the static method. The digital approach to dynamic measures, as opposed to the analog approach to static measures, suggests that dynamic values may contain fewer occurrences of outliers and manual errors in the testing process. Otherwise, there is no evidence of consistent variations between static and dynamic values.

Figure 54. Static and Dynamic Poisson's Ratios of Concrete Specimens

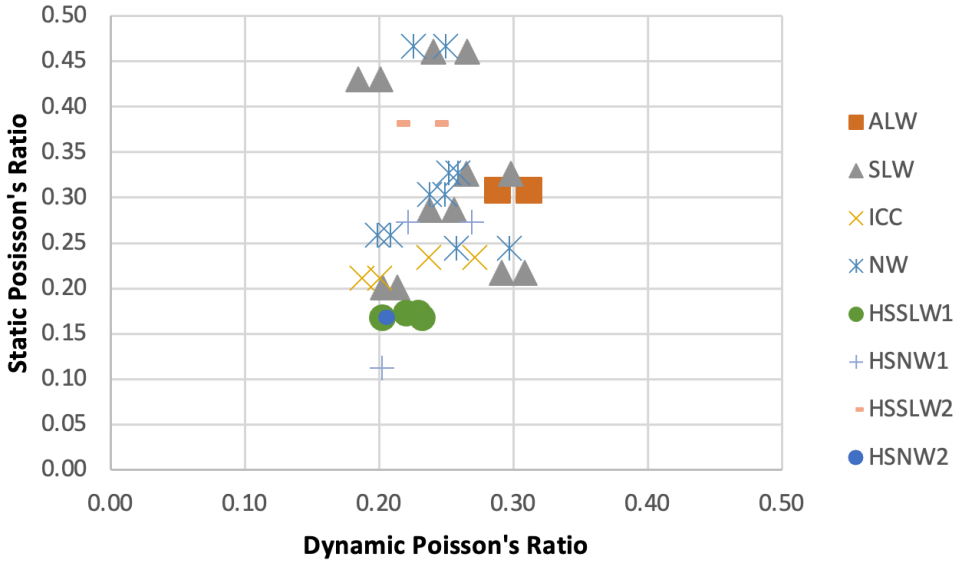

Figures 55, 56, and 57 illustrate the trends of dynamic Poisson's ratio with respect to compressive strength, density, and age of concrete specimens. These figures confirm prior observations that Poisson's ratio is independent of those measures.

Figure 55. Dynamic Poisson's Ratio and Compressive Strength of Concrete Specimens

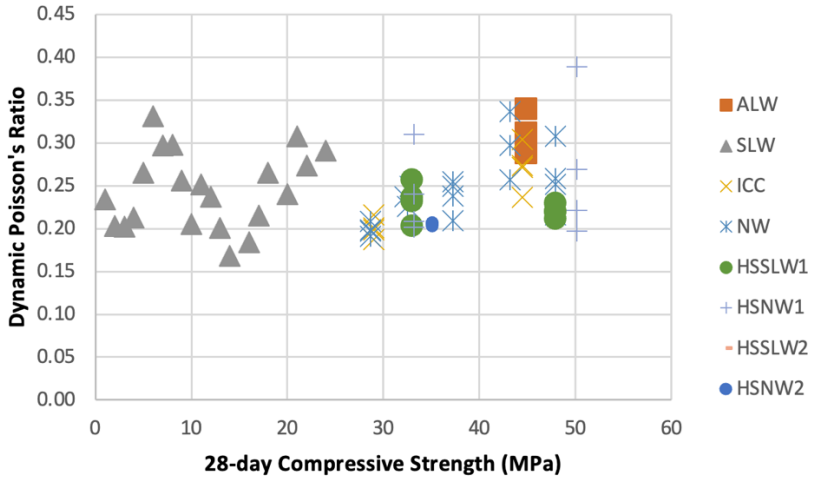

Figure 56. Dynamic Poisson's Ratio and Density of Concrete Specimens

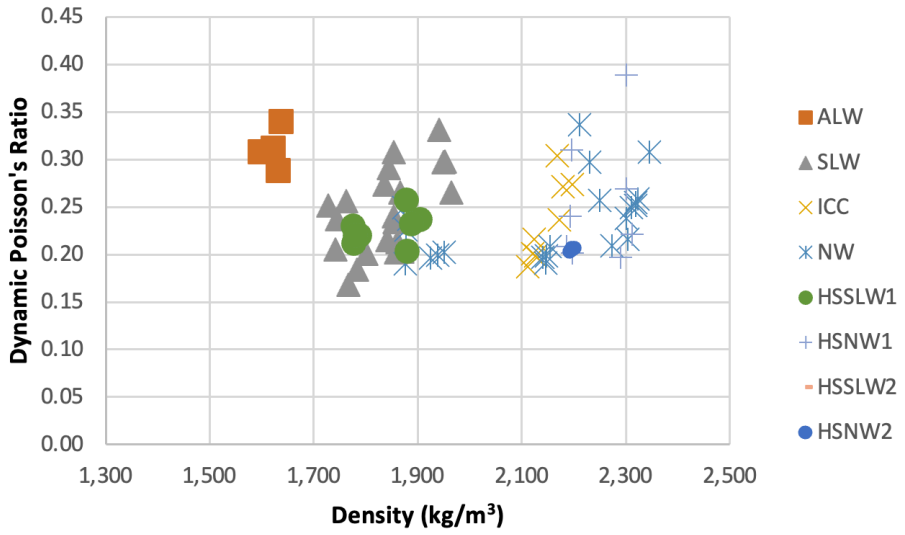

Figure 57. Dynamic Poisson's Ratio and Age of Concrete Specimens

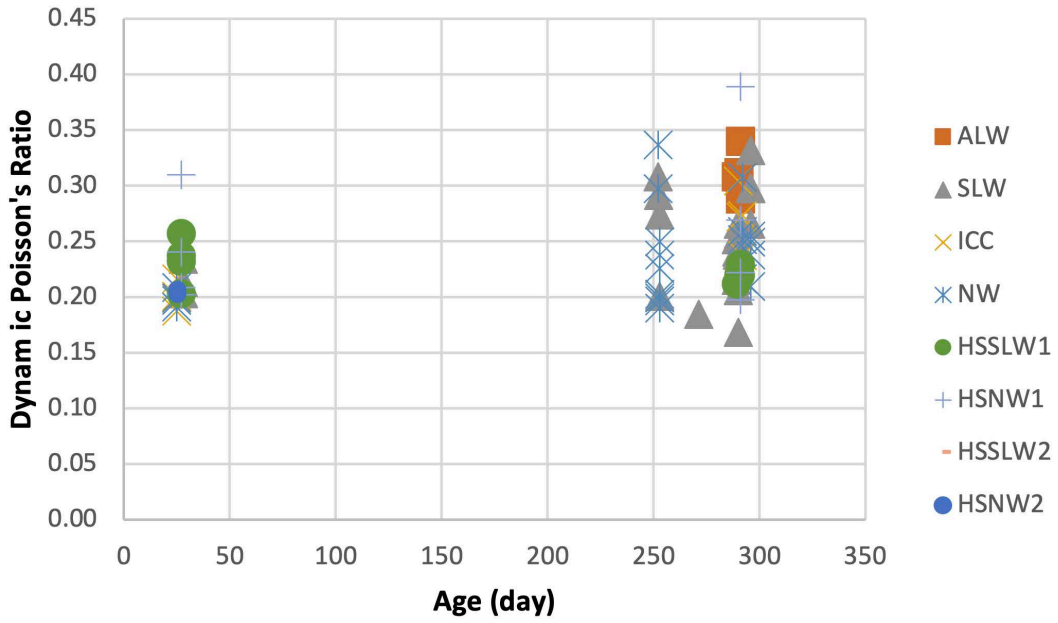

4.2 Service Life Prediction and Lifecycle Analyses

Service Life Prediction

Tehrani (2025) has provided service life predictions using experimental chloride diffusion coefficients following Fick's second law (Figure 58). Disregarding variations in logarithmic decay of diffusion during hydration years and climate characteristics of each location, a general trend

between predicted service life (SL) in years and reference diffusion coefficients (D_{28}) in m2/sec of investigated concrete specimens follows (Tehrani 2025):

$$SL = 8 \times 10^{-7} {D_{28}}^{-0.731} \qquad (30)$$

Figure 58. Service Life Prediction Using Diffusion Coefficient, Adopted from Tehrani (2025)

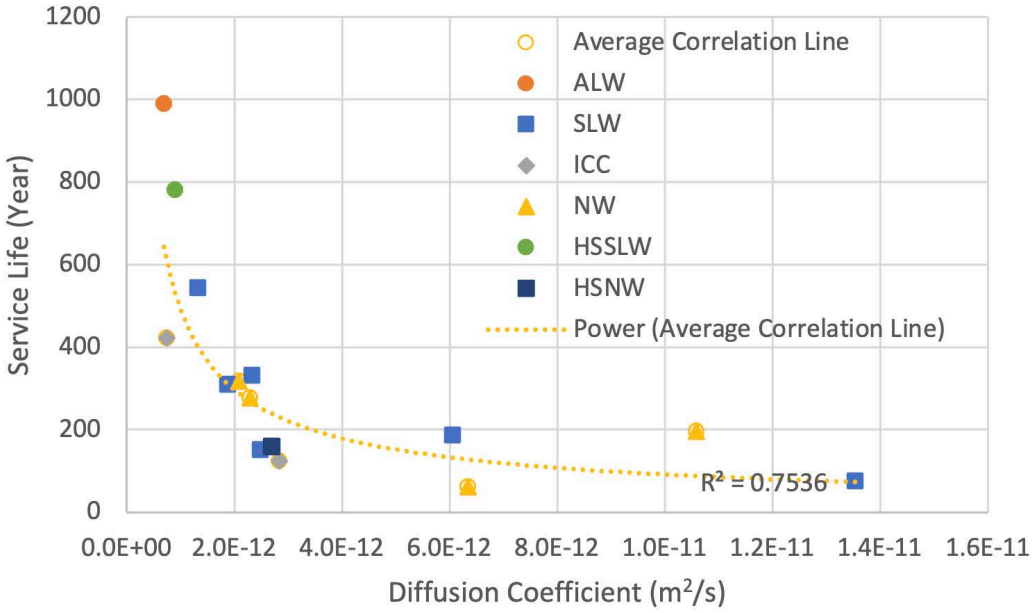

The referenced initial diffusion coefficient represents a homogeneous simulation of uncracked concrete. The diffusion coefficient at the crack is increased as a function of the crack width, leading to a higher efficient value representing the entire section of concrete (Kwon et al. 2009), as shown in Figure 59.

Figure 59. Crack Width Influence on the Diffusion Coefficient of Concrete

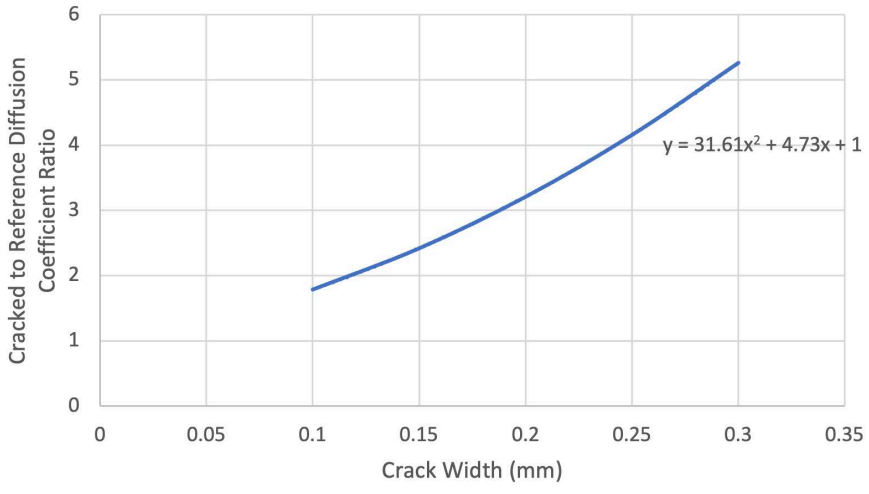

The static and dynamic moduli of elasticity govern the deformations induced by stationary and traffic loads, respectively. Concrete pavement and bridge deck surfaces primarily sustain dynamic loads. Still, bridge girders and other supporting elements are subject to a combination of static and dynamic loads, with dynamic loads accounting for nearly two-thirds of the total (Grubb et al. 2015). Further, the static modulus of elasticity can indirectly represent the stiffness of concrete at early ages and its contribution to associated deformations (Li and Han 2024). Table 12 summarizes the durability and mechanical properties of various concrete specimens.

Table 12. Service Life Prediction Parameters and Results

Concrete Mix	Diffusion Coefficient* (m^2/s)	Logarithmic Decay* Index	Static Modulus of Elasticity (GPa)	Dynamic Modulus of Elasticity (GPa)	Predicted Service Life (Year)
ALW	6.96E-13	0.639518	18.08	19.19	387
SLW	4.6E-12	0.586997	22.33	22.79	87
ICC	1.79E-12	0.44909	29.65	30.45	148
NW	5.33E-12	0.549901	33.23	33.47	59
HSSLW	8.95E-13	0.864436	17.26	20.56	330
HSNW	2.69E-12	0.446228	36.08	33.88	92

* Adapted from Tehrani (2025)

Lifecycle Assessment

Figure 60 demonstrates the trend of lifecycle cost versus predicted service life. This trend represents the initial costs of concrete surfaces obtained from lowest-bid records, along with a breakdown of the costs for materials, labor, and equipment. Maintenance, retrofit, and rehabilitation costs are based on predicted service life and associated durability factors for different mix designs. The trend suggests $LCUC$ in 2025's dollar per m^3 unit volume value as follows (Tehrani 2025):

$$LCUC = 2 \times 10^6 SL^{-1.038} \qquad (31)$$

Figure 60. Lifecycle Cost Using Service Life, Adopted from Tehrani (2025)

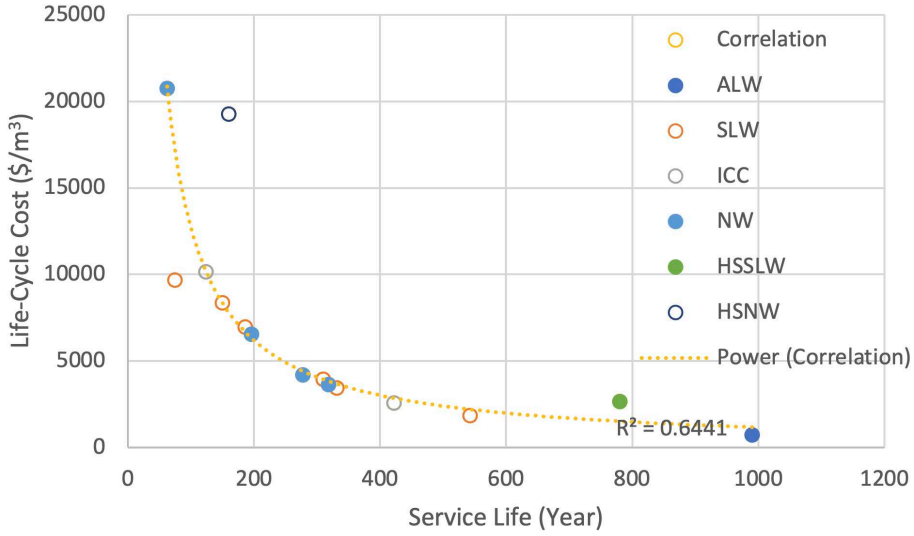

Figure 61 illustrates a similar trend of lifecycle emissions versus predicted service life. The general trend for global warming potential (GWP) in kg CO_2 equivalent per m^3 unit volume follows (Tehrani 2025):

$$LCGWP = 1.35 \times 10^5 SL^{-0.894} \qquad (32)$$

Figure 61. Lifecycle Global Warming Potential Using Predicted Service Life, Adopted from Tehrani (2025)

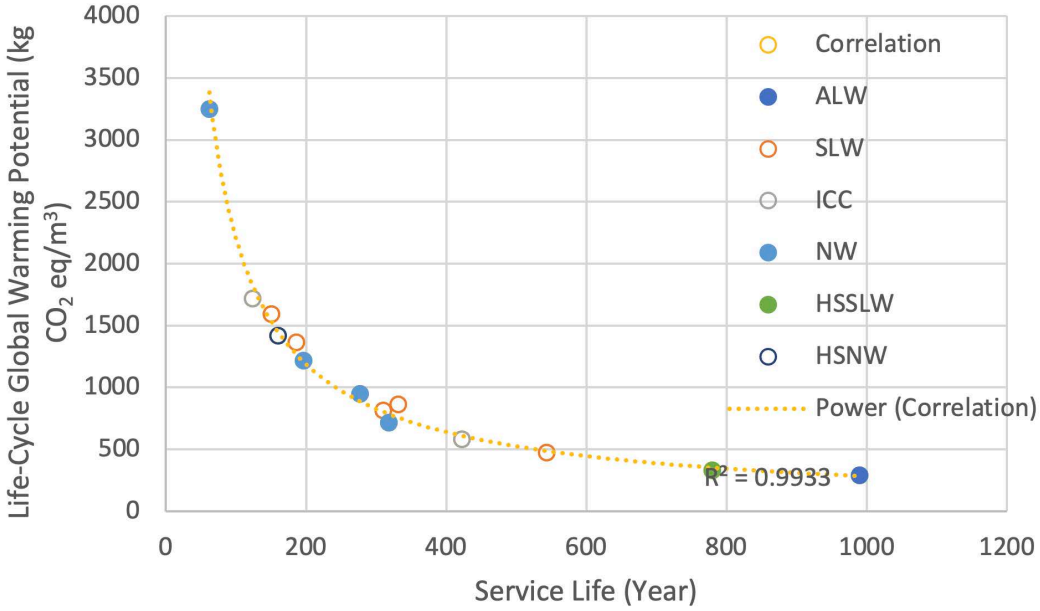

Table 13 shows the results of lifecycle cost and emission analyses per unit volume of concrete. Comparing these values for concrete containing lightweight aggregates and normalweight witness samples indicates that fine lightweight aggregates make a greater contribution to reducing costs and emissions, as a direct result of extended service life. This observation is evident in comparing ICC and ALW, with partial and complete replacement of fine aggregates, respectively, with SLW and HSSLW, with no fine lightweight aggregates, as opposed to NW and HSNW.

Table 13. Lifecycle Analysis Results

Concrete Mix	Cost ($/m^3)	Global Warming Potential (kg-CO_2/m^3)
ALW	4116	657
SLW	19'408	2497
ICC	11'517	1593
NW	28'845	3513
HSSLW	4868	759
HSNW	18'402	2385

5. Summary & Conclusions

5.1 Summary

Scope of Study

The study comprehensively evaluates the mechanical properties, durability, and lifecycle performance of lightweight aggregate concrete and internally cured concrete for transportation applications.

Experimental and Analytical Approach

Experimental investigations examined stress–strain behavior, modulus of elasticity, splitting tensile strength, Poisson's ratio, and their interactions with cracking processes such as early-age shrinkage and with durability indicators such as chloride penetration and electrical resistivity. Analytical modeling predicted service life using chloride-diffusion models and assessed lifecycle costs and environmental impacts through lifecycle assessment.

Findings

Experimental investigations confirmed that all tested LWC and ICC mixes exceeded their target compressive strengths. The modulus of elasticity of LWC was consistently lower than that of NWC, reducing internal stresses and mitigating cracking under restraint and dynamic loads. Splitting tensile strengths of LWC and ICC exceeded the expected values prescribed by design codes, and Poisson's ratio trends indicated improved deformation compatibility for lightweight mixes.

Durability assessments demonstrated that LWC and ICC exhibit superior resistance to chloride penetration, a critical property for bridge decks and pavements exposed to deicing salts and marine environments. Service life predictions using Fick's second law confirmed that high-strength sand-lightweight concrete can last nearly five times longer than NWC under similar exposure conditions. A lifecycle cost analysis revealed that LWC offers significant savings over time, driven by reduced maintenance and extended service life. Environmental assessments showed that LWC substantially reduces greenhouse gas emissions, reinforcing its role in sustainable infrastructure development.

The research also identified limitations in current design codes, which underestimate the modulus of elasticity and require unnecessary reduction factors for lightweight concrete. Revised empirical models and updated specifications are recommended to reflect the actual performance of modern lightweight concretes. Case studies of bridge applications validated these findings, demonstrating reliable performance, reduced dead load, and predictable creep and shrinkage behavior.

5.2 Conclusions

Structural Efficiency

Lightweight aggregate concrete and internally cured concrete provide significant benefits for transportation infrastructure by reducing dead loads, improving seismic resilience, and mitigating cracking. These properties make them structurally efficient alternatives to normal-weight concrete.

Durability and Sustainability

Internally cured LWC enhances resistance to environmental stressors, thereby extending service life and reducing maintenance costs. Lifecycle assessment confirms that these materials substantially reduce greenhouse gas emissions, supporting sustainability goals.

Economic Feasibility

The long-term economic benefits of LWC and ICC outperform those of NWC due to reduced maintenance and extended service life.

Design Recommendations

The study recommends updating design codes to incorporate revised equations for the modulus of elasticity and to eliminate unnecessary reduction factors for LWC. Broader adoption of these materials aligns with federal initiatives and sustainability objectives, making them a practical and environmentally responsible choice for modern transportation infrastructure.

5.3 Further Research

While this study provides insight into the mechanical and service-life-related performance of lightweight concrete, further research is warranted to confirm and extend these findings. Experimental validation under varying aggregate types, mixture proportions, and environmental exposure conditions would help assess the robustness of the observed trends. In particular, future work may investigate the influence of cracking, cyclic loading, and long-term durability mechanisms on material performance, which were beyond the scope of the present study.

Additionally, the results of this research may be applicable to a wider range of civil infrastructure systems beyond transportation infrastructure. Potential applications include building structures, marine and coastal facilities, and energy-related infrastructure, where reduced self-weight, improved durability, or enhanced service life is desirable. Further studies evaluating constructability, structural performance, and life-cycle sustainability in these contexts would support broader adoption of lightweight concrete materials.

5.4 Challenges and Limitations

Despite the demonstrated benefits of lightweight aggregate concrete and internally cured concrete for transportation infrastructure, several challenges may limit their widespread adoption. Conservative design practices and limited contractor familiarity may lead practitioners to favor more traditional concrete materials. However, many of these concerns may be mitigated as experience with lightweight concrete continues to grow, and advancements in design guidance and construction practices may further reduce barriers to implementation.

Bibliography

Standards and Specifications

AASHTO T 277-23. 2023. Rapid Determination of the Chloride Permeability of Concrete, *Standard Specification for Transportation Materials and Methods of Sampling and Testing*. Washington, CD: American Association of State Highway and Transportation Officials.

AASHTO T 358-22. 2022. Surface Resistivity Indication of Concrete's Ability to Resist Chloride Ion Penetration, *Standard Specification for Transportation Materials and Methods of Sampling and Testing*. Washington, CD: American Association of State Highway and Transportation Officials.

ACI 213-14. 2023. *Guide for Structural Lightweight-Aggregate Concrete*, ACI PRC-213R-14(23). Farmington Hill, MI: American Concrete Institute.

ACI 231-10. 2020. *Report on Early-Age Cracking: Causes, Measurement and Mitigation,* ACI PRC-231-10(20). Farmington Hill, MI: American Concrete Institute.

ACI 308R-16. 2016. *Guide to External Curing of Concrete, ACI PRC-308R-16*. Farmington Hill, MI: American Concrete Institute.

ACI 308-213-13(22). 2022. *Report on Internally Cured Concrete Using Pre-wetted Absorptive Lightweight Aggregate*, ACI PRC-308-213-13(22). Farmington Hill, MI: American Concrete Institute.

ACI 318/318M-19(22). 2022, *Building Code Requirements for Structural Concrete and Commentary.* Farmington Hills, MI: American Concrete Institute.

ACI 363R-10, 2010. *Report on High-Strength Concrete*. ACI 363R-10. American Concrete Institute, Farmington Hills, MI.

ABNT, 2008. NBR 8522: Concreto – Determinação do Módulo Estático de Elasticidade à Compressão. Rio de Janeiro: Associação Brasileira de Normas Técnicas.

ASTM C31/C31M-25b. 2025. *Standard Test Practice for Making and Curing Concrete Test Specimens in the Field.* West Conshohocken, PA: American Society for Testing and Materials.

ASTM C33/C33M-18. 2023. *Standard Specification for Concrete Aggregates*. West Conshohocken, PA: American Society for Testing and Materials.

ASTM C39/C39M-24. 2024. *Standard Test Method for Compressive Strength of Cylindrical Concrete Specimens*. West Conshohocken, PA: American Society for Testing and Materials.

ASTM C138/C138M-24a. 2024. Standard Test Method for Density (Unit Weight), Yield, and Air Content (Gravimetric) of Concrete. West Conshohocken, PA: American Society for Testing and Materials.

ASTM C143/C143M-20. 2020. *Standard Test Method for Slump of Hydraulic-Cement Concrete.* West Conshohocken, PA: American Society for Testing and Materials.

ASTM C192/C192M-25. 2025. *Standard Practice for Making and Curing Concrete Test Specimens in the Laboratory*. West Conshohocken, PA: American Society for Testing and Materials.

ASTM C215-19. 2020. Standard Test Method for Fundamental Transverse, Longitudinal, and Torsional Resonant Frequencies of Concrete Specimens. West Conshohocken, PA: American Society for Testing and Materials.

ASTM C231/C231M-25. 2025. *Standard Test Method for Air Content of Freshly Mixed Concrete by the Pressure Method.* West Conshohocken, PA: American Society for Testing and Materials.

ASTM C330/C330M-23. 2023. *Standard Specification for Lightweight Aggregates for Structural Concrete.* West Conshohocken, PA: American Society for Testing and Materials.

ASTM C469-22. 2022. Standard Test Method for Static Modulus of Elasticity and Poisson's Ratio of Concrete in Compression. West Conshohocken, PA: American Society for Testing and Materials.

ASTM C496/C496M-17. 2017. *Standard Test Method for Splitting Tensile Strength of Cylindrical Concrete Specimens.* West Conshohocken, PA: American Society for Testing and Materials.

ASTM C567/C567M-19. 2019. *Standard Test Method for Determining Density of Structural Lightweight Concrete.* West Conshohocken, PA: American Society for Testing and Materials.

ASTM C597-22. 2023. *Standard Test Method for Ultrasonic Pulse Velocity Through Concrete.* West Conshohocken, PA: American Society for Testing and Materials.

ASTM C1202-25. 2025. Standard Test Method for Electrical Indication of Concretes Ability to Resist Chloride Ion Penetration. West Conshohocken, PA: American Society for Testing and Materials.

ASTM C1760-12. 2012. *Standard Test Method for Bulk Electrical Conductivity of Hardened Concrete.* West Conshohocken, PA: American Society for Testing and Materials.

ASTM C1761/C1761M-23. 2023. *Standard Specification for Lightweight Aggregate for Internal Curing of Concrete.* West Conshohocken, PA: American Society for Testing and Materials.

ASTM C1876-25. 2025. Standard Test Method for Bulk Electrical Resistivity or Bulk Conductivity of Concrete. West Conshohocken, PA: American Society for Testing and Materials.

ISO 14025. 2006. Environmental labels and declarations — Type III environmental declarations — Principles and procedures. Vernier (Geneva), Switzerland: International Standard Organization (ISO).

Authored References

AASHTO. 2015, *LRFD Bridge Design Specifications*. Washington, DC: American Association of State Highway and Transportation Officials.

ACCO. 2004. *The applied cost analysis of construction works*. [in Persian]. Tehran, Iran: Association of Construction Companies. acco.ir.

Ahmad, S. H., and S. P. Shah. 1982. "Stress-Strain Curves of Concrete Confined by Spiral Reinforcements." *ACI Journal, Proceedings* 79 (6): 484–490. https://doi.org/10.14359/10922.

Ashrafi, E., and M. Farzam. 2021. "Experimental Investigation on the Triaxial Behavior of Lightweight Concrete." *Construction and Building Materials* 312: 125348. https://doi.org/10.1016/j.conbuildmat.2021.125348.

Bentz, Dale P., Pietro Lura, and John W. Roberts. 2005. "Mixture Proportioning for Internal Curing." *Concrete International* 27 (2): 35–40.

Bjerkeli, L., Tomaszewicz, A., and Jensen, J. J., (1990), "Deformation Properties and Ductility of High-Strength Concrete", Proceedings o f the Second International Symposium on Utilization o f High-Strength Concrete, University of California, Berkeley, May 20-23, pp. 215-238.

Bogas, J. A., M. G. Gomes, and S. Real. 2014. "Bonding of Steel Reinforcement in Structural Expanded Clay Lightweight Aggregate Concrete." *Construction and Building Materials* 65: 350–359. https://doi.org/10.1016/j.conbuildmat.2014.04.122.

Bonifácio, A. L., J. C. Mendes, M. C. R. Farage, F. S. Barbosa, and A. L. Beaucour. 2020. "Predicting the Mechanical Properties of Lightweight Aggregate Concrete Using Finite Element Method." *Revista IBRACON de Estruturas e Materiais* 13 (4): e13410. https://doi.org/10.1590/S1983-41952020000400010.

Bonyadi, M., Ali-Akbar Shakeri, Abbas Navidkia, Mohammad-Ali Dastan Diznab, and Fariborz M. Tehrani. 2022. "Assessing the Curing Time Effect on Compressive Strength of Structural Concrete." In *Proceedings of the Eight National Conference on Applied Research in Civil Engineering, Architecture and Urban Management*, Tehran, February 16, 2022. https://civilica.com/doc/1479219.

Bonyadian, Sara, Makan Mohammadi, Babak Foroutanmehr, and Fariborz M. Tehrani. 2019. "An Experimental Investigation of Internally-Cured Concrete Application for Bridge Decks." In *Proc. The Fifth International Conference on Bridges*, Tehran: Amirkabir University of Technology, December 17–18, 2019: MS02. http://ibc.aut.ac.ir.

Bonyadian, Sara, Makan Mohammadi, Babak Foroutanmehr, Arsalan Ghofrani, and Fariborz M. Tehrani. 2024. "An Experimental Investigation of Internally Cured Concrete Using Palletized Lightweight Expanded Clay Aggregates." In *Engineering Mechanics Institute Conference and Probabilistic Mechanics & Reliability Conference (EMI/PMC 2024)*, Urbana-Champaign, Chicago, IL: University of Illinois, May 28–31, 2024. Paper EP241182.

Brown III, W. R., Torbjorn J. Larsen, and Thomas A. Holm. 1995. "Long-Term Service Performance of Lightweight Concrete Bridge Structures." In *International Symposium on Structural Lightweight Aggregate Concrete*. https://www.escsi.org/wp-content/uploads/2017/10/4700.5-Long-Term-Service-Performance-of-LWC-Bridge-Structures.pdf.

BSI. 1985. BS 8110-2: Structural Use of Concrete – Part 2: Code of Practice for Special Circumstances. London: British Standards Institution.

Byard, Benjamin E., and Anton K. Schindler. 2010. "Cracking Tendency of Lightweight Concrete." Highway Research Center, Auburn University, Auburn, AL. https://www.escsi.org/wp-content/uploads/2017/10/ESCSI-Final-Report-Auburn-University.pdf.

Caltrans. 2007. "Contract Cost Data." State of California. https://sv08data.dot.ca.gov/contractcost/. Accessed January 28, 2025.

Castrodale, Reid. 2021. *Lightweight Concrete Bridge Design Primer*. No. FHWA-HIF-19-067. United States. Federal Highway Administration. Office of Bridges and Structures, 2021.

Chapman, D. D., and R. W. Castrodale. 2016. "Sand Lightweight Concrete for Prestressed Concrete Girders in Three Washington State Bridges." In *Proceedings of the PCI/NBC 2016*.

Costa, H., R. N. F. Carmo, and E. Júlio. 2018. "Influence of Lightweight Aggregates Concrete on the Bond Strength of Concrete-to-Concrete Interfaces." *Construction and Building Materials* 180: 519–530.

Cousins, T., C. Roberts-Wollmann, and M. C. Brown. 2013. *High-Performance/High-Strength Lightweight Concrete for Bridge Girders and Decks*. NCHRP Report 733. Washington, DC: Transportation Research Board.

Cowan, H. J. 1956. "Discussion on Concrete Stress Distribution in Ultimate Strength Design." *Journal of the American Concrete Institute, Proceedings* 52 (Part 2).

CRSI. 2017. "Environment Product Declaration." Schaumburg, IL: Concrete Reinforcing Steel Institute.

Cui, H. Z., T. Y. Lo, S. A. Memon, and W. Xu. 2012a. "Effect of Lightweight Aggregates on the Mechanical Properties and Brittleness of Lightweight Aggregate Concrete." *Construction and Building Materials* 35: 149–158. https://doi.org/10.1016/j.conbuildmat.2012.02.053.

Cui, H. Z., T. Y. Lo, S. A. Memon, F. Xing, and X. Shi. 2012b. "Analytical Model for Compressive Strength, Elastic Modulus and Peak Strain of Structural Lightweight Aggregate Concrete." *Construction and Building Materials* 36: 1036–1043. https://doi.org/10.1016/j.conbuildmat.2012.06.034.

Cui, H. Z., T. Y. Lo, S. A. Memon, F. Xing, and X. Shi. 2012c. "Experimental Investigation and Development of Analytical Model for Pre-Peak Stress–Strain Curve of Structural Lightweight Aggregate Concrete." *Construction and Building Materials* 36: 845–859. https://doi.org/10.1016/j.conbuildmat.2012.06.041.

Davodijam, Fateme, Mohammad Ali Dastan Diznab, and Fariborz M. Tehrani. 2022. "Sustainability Rating of Internally Cured Concrete in Marine Environments Using Service Life Prediction Models." In *Proc. ASCE Int. Conf. on Sustainable Infrastructure 2021: Leveraging Sustainable Infrastructure for Resilient Communities*, edited by M. F. Bloom and K. R. Reddy, 141–151. https://doi.org/10.1061/9780784483879.013.

Deng, Y., B. Phares, and D. Harrington. 2016. *Causes of Early Cracking in Concrete Bridge Decks*. The Long-Term Plan for Concrete Pavement Research and Technology (CP Road Map).

Dhungel, S., A. Bahadori, D. Darwin, M. O'Reilly, and K. Truman. 2024. *Evaluation of Cracking Performance of Bridge Decks With and Without Overlays and With and Without Fibers*. University of Kansas Center for Research, Inc.

Diógenes, H. J. F., L. C. Cossolino, A. H. A. Pereira, M. K. El Debs, and A. L. H. C. El Debs. 2011. "Determination of Modulus of Elasticity of Concrete from the Acoustic Response." *IBRACON Structures and Materials Journal* 4 (5): 792–813.

Du, Y., H. Qi, J. Jiang, and J. Y. R. Liew. 2022. "Experimental Study on the Dynamic Behaviour of Expanded-Shale Lightweight Concrete at High Strain Rate." *Materials and Structures* 55 (4). https://doi.org/10.1617/s11527-021-01846-z.

Ehlen, Mark A., and Anthony N. Kojundic. 2014. "Life-365 v2.2 – Adding user estimates of chloride exposure." *Concrete International* 36 (5): 41–44.

Ehlen, Mark A., Michael D. A. Thomas, and Evan C. Bentz. 2009. "Life-365 Service Life Prediction Model™ Version 2.0." *Concrete International* 31 (5): 41–46.

El-Dash, K. M. 1995. Strength and Ductility of Confined High-Strength Lightweight Aggregate Concrete Columns. PhD diss., North Carolina State University.

EPD. 2021. "What Is an EPD?" Environmental Product Declarations. The International EPD System. https://www.environdec.com/all-about-epds/the-epd (accessed 2025).

ESCSI. 2006. "Internal Curing Using Expanded Shale, Clay and Slate Lightweight Aggregate." ESCSI 4362.0. Chicago, IL: Expanded Shale, Clay and Slate Institute. https://www.escsi.org/wp-content/uploads/2017/10/4362.0-Internal-Curing-Using-ESCS-LWA-1.pdf.

ESCSI. 2024a. "Embodied Energy to Manufacture Expanded Shale, Clay and Slate (ESCS) Lightweight Aggregate." Information Sheet 9153. Chicago, IL: Expanded Shale, Clay and Slate Institute.

ESCSI. 2024b. "Freeze-Thaw Durability of Structural Lightweight Concrete Made with ESCS Aggregates." Information Sheet 7900.093-2024. Chicago, IL: Expanded Shale, Clay and Slate Institute.

FHWA. 2023. "EDC-7 Innovations (2023–2024)." U.S. Department of Transportation, Federal Highway Administration. https://www.fhwa.dot.gov/innovation/everydaycounts.

FHWA. 2024. "Innovation of the Month: Enhancing Performance with Internally Cured Concrete." *EDC News* (June 27, 2024). Washington, DC: U.S. Department of Transportation, Federal Highway Administration. https://doi.org/10.21949/1521785.

Fluge, Finn, and A. Blankvoll. 1995. "Chloride Exposure on Gimsøystraumen Bridge—Results from Extended Condition Survey." In *Nordic Mini Seminar on Field Measurements for Modelling Service Life—Reinforcement Corrosion*, 131–41. Lund: Lund Institute of Technology.

Furouhi, Fereidun, Fariborz M. Tehrani, and Amid Zand. 1996. "Two Macro-Economic Viewpoints on Light Concrete Application Effect on National Economic Development." [in Persian]. *Ravesh* [Industrial Engineering, in Persian] 6 (35): 9–11.

Frosch, R. J. 1999. "Another Look at Cracking and Crack Control in Reinforced Concrete." *ACI Structural Journal* 96 (3): 437–442. https://doi.org/10.14359/630.

Frosch, Robert J., David T. Blackman, and Roger D. Radabaugh. 2003. *Investigation of Bridge Deck Cracking in Various Bridge Superstructure Systems*. FHWA/IN/JTRP-2002/25. West Lafayette, IN: Joint Transportation Research Program. https://doi.org/10.5703/1288284313257.

Gerami, Mahmoud A., Fariborz M. Tehrani, and Alireza N. Esfahani. 2007. *A Comprehensive Guide to LECA in Agriculture*. [in Persian]. Tehran, Iran: Omīdān. https://leca.ir/wp-content/uploads/maghalat/Aggriculture%20book%2088.pdf.

Gergely, Peter, and LeRoy A. Lutz. 1968. "Maximum Crack Width in Reinforced Concrete Flexural Members." *ACI Special Publication* 20: 87–117. https://doi.org/10.14359/17348.

Ghavami, Nava. 2022. Assessing the Design Strength Modification Factors for Rotary-Kiln Produced Expanded Aggregates. Master's thesis, California State University, Fresno.

Ghavami, Nava, Kianoush Kadkhodaie, Sara Kalantari, and Fariborz M. Tehrani. 2024. "Assessing the Variability of Lightweight Concrete Inter- and Intra-Rater Design Parameters Concerning Aggregate Sources." In *Proceedings of the 1st International Conference on the Exchange of Scientific Information in the Fields of Concrete Structures and Materials (IC Concrete)*, Tehran, Iran, May 6–7, 2024, 1029:1–9. https://civilica.com/doc/1994518.

Graybeal, Benjamin A., and Gary Greene. 2015. "FHWA Research Program on Lightweight High-Performance Concrete – Shear Performance of Prestressed Girders." *PCI National Bridge Conference*, Salt Lake City, Utah.

Greene, Gary, and Benjamin A. Graybeal. 2013. *Lightweight Concrete: Mechanical Properties*. FHWA-HRT-13-062. Washington, DC: Federal Highway Administration. https://rosap.ntl.bts.gov/view/dot/49980.

Grubb, Michael A., Kenneth E. Wilson, Christopher D. White, and William N. Nickas. 2015. *Load and Resistance Factor Design (LRFD) for Highway Bridge Superstructures: Reference Manual*. FHWA-NHI-15-047. Washington, DC: National Highway Institute. https://rosap.ntl.bts.gov/view/dot/43721.

Hadidi, R., and M. A. Saadeghvaziri. 2005. "Transverse Cracking of Concrete Bridge Decks: State-of-the-Art." *Journal of Bridge Engineering* 10 (5): 503–510. https://doi.org/10.1061/(ASCE)1084-0702(2005)10:5(503).

Han, B., and T.-Y. Xiang. 2017. "Axial Compressive Stress-Strain Relation and Poisson Effect of Structural Lightweight Aggregate Concrete." *Construction and Building Materials* 146: 338–343. https://doi.org/10.1016/j.conbuildmat.2017.04.101.

Han, F., D. H. Dan, and H. Wang. 2018. "A Study on Dynamic Amplification Factor and Structure Parameter of Bridge Deck Pavement Based on Bridge Deck Pavement Roughness." *Advances in Civil Engineering* 2018: 9810461. https://doi.org/10.1155/2018/9810461.

Hassan, M., and L. Amleh. 2025. "Influence of Various Crack Widths in RC Bridge Decks on the Initiation of Chloride-Induced Corrosion." *Journal of Composites Science* 9 (5): 242. https://doi.org/10.3390/jcs9050242.

Hassanain, Mostafa A. 2010. "The New Sitra Bridges." *Concrete International* 32 (9): 38–45.

Helland, Steinar. 2005. "Lightweight Aggregate Concrete in Norwegian Bridges." *HPC Bridge Views*, 1–38. https://www.escsi.org/wp-content/uploads/2017/10/4700.10-Lightweight-Aggregate-Concrete-in-Norwegian-Bridges.pdf.

Henkensiefken, Ryan. 2008. "Internal Curing in Cementitious Systems Made Using Saturated Lightweight Aggregate." Master's thesis, Purdue University.

Henriksen, C. F., and E. Stoltzner. 1993. "Chloride Corrosion in Danish Road-Bridge Columns." *Concrete International* 15 (8): 55–60.

Hognestad, Eivind, N. W. Hanson, and Douglas McHenry. 1955. "Concrete Stress Distribution in Ultimate Strength Design." *Journal of the American Concrete Institute* 52 (12): 455–480. Portland Cement Association Bulletin D6A. https://doi.org/10.14359/11609.

Holm, Thomas A. 1980. "Performance of Concrete in Marine Environment." In *ACI Special Publication* 65: International Symposium, Canada Centre for Mineral and Energy Technology. https://doi.org/10.14359/14117.

Holm, Thomas A., and J. P. Ries. 2007. Reference Manual for the Properties and Applications of Expanded Shale, Clay and Slate Lightweight Aggregate. Chicago, IL: Expanded Shale, Clay, and Slate Institute.

Holm, Thomas A., and Theodore W. Bremner. 2000. State-of-the-Art Report on High-Strength, High-Durability Structural Low-Density Concrete for Applications in Severe Marine Environments. ERDC/SL TR-00-3. Washington, DC: U.S. Army Corps of Engineers, Engineer Research and Development Center. https://www.escsi.org/wp-content/uploads/2017/10/4710.4-USACE-State-of-the-Art-Report.pdf.

Hopper, Travis, Amir Manafpour, Gordon Warn, Farshad Rajabipour, Dennis Morian, Shervin Jahangirnejad, and David Thomas. 2015. *Bridge Deck Cracking: Effects on In-Service Performance, Prevention, and Remediation*. FHWA-PA-2015-006-120103. Pennsylvania Department of Transportation, Bureau of Planning and Research. https://rosap.ntl.bts.gov/view/dot/29302.

Hoyt, P. M. 1961. "Load-Deflection Relationships in Lightweight Aggregate Concrete." Master's thesis, University of Wyoming.

Hruban, Konrad E. 1956. "Discussion on Concrete Stress Distribution in Ultimate Strength Design." *Journal of the American Concrete Institute* 52 (Part 2): 1305–1330. https://doi.org/10.14359/11609.

Ivey, Don L., and Eugene Buth. 1967. "Shear Capacity of Lightweight Concrete Beams." *ACI Journal* 64 (10): 634–643. https://doi.org/10.14359/19118.

Jensen, Vernon P. 1943. *Ultimate Strength of Reinforced Concrete Beams as Related to the Plasticity Ratio of Concrete*. Bulletin No. 345. Urbana, IL: University of Illinois Engineering Experiment Station. https://hdl.handle.net/2142/4399.

Kaar, Paul H., and Alan H. Mattock. 1963. "High Strength Bars as Concrete Reinforcement—Part 4: Control of Cracking." *Journal of the PCA Research and Development Laboratories* 5 (1): 15–38.

Kaar, Paul H., N. W. Hanson, and H. T. Capell. 1977. "Stress-Strain Characteristics of High-Strength Concrete." *ACI Symposium Paper* 55: 161–186. https://doi.org/10.14359/6613.

Kadkhodaie, Kianoush, Sara Kalantari, Nava Ghavami, and Fariborz M. Tehrani. 2024. "Statistical Analysis of Structural Lightweight Aggregate Concrete Modification Factors." In *Proceedings of the 1st International Conference on the Exchange of Scientific Information in the Fields of Concrete Structures and Materials (ICConcrete)*, Tehran, Iran, May 6–7, 2024, 1028: 1–10. https://civilica.com/doc/1994519.

Kalantari, Sara, and Fariborz M. Tehrani. 2021. "Enhancing the Resilience of Concrete Pavements Using Service Life Prediction Models." In *Proceedings of the ASCE International Airfield & Highway Pavements Conference: Pavement Design, Construction, and Condition Evaluation*, edited by Hasan Ozer, Jeb S. Rushing, and Zhanping Leng, 178–185. Austin, TX: Transportation & Development Institute of ASCE. https://doi.org/10.1061/9780784483503.018.

Kalantari, Sara, and Fariborz M. Tehrani. 2022. "Performance-Based Specifications for the Enhancement of Service-Life and Durability of Concrete Infrastructures." In *Proceedings of the ASCE Lifelines Conference*, Los Angeles, CA, February 7–11, 2022: 311. https://doi.org/10.34948/N3QP4X.

Kalantari, Sara, and Fariborz M. Tehrani. 2024. "Predicting Concrete Service Life in Climate Zones of Iran." In Proceedings of the 1st International Conference on the Exchange of Scientific Information in the Fields of Concrete Structures and Materials (ICConcrete), Tehran, Iran, May 6–7, 2024, 1003: 1–8. https://civilica.com/doc/1994535.

Kalantari, Sara, Mohammad-Ali Dastan Diznab, and Fariborz M. Tehrani. 2021. "Sustainability of Internally-Cured Concrete for Mitigating Shrinkage Cracking Using Service Life Prediction Models." In *Proceedings of the International RILEM Conference on Early-Age and Long-Term Crack Width Analysis in RC Structures (CRC 2021)*, edited by Fotis Kanavaris, Farid Benboudjema, and Miguel Azenha, 277–289. RILEM Bookseries 31. Cham: Springer. https://doi.org/10.1007/978-3-030-72921-9_23.

Kalantari, Sara, Rojina Ehsani, and Fariborz M. Tehrani. 2023. "A Worldwide Survey of Concrete Service Life in Various Climate Zones." In *Adapting the Built Environment for Climate Change: Design Principles for Climate Emergencies*, edited by F. Pacheco-Torgal and C.-G. Granqvist, 183–200. Cambridge, MA: Elsevier. https://doi.org/10.1016/B978-0-323-95336-8.00015-9.

Khajehdehi, Reza, and David Darwin. 2018. *Controlling Cracks in Bridge Decks*. Lawrence, KS: University of Kansas Center for Research, Inc.

Kim, Kyung-Taek, and Sang-Kyun Chun. 2015. "Evaluation of Internally Cured Concrete Pavement Using Environmental Responses and Critical Stress Analysis." *International Journal of Concrete Structures and Materials* 9 (4): 463–473. https://doi.org/10.1007/s40069-015-0115-6.

Klein, A., and E. Kluge. 1961. "Tensile Strength of Lightweight Concrete Beams." *ACI Journal* 58 (6): 123–130. https://doi.org/10.14359/7928.

Kneifel, Joshua D., and Priya D. Lavappa. 2024. "Energy Price Indices and Discount Factors for Life-Cycle Cost Analysis—2024." *Annual Supplement to NIST Handbook 135*. NIST Interagency Report NIST IR 85-3273-39. Gaithersburg, MD: National Institute of Standards and Technology. https://doi.org/10.6028/NIST.IR.85-3273-39.

Korolev, A. S., A. Kopp, D. Odnoburcev, V. Loskov, P. Shimanovsky, Y. Koroleva, and N. I. Vatin. 2021. "Compressive and Tensile Elastic Properties of Concrete: Empirical Factors in Span Reinforced Structures Design." *Materials* 14 (24): 7578. https://doi.org/10.3390/ma14247578.

Kosmatka, Steven H., Beatrix Kerkhoff, and William C. Panarese. 2021. *Design and Control of Concrete Mixtures*. CD100. Washington, DC: Portland Cement Association.

Kwon, Seung-Jun, U. J. Na, S. S. Park, and S. H. Jung. 2009. "Service Life Prediction of Concrete Wharves with Early-Aged Crack: Probabilistic Approach for Chloride Diffusion." *Structural Safety* 31 (1): 75–83. https://doi.org/10.1016/j.strusafe.2008.04.001.

Li, W. A., and L. Han. 2024. "Study on Predictive Method for Time-Dependent Elastic Modulus of Early-Age Concrete in Continuous Rigid-Frame Bridges." In *Proceedings of the 4th International Conference on Computational Modeling, Simulation and Data Analysis*, December 6, 2024, 257–262.

Li, S., and C. Song. 2019. "Mechanical Performance Test and Analysis of Prestressed Lightweight Aggregate Concrete Hollow Slab." *Advances in Structural Engineering* 22 (8): 1830–1844. https://doi.org/10.1177/1369433219831926.

Life-365™ Consortium III. 2020. *Life-365™ Service Life Prediction Model™*. https://www.life-365.org.

Lim, J. C., and T. Ozbakkaloglu. 2014. "Stress–Strain Model for Normal- and Light-Weight Concretes under Uniaxial and Triaxial Compression." *Construction and Building Materials* 71: 492–509. https://doi.org/10.1016/j.conbuildmat.2014.08.050.

Love, A. E. H. 1944. *The Mathematical Theory of Elasticity*. New York: Dover Publications.

Lu, Xinying. 1997. "Application of the Nernst-Einstein Equation to Concrete." *Cement and Concrete Research* 27 (2): 293–302. https://doi.org/10.1016/S0008-8846(96)00200-1.

Lyndon, F. D., and R. V. Baladran. 1986. "Some Observations on Elastic Properties of Plain Concrete." *Cement and Concrete Research* 16 (3): 314–324. https://doi.org/10.1016/0008-8846(86)90126-9.

Mark, Eric Charles. 2006. "Using Internal Curing to Prevent Concrete Bridge Deck Cracking." PhD diss., Cleveland State University.

Martinez, S., A. H. Nilson, and F. O. Slate. 1984. "Spirally Reinforced High-Strength Concrete Columns." *ACI Journal* 81 (4): 431–442. https://doi.org/10.14359/10498.

Mesbah, H. A., M. Lachemi, and P. Aïtcin. 2002. "Determination of Elastic Properties of High-Performance Concrete at Early Ages." *ACI Materials Journal* 99 (1): 37–41. https://doi.org/10.14359/11294.

Mn/DOT (Minnesota Department of Transportation). 2011. *Bridge Deck Cracking*. Transportation Research Synthesis 1105. St. Paul, MN: Minnesota Department of Transportation. https://lrrb.org/media/reports/TRS1105.pdf.

Murillo, Juan A., Steve Thoman, and Dennis Smith. 1994. "Lightweight Concrete for a Segmental Bridge." *Civil Engineering* 64 (5): 68. https://www.escsi.org/wp-content/uploads/2017/10/4700.8-Lightweight-Concrete-for-a-Segmental-Bridge.pdf.

Myers, J., and R. Morales. 2000. *Modulus of Elasticity Predictions for Lightweight Concrete*. Internal Technical Dataset, Kiln Production Records and Modulus Analysis, July–October 2000.

Nelson, Denise, and Fariborz M. Tehrani. 2018. "Is Resilience … Sustainable?" *APWA Reporter* 85 (8): 53–56. www3.apwa.net/Resources/Reporter/Articles/2018/8/Is-resilience-sustainable.

Neville, A. M. 1997. *Properties of Concrete*. 4th ed. New York: John Wiley & Sons Inc.

NRMCA (National Ready Mixed Concrete Association). 2020. "Environmental Product Declaration." Silver Spring, MD: NRMCA.

Nunley, K. 2018. "Williams Creek Bridge Replacement Chooses IC Concrete." *Lightweight Design News*, April. https://www.escsi.org/e-newsletter.

Ozyildirim, H. C., and H. Nair. 2023. "Controlling Bridge Deck Cracking in Virginia." *Aspire Magazine*, Winter: 32–34.

PBO (Plan and Budget Organization). 2018. *Cost Analysis of Referenced Units* [in Persian]. Tehran, Iran: Plan and Budget Organization. sama.mporg.ir.

PCA (Portland Cement Association). 2016. "Environmental Product Declaration." Skokie, IL: Portland Cement Association.

Peurifoy, Robert B., Clifford J. Schexnayder, Aviad Shapira, and Robert L. Schmitt. 2018. *Construction Planning, Equipment, and Methods*. New York, NY: McGraw-Hill.

Popovics, J. S., J. Zemajtis, and I. Shkolnik. 2008. *A Study of Static and Dynamic Modulus of Elasticity of Concrete*. ACI-CRC Final Report. Urbana, IL: University of Illinois.

Popovics, Sandor. 1982. Concrete: Structure, Properties and Materials. São Paulo: Pini.

Pouramini, Mohammad, Fariborz M. Tehrani, Saman Sezavar Keshavarz, and Arjang Sadeghi. 2021. "Durability of Concrete Pavements Exposed to Freeze-Thaw Cycles in Different Saline Environments." In *Proceedings of the ASCE International Airfield and Highway Pavements Conference: Pavement Design, Construction, and Condition Evaluation 2021*, edited by Hasan Ozer, Jeb S. Rushing, and Zhanping Leng, 159–168. https://doi.org/10.1061/9780784483503.016.

Pouramini, M., A. Torabian, and F. M. Tehrani. 2019. "Application of Lightweight Expanded Clay Aggregate as Sorbent for Crude Oil Cleanup." *Desalination and Water Treatment*. 160(2019), 366-377. https://doi.org/10.5004/dwt.2019.24232.

Richart, F. E., A. Brandtzaeg, and R. L. Brown. 1928. *A Study of the Failure of Concrete under Combined Compressive Stresses*. University of Illinois Engineering Experiment Station Bulletin No. 185. Urbana, IL: University of Illinois. https://hdl.handle.net/2142/4277.

Ritchie, D. D., and S. H. Graf. 1951. *Expanded Shale Aggregate in Structural Concrete*. Bulletin No. 30. Corvallis, OR: Oregon State College, Engineering Experiment Station. https://ir.library.oregonstate.edu/concern/technical_reports/6969z175s.

Roberts, James E. 1997. "Lightweight Concrete for California's Highway Bridges." *Engineered Concrete Structures* 10 (3). https://www.escsi.org/wp-content/uploads/2017/10/4700.11-Lightweight-Concrete-for-California.pdf.

Roberts, John W. 2004. "The 2004 Practice and Potential of Internal Curing of Concrete Using Lightweight Sand." In *Advances in Concrete through Science and Engineering*, edited by J. Weiss, K. Kovler, J. Marchand, and S. Mindess. Bagneux, France: RILEM Publications SARL. https://doi.org/10.1617/2912143926.035.

Rosenblueth, E. 1956. "Discussion on Concrete Stress Distribution in Ultimate Strength Design." *Journal of the American Concrete Institute* 52 (Part 2): 1305–1330. https://doi.org/10.14359/11609.

Schindler, Anton K., and B. Frank McCullough. 2002. "Importance of Concrete Temperature Control during Concrete Pavement Construction in Hot Weather Conditions." *Transportation Research Record* 1813 (1): 3–10. https://doi.org/10.3141/1813-01.

Schmitt, Tony R., and David Darwin. 1995. *Cracking in Concrete Bridge Decks*. SM Report No. 39. Lawrence, KS: University of Kansas Center for Research, Inc. https://kuscholarworks.ku.edu/bitstreams/ba3d58f9-1f70-4cb1-afad-129efe51081d/download.

Shah, Surendra P., and W. Jason Weiss. 2000. "High Performance Concrete: Strength, Permeability, and Shrinkage Cracking." In *PCI/FHWA/FIB International Symposium on High Performance Concrete*, 331–340. Orlando, FL: Precast/Prestressed Concrete Institute.

Shakeri, Ali-Akbar, S. Dardaei Joghan, and Fariborz M. Tehrani. 2024. "Optimal Mixture Design of Bio-Concrete Containing *Bacillus Subtilis* for Compressive Strength Enhancement: A Review." In *Proceedings of the 14th National Congress on Civil Engineering*, University of Zanjan, Zanjan, Iran, June 11–12, 2024, MM-01-665: 1–18. https://proceeding.14ncce.ir/#articles.

Sheikh, Shamim A., and Murat T. Toklucu. 1993. "Reinforced Concrete Columns Confined by Circular Spirals and Hoops." *ACI Structural Journal* 90 (5): 542–553. https://doi.org/10.14359/3949.

Sheikh, Shamim A., and Suzru M. Uzumeri. 1980. "Strength and Ductility of Tied Concrete Columns." *Journal of the Structural Division* 106 (5): 1079–1102. https://doi.org/10.1061/(ASCE)0733-9445(1980)106:5(1079).

Shkolnik, Iosif E. 1996. "Evaluation of Dynamic Strength of Concrete from Results of Static Tests." *Journal of Engineering Mechanics* 122 (12): 1133–1138. https://doi.org/10.1061/(ASCE)0733-9399(1996)122:12(1133).

Shkolnik, Iosif E. 2005. "Effect of Nonlinear Response of Concrete on Its Elastic Modulus and Strength." *Cement and Concrete Composites* 27: 747–757. https://doi.org/10.1016/j.cemconcomp.2004.09.001.

Subramaniam, V. Kolluru, John S. Popovics, and Surendra P. Shah. 2000. "Determining Elastic Properties of Concrete Using Vibrational Resonance Frequencies of Standard Test Cylinders." *Cement, Concrete & Aggregates* 22 (2): 81–89. https://doi.org/10.1520/CCA10467J.

SUDAS (Statewide Urban Design and Specifications Program). 2021. "Roadway Design." Chapter 5 in *SUDAS Design Manual*. Iowa: SUDAS Program. https://iowasudas.org/manuals/design-manual.

Swamy, R. N., and J. Bandyopadhyay. 1982. *BS8110 Part 2: Structural Use of Concrete – Code of Practice for Special Circumstances*. London: British Standards Institution. https://doi.org/10.3403/BS8110.

Tehrani, F. M., and Makan M. Ziarani. 2010. *Rāhnamā-ye Jāmeʿ-e Līkā* [A Comprehensive Guide to LECA, in Persian]. Tehran, Iran: Omīdān. Accessed November 26, 2025. https://leca.ir/wp-content/uploads/maghalat/Handbook%20Leca%2088.pdf.

Tehrani, F. M. 1994. "Technical and Economical Evaluation of Lightweight Materials in Construction." [In Persian]. In *Proceedings of the 2nd Seminar of Housing Development Policies*, 335–351. Tehran, Iran.

Tehrani, F. M. 1996. "Light Expanded Clay Applications in Road Construction." [In Persian]. *Journal of Department of Road and Transportation (Rāh-va-Tarābari)* 3 (5): 50–51.

Tehrani, F. M. 1998. *Rāhnamā-ye Jāmeʿ-e Līkā* [A Comprehensive Guide to LECA, in Persian]. Tehran, Iran: LECA Co. Accessed November 26, 2025. https://leca.ir/wp-content/uploads/maghalat/LECA-Handbook.pdf.

Tehrani, F. M. 2019a. "Deploying and Rating Sustainable Practices for Resilient Bridge Infrastructure." Keynote Lecture. In *Proceedings of the Fifth International Conference on Bridges*, MS05. Tehran, Iran: Amirkabir University of Technology, December 17–18, 2019.

Tehrani, F. M. 2019b. "Guide to ACI 213R-14 Structural Lightweight-Aggregate Concrete (3-part series)." ACI University, November 5–7, 2019. Accessed November 26, 2025. https://www.concrete.org/store/productdetail.aspx?ItemID=W1917.

Tehrani, F. M. 2020. "Service Life Prediction of Structural Lightweight Concrete Using Transport Properties." *ESCSI Report 4363*, October 2020. Chicago, IL: Expanded Shale, Clay, and Slate Institute. Accessed November 26, 2025. https://www.escsi.org/wp-content/uploads/2020/10/ESCSI-4363-Service-Life-Prediction-SLWC-Transport-Properties.pdf.

Tehrani, F. M. 2021a. "Application of Expanded Shale, Clay, and Slate Aggregate in Award-Winning Bridge Projects to Accomplish Excellence in Upgrade and Replacement." *ESCSI E-Newsletter* (Winter). Accessed November 26, 2025. https://www.escsi.org/e-

newsletter/application-of-expanded-shale-clay-and-slate-aggregate-in-award-winning-bridge-projects-to-accomplish-excellence-in-upgrade-and-replacement.

Tehrani, F. M. 2021b. "Service Life Prediction of Internally Cured Concrete Pavements Using Transport Properties." In Proceedings of ASCE International Airfield & Highway Pavements Conference: Pavement Design, Construction, and Condition Evaluation, edited by H. Ozer, J. F. Rushing, and Z. Leng, 82–91. Austin, TX: Transportation & Development Institute of ASCE, June 8–10, 2021. https://doi.org/10.1061/9780784483503.008.

Tehrani, F. M. 2022. "Deployment of Sustainable Practices Using Lightweight Aggregates for Bridge Infrastructures." In *Proceedings of ASCE Lifelines 2022: 1971 San Fernando Earthquake and Lifeline Infrastructure*, edited by C. A. Davis, K. Yu, and E. Taciroglu, 187–197. Los Angeles, CA: University of California, Los Angeles, February 7–11, 2022. https://doi.org/10.1061/9780784484432.018.

Tehrani, F. M. 2023a. "Applied Development of Environmental Declarations for Rotary-Kiln Manufactured Expanded Aggregates." *ASCE Engineering Mechanics Institute 2023 Conference*, Atlanta, GA, June 6–9, 2023.

Tehrani, F. M. 2023b. "Objective Sustainability of Lightweight Aggregate Concrete Using Environmental Product Declarations." Session on Role of Life Cycle Assessment (LCA) and Environmental Product Declarations (EPDs) in Concrete Sustainability Evaluation, Part 2 of 2, *ACI Concrete Convention*, Boston, MA, October 29–November 2, 2023.

Tehrani, F. M. 2024a. "ESCSI Plays Pivotal Role in NRMCA's EPA Grant for EPD Development." *Lightweight Design eNews* (Winter). Accessed November 26, 2025. https://www.escsi.org/e-newsletter/escsi-plays-pivotal-role-in-nrmcas-epa-grant-for-epd-development/.

Tehrani, F. M. 2024b. "Lifecycle Environmental Assessment of Internally-Cured Concrete for Bridge Deck." Session on How Lightweight Aggregate & Concrete Can Reduce Global Warming Potential and Increase Sustainability of Concrete, Part 1 of 2, *ACI Concrete Convention*, Philadelphia, PA, November 3–6, 2024.

Tehrani, F. M. 2024c. "Lifecycle Environmental Footprints Assessment of Jointed Reinforced Internally Cured Concrete Pavements." In *Proceedings of the 1st International Conference on the Exchange of Scientific Information in the Fields of Concrete Structures and Materials (ICConcrete)*, 1005: 1–10. Tehran, Iran, May 6–7, 2024. Accessed November 26, 2025. https://civilica.com/doc/1994534/.

Tehrani, F. M., and D. Nelson. 2022. "From Sustainability to Resilience: A Practical Guide to ENVISION." Chapter 3 in *Objective Resilience, Book 2: Objective Processes*, edited by M. Ettouney, 81–125. Reston, VA: ASCE Press. https://doi.org/10.1061/9780784415894.ch3.

Tehrani, Fariborz M., G. Homayoun, S. M. Mousavi, M. Goodarzi, M. H. Rafatkhah, and A. N. Esfahani. 2024. "Toward Declaring Environmental Footprints of Lightweight Expanded Clay Aggregate and Concrete Products." In *Proceedings of the 1st International Conference on the Exchange of Scientific Information in the Fields of Concrete Structures and Materials (ICConcrete)*, 1031: 174–182. Tehran, Iran, May 6–7, 2024. Accessed November 26, 2025. https://www.icconcrete.org/p_conferenceproceeding and https://civilica.com/doc/1994517/.

Tehrani, Fariborz M., G. Homayoun, S. M. Mousavi, M. Goodarzi, M. H. Rafatkhah, and A. N. Esfahani. 2025. "Contributions of Lightweight Aggregate and Concrete Products to Building Energy Optimization Across Climate Zones." In *Proceedings of the 2nd International Conference on the Exchange of Scientific Information in the Fields of Concrete Structures and Materials (ICConcrete)*, 1008: 46–55. Tehran, Iran, May 6–7, 2025. Accessed November 26, 2025. https://civilica.com/doc/2286343/.

Tehrani, F. M., R. Farshidpour, M. Pouramini, M. Mousavi, and A. N. Esfahani. 2018. "Sustainability Rating of Lightweight Expanded Clay Aggregates Using Energy Inputs and Carbon Dioxide Emissions in Life-Cycle Analysis." In *Proceedings of the Sixth International Symposium on Life Cycle Civil Engineering*, 2989–2993. Ghent, Belgium: IALCCE, October 2018. Accessed November 26, 2025. https://www.crcpress.com/Life-Cycle-Analysis-and-Assessment-in-Civil-Engineering-Towards-an-Integrated/Caspeele-Taerwe-Frangopol/p/book/9781138626331.

Tehrani, F. M. 2025. Strategized Reduction of Greenhouse Gas Emissions Through Predicting and Extending the Service Life of Concrete Pavements and Bridges. Mineta Transportation Institute, San José State University.

UL. 2022. "Product Category Rules (PCR) Guidance for Building-Related Products and Services, Part B: Expanded Shale, Clay, and Slate Lightweight Aggregate EPD Requirements." UL 10010-37. Northbrook, IL: UL.

Vosoughi, Payam, Steven Tritsch, Halil Ceylan, and Peter Taylor. 2017. "Lifecycle Cost Analysis of Internally Cured Jointed Plain Concrete Pavement." Part of IHRB Project TR-676. Ames, IA: Iowa Highway Research Board.

Vulcan. 2016. "Environmental Product Declaration." Glendale, CA: Vulcan Materials Company, Western Division.

Wall, J., and A. Maloof. 2003. *Early Strength and Modulus Development of Lightweight Concrete.* Carolina Stalite Laboratory. Project Start Date: June 2003.

Wall, J. R., C. Freeman, and M. Robinson. 2002. *Modulus of Elasticity Research Report.* Carolina Stalite Laboratory, Gold Hill, NC.

Wang, P. T., S. P. Shah, and A. E. Naaman. 1978. "Stress–Strain Curves of Normal and Lightweight Concrete in Compression." *ACI Journal* 75 (62): 603–611.

Wei, H., T. Wu, X. Liu, and R. Zhang. 2020. "Investigation of Stress-Strain Relationship for Confined Lightweight Aggregate Concrete." *Construction and Building Materials* 256: 119432. https://doi.org/10.1016/j.conbuildmat.2020.119432.

Whitney, C. S. 1937. "Design of Reinforced Concrete Members Under Flexure or Combined Flexure and Direct Compression." *ACI Journal* 33 (2): 483–498.

Wolfe, Bill. 2017. "Bayonne Bridge Rises to New Heights." *Lightweight Design News* (October). Accessed November 26, 2025. https://www.escsi.org/e-newsletter.

Wu, T., H. Wei, Y. Zhang, and X. Liu. 2018. "Axial Compressive Behavior of Lightweight Aggregate Concrete Columns Confined with Transverse Steel Reinforcement." *Advances in Mechanical Engineering* 10 (3): 1–14. https://doi.org/10.1177/1687814018766632.

About the Author

Dr. Fariborz M. Tehrani is a Professor and Director with nearly four decades of academic and industry background in engineering design, management, education, and leadership. His research and practice experiences focus on sustainable and resilient structural engineering, mechanics, and materials (SR-SEMM). Fariborz is a Fellow ASCE, the Director of the ESCSI, and a voting member of several ACI and ASTM Committees. He has also served as the ISI Academic Committee Chair and EWB professional mentor at University of Southern California; University of California, San Diego; and California Polytechnic State University, San Luis Obispo. He has over 130 published and over 160 presented scholarly works. Dr. Tehrani received the ASCE Region 9 Outstanding Faculty Advisor Award, the CHESC Best Practice Award, and two ASCE Research Awards from Fresno and San Francisco. He received his BSc from Sharif University of Technology, his MSc from Amirkabir University of Technology, and his MS, Degree of Engineering, and PhD from the University of California, Los Angeles.

MTI FOUNDER

Hon. Norman Y. Mineta

MTI BOARD OF TRUSTEES

Directors